TAMPEREEN TEKNILLINEN YLIOPISTO
TAMPERE UNIVERSITY OF TECHNOLOGY

Janne Juoksukangas

Modelling and Experimental Analysis of Fretting Fatigue in Complete and Bolted Contacts

Julkaisu 1472 • Publication 1472

Tampere 2017

Tampereen teknillinen yliopisto. Julkaisu 1472
Tampere University of Technology. Publication 1472

Janne Juoksukangas

Modelling and Experimental Analysis of Fretting Fatigue in Complete and Bolted Contacts

Thesis for the degree of Doctor of Science in Technology to be presented with due permission for public examination and criticism in Festia Building, Auditorium Pieni Sali 1, at Tampere University of Technology, on the 24th of May 2017, at 9 a.m.

Tampereen teknillinen yliopisto - Tampere University of Technology
Tampere 2017

ISBN 978-952-15-3944-2 (printed)
ISBN 978-952-15-3960-2 (PDF)
ISSN 1459-2045

Abstract

Fretting is the micrometer-level relative movement between contacting surfaces that can lead to fretting fatigue and fretting wear in practical connections in machine components. Fretting has a clear tendency to nucleate cracks that can continue to grow as a result of the cyclic loads in a component, leading to premature failure. The lack of fundamental knowledge of the fretting mechanism and a universal model poses challenges for the design of modern machine components having contacts under high loading.

This thesis comprises seven publications. Its purpose is to study the effect of various design parameters on the fretting fatigue behavior in practical connections and also to apply the Digital Image Correlation method to fretting contact in order to measure displacement fields. Both experimental and modelling methods were employed to study complete and bolted contacts. The material used was self-mated quenched and tempered steel. A complete contact fretting test device was developed that had a large contact area and transverse loading resembling practical connections. Numerous fatigue tests were carried out. The Finite Element Method was used to analyze the contacts in greater detail.

Fretting significantly decreased the fatigue life in complete and bolted contacts. Increasing contact normal load decreased life in both types of contact while rounding of the sharp contact edge did not extend fatigue life. Fatigue life decreased when the amplitude of cyclic loading of the test specimen was increased. In complete contact tests, the cracking point was at the contact edge whereas in the bolted joints the area of fretting damage and cracking point was away from the geometric stress concentration (bolt hole) and corresponded to the distribution of frictional energy dissipation. Shot peening and nitriding were particularly effective in increasing fatigue life in sharp ended contacts. Cyclic relative displacement fields close to the contact interface were measured using the Digital Image Correlation method so that bulk compliances were minimized. These displacement measurements were successfully compared with numerical results. The modelling results agreed with the experiments in terms of cracking prediction and contact quantities.

Preface

This study was carried out at the Tampere University of Technology, first at the Department of Mechanics and Design, then at the Department of Engineering Design and lastly at the Department of Materials Science, in the Tribology group led by Professor Arto Lehtovaara. The main funding was received from the Graduate School of Concurrent Mechanical Engineering whose sponsorship is gratefully acknowledged. This thesis is part of two industry-based projects that I was involved with. FREDA (Fretting damage in mechanical engineering) was part of the FIMECC Demanding Applications Program funded by Tekes (the Finnish Funding Agency for Innovation), Wärtsilä Finland Oy and Metso Paper Oy, and Scarface (Short crack and fretting fatigue damage in mechanical engineering, decision no. 40205/12) project was funded by Tekes, Wärtsilä Finland Oy, Nome Oy, and Global Boiler Works Oy. I am grateful to all of these for their financial support which was especially important in allowing extensive experimental testing. Some of the tests are presented here. I also wish to acknowledge the Foundation of K.F. and Maria Dunderberg, Otto A. Malm Foundation and the Foundation of Henry Ford for their financial support of this thesis.

Numerous people deserve my thanks and are mentioned in the individual articles. I am especially indebted to my supervisor, Professor Arto Lehtovaara, for his much valued guidance, advice and support. I would like to thank Antti Mäntylä, Msc and Christian Lönnqvist, Msc for their important collaboration in fretting research and co-authoring the articles. I would also like to thank Tomi Koivula, MSc, Atte Hokkanen, MSc, Taro Salonen, MSc, Olli Nuutila, Lic. Tech, Juha Miettinen, PhD, Mikko Hokka, PhD and Professor Pentti Saarenrinne for their help with the measurement equipment. Alan Thompson, MPhil, MA, is acknowledged for helping with the English language. The people working in the projects are also acknowledged as well as the members of the Graduate School of Concurrent Mechanical Engineering. Finally, I would like to thank all my colleagues in the various departments and especially the members of the research group of Tribology.

My thanks are also due to thank several people who were not directly involved in my work. During my studies, it was greatly honoured to be nominated to the board of the Finnish Society for Tribology and to work alongside some of the leading tribologists in Finland. I am also very grateful to Janne, Jokke, Juha, Pete and Sussu; those thousands of kilometers on the road were a welcome counterbalance to daily routine. Finally, I am greatly indebted to my parents Anja and Markku and brother Juho for their support and encouragement. My most heartfelt gratitude during these busy years of establishing a family and house building goes to Piritta, Sofia, Aleksi and Aino.

Tampere, March 2017

Janne Juoksukangas

Contents

List of Figures

Symbols and Abbreviations

a	Half-width of a punch, [m]
d	Findley cracking risk, [-]
E_d	Frictional energy dissipation, [J]
f_F	Findley constant, [Pa]
F_f	Tangential (friction) force, [N]
F_n	Normal force, [N]
k	Slope exponent of *S-N* curve, [-]
k_F	Findley constant, [-]
K_t	Stress concentration factor, [-]
N	Number of loading cycles, [-]
N_1	Number of loading cycles to macroscopic crack nucleation, [-]
N_2	Number of loading cycles to complete fracture, [-]
N_{af}	Number of cycles at the point when *S-N* curve reaches the fatigue limit, [-]
p	Contact pressure, [Pa]
p_0	Constant clamping load (normal pressure), [Pa]
p_{nom}	Nominal contact pressure, [Pa]
P	Normal load, [N]
q	Shear traction, [Pa]
Q	Tangential load, [N]
R	Load ratio, [-]
S	Stress, [Pa]
S_{11}	Axial (tangential) normal stress in *x* direction, [Pa]
S_a	Surface roughness over an area (3D surface roughness), [m]
S-N	Stress-life
t	Time, [s]
$u_{i\_spec}(t)$	Displacement of a point in specimen at time moment *t*, [m]
$u_{i\_pad}(t)$	Displacement of a point in pad, [m]
$u_{spec\_i}(t)$	Displacement of a point in specimen *i,* [m]
U_x	Displacement in *x* direction, [m]
U_y	Displacement in *y* direction, [m]
x,y,z	*x, y* and *z* coordinate, [m]
x_1	Point at hole edge, [m]
x_2	Point at about 9 mm away from bolt's hole edge, [m]
δ	Relative tangential movement, displacement, [m]
δ_{disp}	Transverse bulk loading (displacement), [m]
$\delta_i(t)$	Relative tangential movement at time moment *t*, [m]
ΔK_I	Stress intensity factor, [-]

ε	Strain, [-]
μ	Coulomb coefficient of friction (COF), [-]
σ	Normal stress, [Pa]
σ_a	Bulk stress amplitude, [Pa]
σ_{af}	Fatigue limit, [Pa]
σ_n	Normal stress, [Pa]
$\sigma_{1,max}$	Maximum principal stress, [Pa]
τ_a	Shear stress amplitude, [Pa]
τ_{crit}	Critical shear traction (below of which contact sticks), [Pa]

2D	Two-dimensional
3D	Three-dimensional
COF	Coefficient of friction
C3D8I	Element type in Abaqus FE-programme
CPE4I	Element type in Abaqus FE-programme
CSLIP1	Computed slip in Abaqus FE-programme
D24	Bolted joint series (no. 3) with spacer diameter of 24 mm
DIC	Digital Image Correlation
Exp. fat. limit	Experimental fatigue limit
FE	Finite element
FF	Fretting fatigue
FEM	Finite element method
FOV	Field of view
GSR	Gross sliding regime
LSM	Least Squares Matching approach in Davis DIC software
LVDT	Linear Variable Differential Transformer
Mod	Modelling (result)
MSR	Mixed slip regime
NLGEOM	Nonlinear geometry option in Abaqus FE-programme
PSR	Partial slip regime
QT_i	Quenched and tempered steel specimen (i^{th})
RH	Relative humidity
SEM	Scanning electron microscope
SG_i	Strain gauge (i^{th})
TCD	Theory of Critical Distances
x102	Bolted joint series no. 4

List of Publications

This thesis is formed of the following seven publications. In the text they are referred to using Roman numerals.

I. J. Juoksukangas, A. Lehtovaara, A. Mäntylä, **Development of a complete contact fretting test device**, Proc. IMechE, Part J: J. Engineering Tribology, 227(6), 2013, 570–578, doi:10.1177/1350650112466162

II. J. Juoksukangas, A. Lehtovaara, A. Mäntylä, **Response to discussion with DA Hills et al., concerning the article "Development of a complete contact fretting test device" by J Juoksukangas et al.**, Proc. IMechE, Part J: J. Engineering Tribology, 228(1), 2014, 127–128, doi:10.1177/1350650113500947

III. J. Juoksukangas, A. Lehtovaara, A. Mäntylä, **The effect of contact edge geometry on fretting fatigue behavior in complete contacts**, Wear, 308(1–2), 2013, 206–212, doi:10.1016/j.wear.2013.06.013

IV. J. Juoksukangas, A. Lehtovaara, A. Mäntylä, **Applying the digital image correlation method to fretting contact for slip measurement**, Proc. IMechE, Part J: J. Engineering Tribology, Published online August 20 2015, doi:10.1177/1350650115601695

V. J. Juoksukangas, A. Lehtovaara, A. Mäntylä, **A comparison of relative displacement fields between numerical predictions and experimental results in fretting contact**, Proc. IMechE, Part J: J. Engineering Tribology, 230(10), 2016, 1273–1287, doi:10.1177/1350650116633573

VI. J. Juoksukangas, A. Lehtovaara, A. Mäntylä, **Experimental and numerical investigation of fretting fatigue behavior in bolted joints**, Tribology International, 103, 2016, 440–448, doi:10.1016/j.triboint.2016.07.021

Unpublished manuscript

VII. J. Juoksukangas, A. Lehtovaara, T. Koivula, A. Mäntylä, **Influence of a surface treatment on fretting fatigue life in complete contacts**

Author's contribution

Janne Juoksukangas was the main author in all publications and undertook the major part of the writing. Professor Arto Lehtovaara supervised the work, commented on the manuscripts and assisted in the writing. Antti Mäntylä, MSc, was the co-author in Publications II–VII, Christian Lönnqvist, MSc in Publication I and Tomi Koivula, MSc in Publication VII. They also read the manuscripts and provided comments. Juoksukangas was mainly responsible for specimen manufacture and other experimental-related activities (including instrumentation) assisted by the departments' laboratory technicians and sub-contractors.

Publication I: The following collaborated in developing the test device: Janne Kortelainen, MSc, Juhani Vestola, MSc, Christian Lönnqvist, MSc, Olli Nuutila, Lic Tech and the authors of the publication. The authors planned the experiments. Juoksukangas determined some of the experimental parameters, carried out the experiments and analyzed the data. Jussi Laurila, Lic. Tech, performed the fracture surface analysis.

Publication II: As described in the paragraph above.

Publication III: The authors contributed to the experiment planning. Juoksukangas built the finite element model, coded all Matlab and Abaqus/Python scripts, specified some of the experimental parameters, carried out the experiments and also analyzed the experimental and numerical data.

Publication IV: Juoksukangas and Taro Salonen, MSc, were mainly responsible for the DIC measurement setup and the co-authors provided comments. Juoksukangas carried out the experiments and analyzed the data. Juoksukangas devised the presentation of the measurement results.

Publication V: Juoksukangas was responsible for the idea of the article and its contents. He also built the numerical model and carried out the work including all Matlab and Abaqus/Python coding. The co-authors provided comments.

Publication VI: The layout of the test setup was developed by the authors and Atte Hokkanen, MSc Hokkanen was responsible for the design details and drawings and also planned the experiments in collaboration with the authors. Hokkanen carried out the experiments, data analysis and photographic inspections. Juoksukangas built the numerical model and made the numerical analyses.

Publication VII: The authors contributed to the experiment planning. Koivula carried out the experiments, data analysis and microscopic inspections in co-operation with

Juoksukangas. Part of the material analysis was made at the Department of Materials Science and the residual stress measurements were made by a subcontractor.

1 Introduction

Metal fatigue has long represented a serious challenge for designers. Severe fatigue failures were reported as early as the 19th century [1], and much effort has been invested in prevention work since then. However, fatigue originated failures persist with the resultant loss of machine function. Premature machine failure increases costs in several ways. Apart from the need to repair the broken machine, such failure can incur major financial costs, both direct and indirect as well as the possible safety risks such as human injury.

Machines typically have multiple frictional contacts in the assemblies, as in shaft-hub connections (interference fits) and bolted joints. A particularly damaging and insidious mechanism prevailing in such contacts is fretting. Fretting fatigue or fretting wear may occur if short amplitude relative movement exists between parts under normal loading in a recurring manner. Fretting fatigue can significantly decrease fatigue life in joints that are designed to be static, but for some reason slight movement occurs between the parts. One application well-known for its vulnerability to fretting is the gas turbine engine used, for example, in the aviation industry. Fretting is a complex tribological phenomenon that is affected by many parameters [2]. The proper consideration of fretting at the design stage is, therefore, important. Progress towards fatigue-free and more energy-efficient machines as well as increasing power densities in modern machine construction has given rise to numerous sophisticated engineering solutions. Though proper sizing of components is an essential task of an engineer, there is still no universally accepted model for taking fretting into account.

1.1 Tribology, friction and wear

Tribology, the science of friction, wear and lubrication [3], has received increased attention in recent decades due to its importance in machine friction and wear. Though friction is a requirement in certain applications such as the brakes in cars, and in everyday life such as shoestrings or stringed instruments, its effects are usually undesirable. In a passenger car,

for example, 28 % of the fuel energy is consumed to overcome friction (excluding braking friction) [4]. The importance of tribology was first acknowledged in the Jost Report 50 years ago (1966) [5]. The report described the problems of friction in machines and the potential savings by using new technology [3]. It has been calculated that losses due to ignorance of tribology amount to around 4 % of the gross national product of the U.S.A [5]. There is a huge number of contacting surfaces both in machines and in everyday life that lie within the scope of tribology. Combustion engines are just one example of machines that contain multiple frictional contacts. Tribology is clearly an important field of human knowledge.

The word “tribology” comes from the Greek “tribos” that means rubbing. In tribology, the interacting surfaces are studied. The term tribology was first used in the 1960s but the history of tribology can be traced to ancient times. For example, Egyptian chariots used animal tallow as a lubricant (friction reduction). In the Renaissance tribological issues were studied by various people such as Leonardo da Vinci. [6]

Friction is the force resisting relative movement between contacting parts. The following are the three classical laws of friction [3]:

1. Friction force is directly proportional to normal load
2. Friction force is independent of the apparent contact area
3. Friction force is independent of sliding velocity

The relationship between normal F_n and tangential (friction) force F_f (the first law) is as follows:

$$F_f = \mu F_n \tag{1}$$

where μ is the coefficient of friction (COF) between the surfaces. Friction force acts parallel to the surface and its direction is opposite to the motion. When a tangential force is high enough to cause sliding, shear traction (q) is the COF multiplied by the contact pressure p (due to the normal loading):

$$q = \mu p \tag{2}$$

It follows that COF limits the magnitude of shear traction. When a contact (or a certain point) is sticking, i.e., the contact is (at least locally) stuck having no relative motion between surface points, shear traction is below this product. Shear tractions affect the stresses on the surface and sub-surface stresses [7]. The hysteretic behavior of friction also dissipates energy in contacts sliding against each other, thus decreasing efficiency, but, on the other hand, providing structural damping.

Wear is the removal of material from one or both interacting surfaces. Besides a loss of material, it can lead to damage of the surface. Many variables affect wear such as normal

load, sliding distance, contact geometry and contact area. There are different kinds of wear, namely, adhesive, abrasive, surface fatigue, erosion, corrosion, electrical and fretting wear. Fretting wear consists of adhesive, abrasive and corrosion wear mechanisms. Wear and friction are interrelated phenomena because friction is involved in the wearing process. [3,5]

1.2 Fatigue

Machines contain moving parts that can be under complex, two or three dimensional (multiaxial) loading conditions. When a component is under cyclic loading, fatigue failure may occur even with nominal stress markedly below yield level. A crack can develop due to loading or it can be created already in the manufacturing process. A crack is always present in fatigue damage and the crack is typically created at a stress concentration (a notch or material inclusion, for example). Fatigue cracks typically nucleate at the surface, thus manufacturing irregularities and surface roughness can have a profound effect on fatigue life. Plasticity is always present in fatigue process, at least at a microscopic level. Fatigue cracks nucleate at the microscopic level from persistent slip bands (crack nucleation stage) followed by the crack growth (propagation) stage before fracture. Fatigue crack growth can be divided into short crack and long crack regimes. During the short crack regime under micrometer level dimensions, the crack growth rate is typically much higher compared to (millimetre scale) long crack regime [8]. [1,9]

Two regimes are related to fatigue depending on the amount of loading cycles undergone before fracture; low-cycle regime and high-cycle regime. In contrast to high-cycle fatigue, in low-cycle fatigue macroscopic plastic deformation exists in every cycle and fracture can occur in a low number of cycles, even below 1000. Typically, machine components experience high-cycle fatigue. The stress-life approach is used in high-cycle regime to determine the fatigue limit for the material. The strain-life approach, on the other hand, is often used in low-cycle fatigue where local plasticity is to be taken into account. If the plasticity is small, stress-based fatigue models can often be used successfully in the finite life regime [8]. The total fatigue life can be divided into crack nucleation life and propagation life. [1,9]

Different fatigue models have been proposed for multiaxial fatigue, e.g., critical plane approaches such as Findley, Smith-Watson-Topper and Fatemi-Socie, stress invariant based approaches such as von Mises, Crossland and Sines, and mesoscopic scale approaches such as Dang Van. Some of the models cannot be used in non-proportional loading when the orientation of the principal axes does not stay fixed, in contrast to proportional loading. At principal plane, the shear stress is zero and only principal stresses (normal stresses in nature) act on the plane. Non-proportional loading is usually regarded as more damaging than proportional loading. Determining the six components of stress

(strain) describing the state of stress (strain) at a point is needed for fatigue calculations. [8,9]

The basic idea in critical plane approaches is that a critical plane is being sought, where an equation relating, for example, to normal and shear stresses reaches its maximum. Basically, the critical plane is the plane where cracks are expected to nucleate, thus having a physical meaning. For example, in the case of the Findley method, the plane is sought where the following relation reaches its maximum: [8]

$$\tau_a(t) + k_F \sigma_n(t) \tag{3}$$

Shear stress amplitude is τ_a and σ_n is the normal stress acting on the plane. The constant k_F can be determined from experimental fatigue tests.

A typical result of a fatigue test is the *S-N* (Wöhler) curve which is obtained from a number of independent fatigue tests at different load levels. Tests are run until failure to find the finite lifetime, and at loadings below the fatigue limit, specimens become run-outs. Un-notched fatigue results are typically regarded as material properties. The fatigue limit can be determined, for example, by using a staircase test [10]. Laboratory fatigue testing allows testing of different materials, loadings (axial, bending, torsion), load ratios and specimen geometries within a reasonable time frame. [1]

1.3 Fretting

Fretting is a tribological phenomenon occurring between solid parts under clamping (normal load) and having small relative movement (slip) between the parts. Despite extensive research, there is still no general solution to the problem of fretting-induced failures. The topic is challenging because of the large number of (interrelating) parameters [2]. Typical industrial components and locations vulnerable to fretting are shaft-hub connections (shrink and press fits, keys etc.) and bolted and riveted connections (Figure 1), wire ropes, gas turbine parts [11] and also electrical connections and body joints [12]. Basically, fretting can be encountered in nominally static joints that have to transfer loads, are under vibration or some other mechanism creates slip between the clamped parts. In practice, red rust (ferric oxide, Fe_2O_3 [13]) ejecting from a contact is evidence of fretting in steels. [7,12]

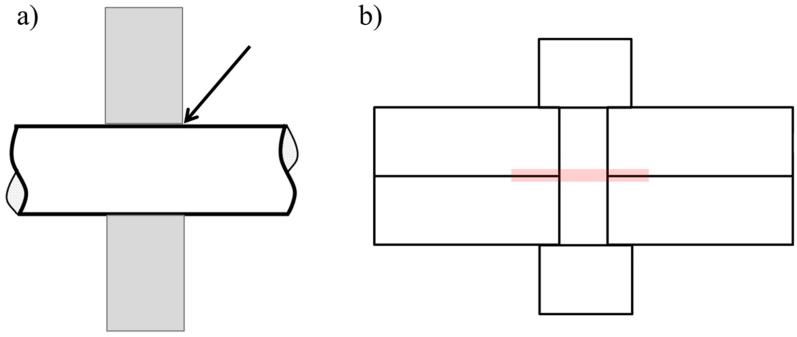

Figure 1. Common examples of fretting fatigue locations, in shaft-hub (a) and bolted (b) connections.

Eden, Rose and Cunningham were one of the first to observe fretting in 1911 when they carried out fatigue tests which produced reddish-brown ‘cocoa’ on the test specimen holders. Later, Tomlinson recognized that the reason for fretting was the tangential motion. An early pioneer in fatigue research, August Wöhler, noticed particles dropping out of shrink fits and called the process “das Bluten des Eisens” (the bleeding of iron) [1]. The effect of fretting on fatigue was first observed in the 1940s. The accelerating effect of fretting on the crack nucleation process was observed in the 1950s. Waterhouse carried out important studies in the 1960s and later. Nishioka and Hirakawa published extensive fretting results in the 1960s and 1970s [14]. [7,12,14,15]. In recent decades, comprehensive fretting research has been carried out and numerical methods have enabled a deeper understanding of fretting. Some of this research is discussed in the following sections.

Fretting can be divided into fretting fatigue and fretting wear. Basically, fretting fatigue may lead to decreased fatigue life. Fretting wear refers to surface damage and/or wear (material loss). Fretting wear can cause loss of fit [16] (or swelling if wear debris cannot escape from the contact) or seizure due to wear debris. The COF can be very high in fretting contact, over unity [17]. In fretting, we are basically interested in sliding friction, at least in the absence of wear debris. In contacts sliding against each other, friction dissipates energy, thus decreasing efficiency (of a machine). However, more important here is that high COF leads to high shear tractions and, therefore, higher stresses on the contact that can lead to nucleation of fatigue crack, even when the nominal ‘bulk’ loading is fairly low. Energy losses in fretting may be relatively minor under small slip.

Plain (normal) fatigue and fretting fatigue share common principles with regard to cracking. First, a crack nucleates, then propagates and finally, complete fracture occurs. However, fretting fatigue can be more complicated due to the contact, since there are high stress concentrations (due to frictional contact stresses) and slip. The stress state in fretting can be multiaxial and non-proportional [18]. In plain fatigue, due to free surface, a single normal stress is zero [8], but in fretting this is not the case because of the contact. The crack nucleation time can often be shorter in fretting than in plain fatigue [7]. After crack nucleation and some crack growth, contact stresses no longer contribute to, or have only a

limited effect on the state of stress and it can be expected that further crack growth is only being caused by bulk loading. When contact stresses are no more influencing, fretting-induced crack growth rate may become smaller and crack may even arrest, if the bulk loading is rather low [19]. It is typical that under the influence of contact loading, the crack propagates at some oblique angle but at some length turns its direction and typically grows perpendicular to the maximum principal stress under pure bulk loading [7]. [20]

1.3.1 Main parameters

Although fretting is affected by several factors, and up to 50 variables have been listed, three primary variables have been identified; normal load, that enables contact between parts, coefficient of friction and relative slip amplitude [2]. These are interrelated since both the increase in normal load [21] and increase in COF [22] decrease slip. Typically, increased normal loading decreases fatigue life [23,24] and the relation can be non-linear [24]. Increased normal load increases stress which can be the reason for decreased fatigue life [23] but increased normal load also increases shear loads.

It is well known that COF changes by increasing the number of loading cycles [7,25]. Non-Coulomb friction behavior has been observed [26,27] in fretting contact which makes it challenging to determine the ‘correct’ value for COF. In addition, COF can vary spatially in the contact [28]. Only the slipping part of contact may contribute to the development of COF [28]. Therefore, the use of a constant value for COF over the whole contact can be more or less an approximation, though a constant value is typically applied in modelling. The COF has a major effect on shear tractions [7] and thus a correct input value for calculations is critically important.

Relative movement (slip) is a strict requirement in fretting; without slip there is, by definition, no fretting. If there is no slip in a contact, it basically becomes a plain fatigue case where possible stress concentration comes from geometry [29]. The range of slip in fretting can be from less than 1 μm up to 100 - 200 μm [30]. Lowering the COF may significantly decrease stresses in the contact but slip, on the other hand, may increase and have further consequences. Fretting fatigue and wear has been experimentally observed to be dependent on slip amplitude [31]. Dissipated energy of a contact due to friction can be calculated from the friction force and relative slip, which is the area enclosed in the fretting loop (i.e., friction force plotted against slip). Fretting wear volume correlates with cumulated dissipated energy [32] and the distribution of dissipated energy is important in fretting [7].

Similar materials are often used in the contacting parts, though dissimilar materials are also used, e.g., [33], which can often be the case in practical connections. A high COF exists typically in a self-mated fretting contact [34]. Much fretting research has been carried out nowadays on titanium and aluminium alloys used in the aviation industry and fewer studies relate to quenched and tempered steels, which are materials that are often used in heavy loaded contacts in machines.

1.3.2 Fretting regimes and maps

An unfortunate aspect in fretting is that only a (small) part of a contact can be slipping whereas the rest of the contact is stuck. Fretting contacts can be divided into gross slip regime (GSR), partial slip regime (PSR) and mixed slip regime (MSR) [21]. In GSR, the contact is fully sliding, i.e., every point in the contacting surface is sliding. In PSR, some points are stuck (no relative movement), while some other points are sliding relative to each other. MSR consists of both GSR and PSR in the loading history. In terms of fretting fatigue, the partial slip contact condition is considered the most dangerous and fretting wear is more closely related to gross slip [32].

At stick area, where the contact is stuck, wear and fatigue damage are limited. At the transition between PSR and GSR (~10 - 30 μm), the fatigue life is at a minimum, increasing in both lower and higher slip values. In PSR, wear is small but is increasing in GSR, having a maximum in a reciprocating sliding regime. In the transition from partial slip to gross slip, there is an increase in wear rate together with an increase in fatigue life. Typically slip amplitudes over a few hundreds of microns to a few millimetres are regarded as the boundary between fretting movement and reciprocating sliding [35]. [31]

By running several experiments, a fretting map [31] can be drawn typically using normal load and displacement amplitude as variables, though other parameters can be used as well. Zhou. et al. [36] called this a “running condition fretting map” and introduced a “material response fretting map” which separates areas of cracking, no degradation and particle detachment. An advantage of these maps are that tests can be compared, even between different researchers and they can also be useful for design engineers. This mapping concept has been widely used in plain fatigue (e.g., Haigh’s diagram) but has later been applied to fretting [37].

1.3.3 Experimental

Due to the complexity of fretting, experimental tests are usually carried out to understand the damage mechanisms. Tests in well-controlled conditions are important in providing fretting data and also for verifying fretting models. Typically, complex loading conditions in real applications are simplified in test conditions [38]. Test devices resembling real applications have been also developed, e.g., using real interference fits [39,40]. On the other hand, a bolted joint test arrangement in a laboratory may closely resemble practical joints.

1.3.3.1 Fretting fatigue test devices

So far, no generic standardized fretting test device has been defined [38,41]. Typically, a fatigue testing machine is used as a base construction for a fretting test device, with the insertion of a pad holding frame that can be fixed, e.g., [42] or be supported by springs. A

bridge type pad is commonly used where it is pressed against the specimen and two fretting contacts are created on either side of the specimen. Single fretting pads supported by springs can be used to create one fretting contact on either side [23]. A common way to create normal load is to use springs (proving ring), dead weights or hydraulic loading. The tangential loading can be created by cyclic fatigue (bulk) loading with the aid of strain [42–44], i.e., the pad is stationary and the specimen is strained. The bridge type device is robust, but has disadvantages because shear loading and bulk loading cannot be separated and the loading between contacts may be uneven [7]. To allow separate control of the loading quantities, separate actuators for bulk and shear loadings can be utilized [28]. Applying the displacement directly enables more accurate control of displacement, however, the micrometer-level displacements are still challenging to produce in a controlled way [7]. The specimen is typically loaded axially, but bending loading can be also used [40,45]. Experimental testing of fretting fatigue in bolted joints is typically carried out in a fatigue machine with two or three specimens bolted together and the bolt's preload and the cyclic bulk loading is measured, e.g. [46]. The bolt's hole obviously creates a point of stress concentration and a possible cracking point but the applied preload can move the point of cracking away from the hole [46]. Thus, the fatigue life can be increased [47,48] though fretting may prevail [46,49].

In laboratory experiments, contact size is typically much smaller than in a practical application. The contact geometries typically employed in fretting test devices are point (ball-on-flat), line (cylinder-on-flat) (both incomplete contacts) and complete (flat-on-flat) contacts. In complete contacts the applied normal loading does not change the nominal contact area, in contrast to incomplete contacts. In complete contacts, misalignment should be avoided because it can have an major effect on stress distribution [28].

1.3.3.2 About measurements

Relative displacement values are typically measured and reported within experimental results. Experimental measurement of the micrometer-level motion between the contacting parts is challenging and the actual slip is always smaller than the applied displacement due to the elastic compliances of the structure. A displacement sensor, such as a linear variable differential transformer (LVDT) [25,50], an extensometer [51,52] or optical sensor (such as laser [53]) is commonly used to measure slip. However, in practice it can be very difficult to install this kind of sensor close enough to the fretting contact interface and so compliances are invariably included in measurements. Moreover, these sensors measure displacement only at a certain point, yet do not provide slip distribution which in fretting contact is typically uneven. The FE-calculated local slip has been reported to be markedly smaller than the experimentally measured slip and this was affected by the rig compliance and the COF [54]. Comparing the absolute slip values between different cases can therefore be difficult and even misleading. These compliances can be analytically taken into account [55,56] to

estimate the slip, but are restricted to certain geometries. In [57], an equation was formed to match numerically calculated values with the experimental slip results.

Measurement of COF is not always straightforward. In gross sliding, according to Coulomb friction law, the COF is equal to the tangential load divided by the normal load Q/P, but the equation does not apply in partial slip conditions due to the presence of the stick zone. In partial slip case, the COF can be determined from the dissipated energy [58]. The COF has been determined by comparing fretting scars to numerically calculated slip [34] and comparing the accumulated relative displacements between experiments and numerical results [59].

1.3.3.3 Fretting fatigue life

A conventional way in fretting fatigue tests is to compare fretting fatigue results to plain fatigue results to find the effect of fretting by a means of “knock-down” factor. However, if nominal stress values are used and the stress states are very different, the generalization of results is limited [60]. Naturally, local stresses can be calculated and results compared, e.g., using some fatigue criteria [61] or within asymptotes as proposed [60], thus improving the usefulness of the results.

In fretting fatigue tests, a cyclic bulk loading is typically applied to the specimen which allows a fretting-induced crack to grow. Fretting fatigue cracks usually nucleate at the contact edge or the stick/slip boundary (regime of maximum stress concentration) [7]. Fretting can decrease fatigue life dramatically. A decrease in fatigue life of at least tens of percent are commonly reported [13,40]. In addition, surface wear can grind embryonic cracks away. Contact size effect can have an major impact on fretting fatigue response since there can be a certain contact size above which cracking arises [19]. Contact size can also have a dramatic effect on wear; in [62] wear was significantly decreased when contact size was increasing.

1.3.3.4 Fretting in steels

A significant decrease in fatigue life with steels has been reported [40,63]. Fretting fatigue life decreased mostly with self-mated material [64]. Failure analysis of steel components (including 4340 alloy steel) revealed multiple crack nucleation sites, reddish brown powder, surface roughening and crack nucleation in the fretting region [65].

Friction coefficients over unity has been reported (either self-mated or different steels in contact) [17,66]. For the same steel used here, a steady-state friction coefficient around 0.8 has been measured [27] and adhesion and material transfer has been observed.

1.3.3.5 Fretting palliatives

Many surface treatment methods have been applied in fretting as palliatives [64]. Two popular surface treatments to increase fretting fatigue life are nitriding and shot peening, which are also used to increase plain fatigue life. Both methods create high compressive stresses on the surface and some depth below, thus modifying the stress state in a more favourable direction in terms of fretting [63,67,68] and plain fatigue [69,70]. Both shot peening and nitriding can markedly increase fretting fatigue life. For example, the fatigue life of nitrided fretting specimens increased to the level of nitrided plain fatigue specimens [63]. Using both shot peening and plasma nitrided steel increased the fatigue limit by 500 % compared to the untreated specimen [68].

1.3.4 Contact mechanics and modelling of fretting fatigue

Contact mechanism is the study of solid parts in contact. The origin of the contact mechanics dates back to Hertz's studies in the 19th century [55]. In recent decades, much progress has been made in the field of contact mechanics, partly due to the improvement in numerical methods and increased computational capacity.

Fretting contacts can be divided into several categories. Most widely used geometries in fretting studies are incomplete (i.e., Hertzian contacts), complete and almost complete contacts. Almost complete contacts have a flat part and rounded contact edge. Practical connections resemble complete and almost complete contacts are shaft-hub connections, for example. These kind of contacts have been studied in [12]. Infinite (singular) stresses are observed theoretically at the contact edges in complete contacts. In practice, infinite stresses are relieved by material plasticity or rounding of the contact edge, because truly sharp contact edges exist only in theory. Sharp edges may be also worn due to wear. It is a common practice for a designer to remove sharp edges of a complete contact by rounding (or chamfering). In receding contact, the application of a normal force lifts the edges of a nominally flat-on-flat contact [71]. A practical application would be a bolted joint.

Analytical solutions to solve contact tractions, displacements and stresses in Hertzian contacts exist [55] but analytical solutions in complete and almost complete contacts have been limited, though much improvement has been gained recently. Analytical solutions for rounded edge have been developed mainly since the 1990s [72]. Similarities between notch and contact mechanics [73] and between fracture mechanics and contact mechanics [74] have been addressed. Hills and co-authors have developed the asymptotic approach in analyzing contacts [75]. In the method, the contact is represented by generalized stress intensity factors. The stress state at the contact edge has been solved by the method for the test configuration used here [76].

The COF has a significant effect on the frictional force (the higher the COF, the higher the frictional force) and crack nucleation (the higher the COF, the shorter the crack nucleation

lifetime) [77]. Thus, the use of an accurate value for the COF in fretting analysis is important. Besides the development of analytical solutions, numerical methods are needed if specific contact geometry, for example, is analyzed. With increasing computer performance and the development of models (including numerical packages), the utilization of numerical contact modelling has grown rapidly. Nowadays the Finite Element Method (FEM) [78] is more or less a standard tool for modelling complex geometries and it is widely used in contact modelling, though the boundary element method is also used in fretting [79].

1.3.4.1 Finite element modelling

Contact is a nonlinear problem because the contact can switch from open to closed and also the contact state can change between sliding or sticking (globally or locally) [80]. Material nonlinear behavior and geometric nonlinearity due to large strains are sources of nonlinearity as well. The finite element method can solve the non-linear contact problem with a wide variety of boundary and loading conditions (including non-proportional loading) together with complex geometries and different material models and calculate displacements (including contact slip), tractions, stresses and strains. Local contact parameters can be achieved which are difficult or impossible to measure experimentally, such as contact tractions and stresses as well as slip and the size of slip regimes.

FEM has been used in numerous fretting studies e.g., [54,81–85]. When using the FEM in fretting, unfortunately, very fine meshes must be used at the contact and the points of stress concentration in order to capture the steep stress gradients, thus possibly requiring powerful computation capability. Sub-modelling technique is effective in these cases [86]. Linear (first order) elements are inherently used in fretting contact analysis due to the possible problems with calculation accuracy in terms of contact forces in mid-side nodes. The use of full integrated elements have been proposed to accurately calculate longitudinal stresses under bulk stresses [87]. The contact size effect has been successfully predicted using different mesh densities [88]. Load incrementation can affect slip distribution [89].

Normal and tangential (when friction is taken into account) forces are transferred between the contacting surfaces. In normal direction, the contacting bodies may not interpenetrate. Various algorithms are used to describe the normal direction. In Abaqus, one of the commercial FE-packages, three contact algorithms exist (in implicit side), namely contact pairs, general contact and contact elements [90]. In the contact pairs method, a user can choose the master and slave surfaces, between which the contact is formed. The contact surfaces can be node-based or element-based. Surface-to-surface, which is typically used in fretting studies, is more accurate compared to node-to-surface [90]. Penalty, Lagrange multiplier and Augmented Lagrange methods are used in Abaqus to describe the normal direction. The Lagrange multiplier method is the most accurate, but the penalty method may give equally accurate results (or very nearly) with shorter computation time, if some

interpenetration is allowed. Augmented Lagrange method combines both these methods. [90,91]

Tangential contact behavior in Abaqus can be basically described by using the Lagrange multiplier method or the penalty method. In the penalty method, the surfaces are allowed to have certain slip when the surfaces should be sticking. This may affect the accuracy of the results, and it is important to choose the parameters correctly [82,92]. The Lagrange multiplier method allows slip only when shear traction exceeds the critical shear traction. However, the penalty method can greatly improve convergence and lead to shorter calculation time [90] because additional degrees of freedom are inserted in the Lagrange multiplier method. Two sliding formulations exist in Abaqus, finite sliding and small sliding. Small sliding is used when slip between surfaces is small in terms of element size. If slip is large, surface separation occurs, or curved surfaces are interacting, finite sliding is used because the formulation allows continuous tracking of local contact status. [90]

1.3.4.2 Fretting fatigue life prediction

The ultimate goal in fretting studies is the ability to predict the lifetime of a practical engineering contact. A number of fatigue methodologies have been analyzed and compared to experimental data [93] and successfully applied to predict cracking [94] and cracking location [93]. Multiaxial fatigue models have been used widely in fretting fatigue, for example the Findley criterion [40,95]. Fretting fatigue parameters have been also developed to take into account the interfacial slip [96,97]. As the crack propagating regime is typically long in fretting fatigue, fracture mechanics is an effective method to study fretting crack propagation and it is widely used, e.g., [98,99]. Nowadays, there is an interest to ‘match’ the state of stress between contacts and plain fatigue notches such that the results of more inexpensive experiments in notched specimens can be used for fretting contact analysis [29].

The fatigue criteria may be over conservative due to the steep stress gradients. It has been shown that some form of averaging method should be used to overcome stress gradient effects relating to fretting [58,100,101]. The size of this structural volume used to average stresses has been linked to the size of a material’s microstructure [100,102]. The theory of critical distances (TCD) [103] has been used to analyze fretting fatigue, e.g. [104]. TCD can be used to overcome these stress gradient effects and is also able to predict the size effect [104].

Fretting wear has been shown to have a major effect on stress state and fatigue life [57]. Fatigue models do not usually take into account the effect of wear but critical plane methods have been successfully used to predict fatigue cracking in cases where wear is significant when wear was taken into account in the model [57]. At least local plasticity may occur in fretting, but in many fretting studies elastic material properties are assumed, though plastic analysis has been suggested [83]. The material hardening behavior can be divided into two

basic cases that either deal with expansion or translation of yield surface. In isotropic hardening, the size of the yield surface increases uniformly in all directions, whereas in kinematic hardening the yield surface translates in stress space [105]. Isotropic hardening is widely used in fretting studies when material plasticity is taken into account [83,106,107].

1.3.5 Press fits and bolted joints

Press fits and bolted joints are typical practical connections that are vulnerable to fretting [39,40,108]. Press (and shrink) fits are frictional joints that are formed between cylindrical shaped shafts and hubs to transfer tangential or axial loads. Press fit is created by mechanically forcing and heating/cooling is employed in shrink fit. According to the Finnish standard for the calculation and design of interference fits SFS 5595 [109], the transfer of torque/axial force is proportional to contact pressure and “adhesive factor” that resembles COF and depends on material and lubrication. Practical connections may involve some lubricant, for example, due to the assembly process, which decreases the COF. However, small sliding speeds in fretting (due to the small amplitude) is not expected to allow hydrodynamic lubrication. The standard [109] instructs the use of as high a contact pressure as possible so that slipping is prevented (though there is a limit in loading in the sense of plasticity). Even though the higher contact pressure may eliminate or decrease slip, it leads to higher stresses in the contact. For interference fits, Lame’s equations are used to calculate stresses and dimensioning fits. Having limitations, in terms of geometry, more realistic study of these contacts requires the use of other methods such as the finite element method.

Mechanical parts in assemblies are often clamped together by bolted connections. The parts are clamped by the preload and the parts are not typically allowed to slip against each other. The tension or shear loading is carried by the friction between the parts and/or some form of mechanical locking such as dowel pins. However, slipping may occur between the parts. The fatigue life of bolted connections can be significantly reduced due to fretting [48]. [110]

1.4 The digital image correlation method

In the field of mechanical engineering, an optical method called the Digital Image Correlation (DIC) is a well-known technique to determine the displacements of a loaded structure. The basic principle is that images of an object are acquired (using a digital camera) during loading. Each image, divided into smaller areas (subsets), is compared with a specific software to a reference image, such as the first image, and the displacements for each subset between the two images are then calculated. As an outcome, full-field displacement data is achieved. The method is non-destructive, but the object surface has to be meet certain standards and so, special treatment of the surface is usually needed. [111]

The method has been mainly investigated since the 1980s [111] but has recently become more widespread due to the development of computation capabilities and developments in imaging equipment. DIC has been successfully applied in many fields, ranging from civil engineering and electronic packaging to biomedical applications [111]. DIC has previously been successfully applied to fretting contacts to measure relative displacements, e.g. [59,112,113]. It has been stated that micrometer-scale pixel size must be used to achieve a sufficient spatial resolution in displacements.

1.5 Background and motivation of the study

Fundamentally, fatigue failures still occur in machines despite intensive research and improvements in technology during the past decades. Fretting fatigue is a particularly detrimental mechanism inducing cracks. Fretting has been studied for over a century, but it is still an area that requires further research. Today's trends towards higher power density, longer life and higher energy-efficiency of machines give rise to an even more challenging operational environment for components. Loadings in components increase and this increases the potential risk of fretting in contacting surfaces inside machines. For example, in a medium speed combustion engine, there are several high-strength components under severe loading. Many of the contacts in machines are large and nominally flat-on-flat contacts. Quenched and tempered steels are often the materials used in these components due to their high plain fatigue strength, but fretting data for such materials is somewhat lacking in the literature.

In the modern machine design process, the problem areas should be identified at the design stage and well before the production process. A major challenge is that traditional fatigue design does not necessarily take into account the effect of fretting and there is also no universally accepted model for fretting. At the design stage designers can specify the materials, geometries and loadings (stresses), including bolt preloads, but they also need to ascertain the parameters affecting fretting, fatigue limits, and so on. Although the operating parameters at the component level may be fairly well known, a designer can also influence the local responses (e.g. stresses) that may eliminate or decrease the risk of fretting. The strength of the chosen material could be increased by applying different surface treatments, for example, but again, the designer should be aware of those benefits for the selected materials. To gain a knowledge of these, laboratory testing is essential.

Laboratory measurements are a useful way to achieve fretting data somewhat cost-effectively within a controlled environment. However, laboratory testing also poses certain challenges. One of the most important fretting variables is the micrometer-level relative movement, i.e., slip, between contacting parts, but its measurement can be problematic. Typically, displacements at a certain point are measured (relatively far from the contact

interface) and these also include the compliances of the test device (which can be numerically removed). In addition, slip distribution is typically uneven. To the best of author's knowledge, experimentally measured cyclic relative displacement fields close to the contact interface within reasonable resolution have not previously been reported in the fretting literature.

A part of this work relates to two industrial oriented research projects, in which the objectives have been to model and evaluate friction, fretting fatigue and fretting wear and also to seek preventive solutions for fretting damage and ultimately, to develop a model that can predict fatigue life.

1.6 Objectives and scope of the thesis

The main objectives of the thesis are to study the influence of various design parameters on fretting fatigue behavior in practical fretting contacts made of quenched and tempered steel and to produce useful fretting fatigue data and also to investigate and measure the cyclic relative displacement field during fretting testing.

The research questions of this thesis are the following:

1. What is the effect of essential design parameters on fretting fatigue behavior in complete and bolted connections and how do surface treatments affect the fatigue behavior with quenched and tempered steels?

2. How can the Digital Image Correlation method be exploited in frictional joints and, importantly, used to measure the relative displacement field, and can the method also be used to validate numerical contact models?

The essential design parameters here are the preload (normal load) in contact, friction coefficient, contact geometry, cyclic bulk loading and relative movement between contacting surfaces (slip). The thesis focuses on complete, i.e., 'sharp' ended, and almost complete contacts that can be practically found in press fits, as well as receding contacts (bolted joints in practice). To achieve the research objectives, both experimental and modelling work is carried out. The material used is quenched and tempered steel EN 10083-1-34CrNiMo6+QT, which is used in both the contacting parts (i.e., as self-mated). A complete contact fretting test device was developed for use in the experiments. The device was used to carry out complete contact, bolted joint and plain fatigue tests. The Digital Image Correlation method was applied in both the complete and bolted connections to measure displacement fields close to the contact interface. The Finite Element Method (using Abaqus programme [90]) was used to analyze the smooth contacts in greater detail. The continuum-level models did not consider micromechanics and wear. In fretting fatigue

cracking prediction, the Findley fatigue criterion was used due to previous experience with this [114]. Only dry contacts were considered in this study and temperature effects were neglected. The main focus of this thesis is on fretting fatigue and fretting wear is only briefly discussed. The operating and design parameters were chosen to fit in with practical values.

1.7 Outline and contribution

The introductory chapter contains a literature review of the research topic as well as the background, objectives, scope, scientific contribution and summary of the appended articles of the thesis. The second and third chapters present the materials and methods involved in the experimental work and modelling. The experimental device that was developed and the numerical models used are both presented and explained. The results are presented and discussed in the fourth chapter. A large number of fatigue test results are presented for different parameters. Measurements of the relative displacement fields are presented along with the modelling results. Recommendations for further research are suggested. The final chapter presents the conclusions of the study.

The scientific contributions of the thesis are as follows:

a) Development of a complete contact fretting test device with transverse loading and large nominal contact area resembling practical connections.

b) A novel approach of the method for the measurement of cyclic relative displacement (slip) field close to the contact interface using the Digital Image Correlation method.

c) Successful comparison between the Digital Image Correlation and the Finite Element methods.

d) Enhancement of the knowledge of fretting fatigue performance in complete and bolted contacts made of quenched and tempered steel by means of experiments and modelling in terms of various parameters and surface treatments.

1.8 Summary of appended articles

The thesis is a composite of seven articles dealing with fretting fatigue in complete and bolted contacts. The material in all tests was quenched and tempered steel EN 10083-1-34CrNiMo6+QT.

Publication I: Development of a complete contact fretting test device

The publication describes the complete contact fretting device that was developed. One fretting fatigue test series (*S-N* series) with nominal contact pressure of 100 MPa was carried out and also a plain fatigue test series. Fretting decreased fatigue life significantly.

Publication II: Response to discussion with DA Hills et al., concerning the article "Development of a complete contact fretting test device" by J Juoksukangas et al.

Publication I raised interest in the fretting community and this article is the response to a discussion [60]. This exchange of letters deals with the generalization of the results achieved in Publication I.

Publication III: The effect of contact edge geometry on fretting fatigue behavior in complete contacts

A fretting fatigue test series was carried out for slightly rounded (almost) complete contact and compared to the 'sharp ended' (Publication I) complete contact results by both experimental and modelling means with nominal contact pressure of 100 MPa. Relatively similar fatigue lives were achieved. The Findley criterion was used to calculate cracking risks that were successfully compared with the experiments. Some of the results were first presented at the Nordtrib 2012 conference at Trondheim, Norway.

Publication IV: Applying the digital image correlation method to fretting contact for slip measurement

The article describes the application of the Digital Image Correlation method to the complete contact test device. Fretting fatigue tests were made with nominal contact pressures of 100 MPa and 30 MPa and cyclic relative displacement fields close to the contact interface were measured and analyzed. Some of the results were first presented at the Nordtrib 2014 conference at Aarhus, Denmark.

Publication V: A comparison of relative displacement fields between numerical predictions and experimental results in fretting contact

Operating parameters and conditions in Publication IV were modelled using FEM and the results were compared to the experiments in terms of relative displacement fields. Coefficient of friction was evaluated by combining FEM and DIC. Measured cyclic relative displacement fields were repeated with FEM.

Publication VI: Experimental and numerical investigation of fretting fatigue behavior in bolted joints

A bolted joint was studied experimentally and numerically. The complete contact test device was used with minor modifications. Several experimental series were carried out with various operating (bulk stress, bolt preload) and design parameters. Fretting significantly decreased the fatigue life and there was also clear evidence of fretting wear. DIC was applied and FEM was used to analyze the contact in greater detail.

Publication VII: Influence of a surface treatment on fretting fatigue life in complete contacts

Experimental plain and fretting fatigue tests were carried out with the nitrided and shot peened specimens with a nominal contact pressure of 100 MPa. Both methods increased fatigue life considerably.

2 Experiments

2.1 Complete contact fretting test device

A test device was developed (Publication I) to allow testing of complete contacts having an edge singularity (‘sharp’ edged flat-on-flat contact), which is often characteristic of machine components. In contrast to the typically used fretting test machines having axial bulk loading, the loading is created transversally to the specimen’s longitudinal direction, which is often the case in practice such as in power transmission components. In addition, the nominal contact area is at least a decade larger than in typical laboratory fretting test device contacts. These three features together make the experiments a close approximation of actual contact conditions in machines. In addition to its function as a fretting test device, the device can also serve as a ‘2D presentation’ of a press fit (shaft-hub connection, for example). The test device allows testing of different materials (including surface treatments), contact geometries (rounded contact edge, bolted connections), operating parameters (cyclic bulk loading, nominal contact pressure) and testing of fretting fatigue life and fretting wear. In addition, plain bending fatigue tests can be conducted with the same device for comparison. The purpose of the fatigue experiments here was to determine the nominal stress fatigue limit and also the finite lifetime in various conditions. Figure 2 shows a schematic view of the device.

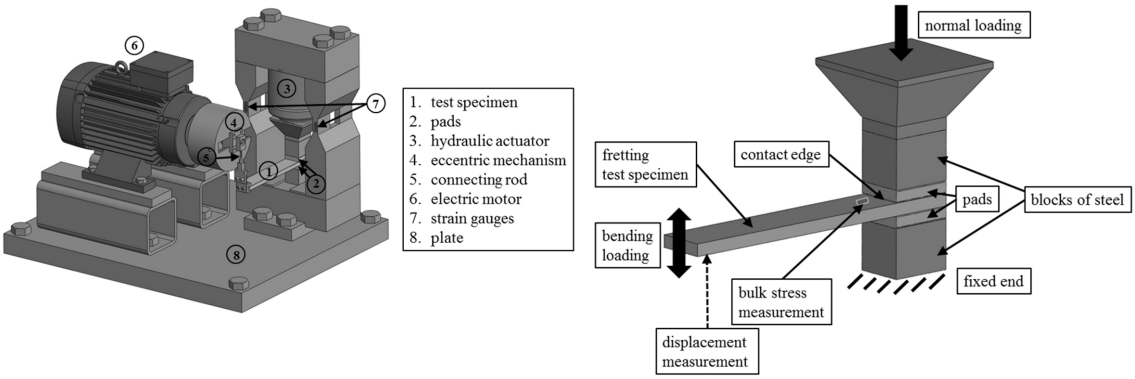

Figure 2. The developed complete contact fretting test device (Publication I).

The two fretting test contacts are formed by the flat fretting specimen and two flat-ended fretting pads that are clamped together. A nominal contact pressure of up to 300 MPa can be created and it can also be adjusted continuously due to hydraulic loading. The cyclic bulk (bending) stresses in the specimen and the contact loading are created by transversally displacing the tip of the free end of the specimen. This is achieved by an eccentric mechanism that allows stepless adjustment of the nominal stress amplitude and mean stress of the specimen and having maximum frequency of 50 Hz. This frequency is assumed to be low enough not to have any frequency effect on fatigue results with steels. In the experiments, the loading frequency was mostly 41 Hz though 20 Hz, and 0.5 - 1 Hz was also used. The cut-off limit was three million cycles in an individual test, after which the specimen was treated as runout if no complete fracture occurred. This corresponds to about 20 hours of testing.

2.2 Test specimens, sample preparation and test conditions

The specimens and pads were made of quenched and tempered steel EN 10083-1-34CrNiMo6+QT. Two batches of material were used, one batch in tests reported in Publications I, III, VII and another batch in Publications IV–VI. In modelling, the elastic modulus was 206 GPa and Poisson's ratio 0.28. If plasticity was taken into account, the ultimate strength was 1030 MPa, yield strength 930 MPa and the relation between true stress and true plastic strain used was:

$$\sigma = 1160\varepsilon^{0.62} + 890 \tag{4}$$

The surface finish of the specimens was kept at a similar level in all tests. After machining, the specimens were ground longitudinally and 3D surface roughness values (*Sa)* of about 0.2 - 0.3 µm were achieved, measured with a Wyko NT1100 optical profilometer. In Publication VII, the specimens were either nitrided or shot peened. The specimen and pads

were cleaned with solvent before testing. The tests were carried out at normal laboratory room temperature and humidity. No lubrication was used in the fretting contacts.

2.2.1 Complete contact and plain fatigue

The complete contact fretting test specimen and pads are shown in Figure 3 (separated for clarity).

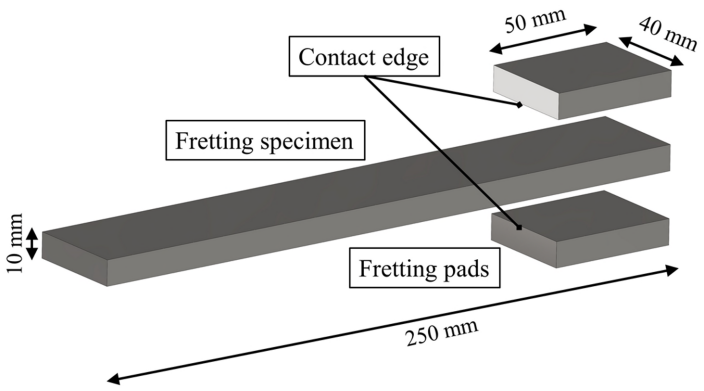

Figure 3. Fretting test specimen and pads.

The fretting specimen has the following dimensions: a length of 250 mm, a width of 40 mm and a thickness of 10 mm. The pads have a length of 50 mm, a width of 40 mm, a thickness of 10 mm, thus creating a nominal contact area of 2000 mm^2. The plain fatigue test specimen is shown in Figure 4. The specimen is narrowed to shift the point of maximum nominal stress away from the contact so that the contact does not contribute to the stresses there.

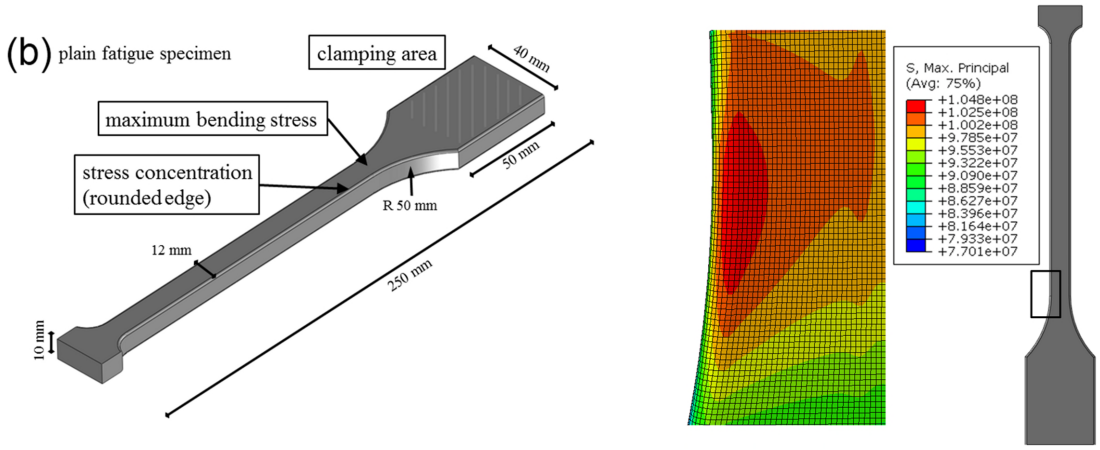

Figure 4. Plain fatigue specimen (Publication I) and stresses in the specimen edge.

A three dimensional (3D) FE-analysis (Figure 4) revealed a stress concentration factor K_t of 1.05 for the specimen in bending.

2.2.2 Bolted joint

The developed complete contact fretting test device was used with minor modifications to study bolted joints. Basically, two fretting test specimens (one on the top of the other) with the bolt holes form the bolted joint specimens. The test setup is shown in Figure 5.

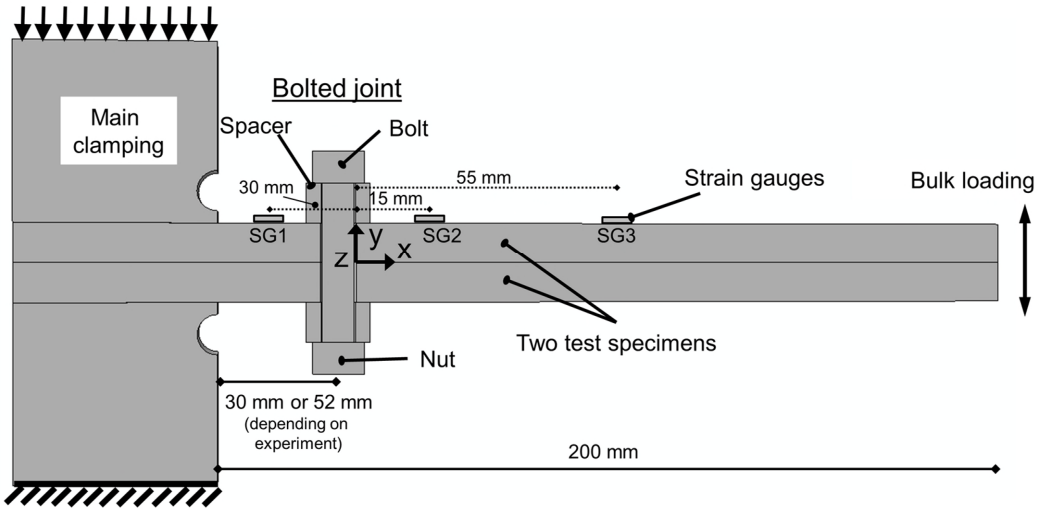

Figure 5. Bolted joint setup (Publication VI).

Preload of a single bolt located in the centreline of the specimen (in *z*-direction) creates the contact normal load of the assembly. The specimens are pressed together at the main clamping and the transverse loading is applied at the free end, which creates the slip between the specimens. Tip clamping obviously induces fretting at the free end but it was assumed that it would have no major effect on the actual test contact. In some tests, the diameter of the spacers under the bolt and nut was adjusted as was the position of the joint in relation to the specimen. In machine design, at least some part of shear load may be carried by dowel pins or the bolt shank under pure shear. Therefore, in this respect, the joint functions as though it was under extreme operating conditions.

2.3 Measurement system

The cyclic bulk stress of the specimen, the normal load (nominal contact pressure) and the bolt preload in the bolted joint tests are measured during testing. In the complete contact case, the maximum bulk stress reported here is the stress at the contact edge (i.e., the point of maximum (nominal) bending stress), which has been linearly scaled from the measurements some distance away from the edge (Publication I). In the plain fatigue tests, the strain gauge is at the point of maximum bending stress. In the bolted joint case, the nominal stresses are reported at the center of the bolt hole and are scaled from the measurements. The number of loading cycles for macroscopic crack nucleation point can

be evaluated in both cases from strain gauge data (Figure 5, Publication I). However, this was not calibrated accurately so that it is used only as a relative value between the tests. It is expected that a crack should already be relatively large when it is observed by this measurement. Here, the loading cycles to complete fracture was the main focus of interest. Displacement of the free tip of the specimen is measured by a laser sensor close to the free end (about 18 mm away). Figure 6 presents the measured tip displacement showing movement that is almost sinusoidal.

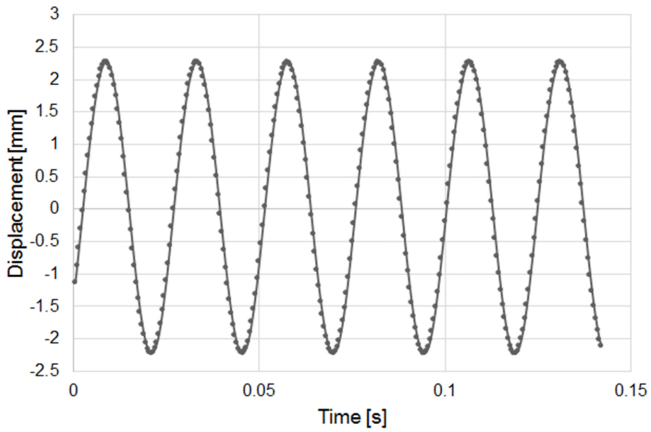

Figure 6. Measured tip displacement as a function of time.

Occasionally, a pressure-sensitive film was used to verify evenness of (nominal) contact pressure distribution. After the fretting tests, the fretting marks were visually inspected for possible misalignment. Evenness of contact pressure can also be evaluated from the strain gauge measurements positioned at each corner of the supporting frame (point 7 in Figure 2).

2.4 Applying the Digital Image Correlation method

The Digital Image Correlation (DIC) method was used to measure displacements in both complete contact and bolted joint cases. A camera equipped with a long-distance microscope [115] was used to capture the images. Davis DIC software [116] was used to calculate the displacements. The DIC measurement setup is shown schematically in Figure 7.

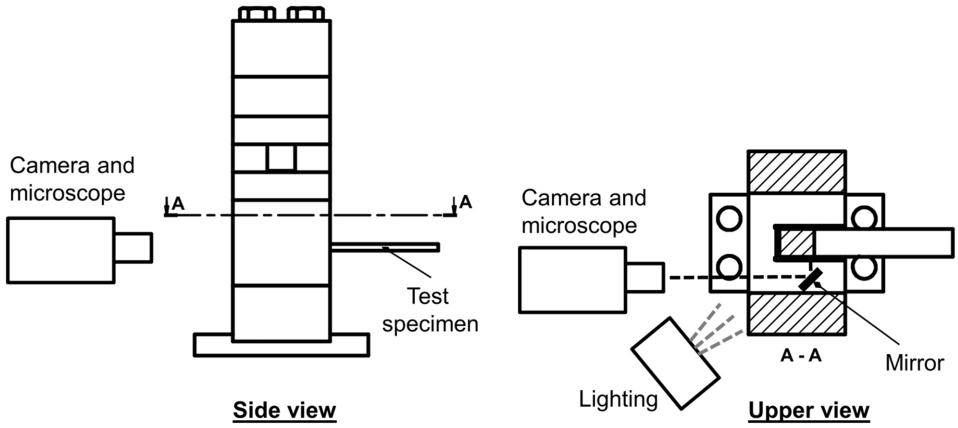

Figure 7. Schematic presentation of the employed DIC setup (Publication IV).

The camera was positioned behind the device and the side face of the specimen and pad were measured using an optical mirror. The pixel size at the target surface varied from about 1.83 μm to about 5 μm. The Least Squares Matching (LSM) approach in Davis software was used to calculate the displacements. The calculation resulted in spatial resolutions from 36.6 μm to 80 μm.

Measurement uncertainties and DIC verification were studied in several ways. A comparison was made between the displacements measured by DIC and those by an external LVDT sensor at some distance away from the contact where it was possible to install the LVDT sensor. DIC results were found to be in very close agreement with the LVDT results. Different kinds of speckle patterns were studied in the fretting environment. Although the setup was slightly different to the one used in the actual tests, plain and painted (air brush) gave rather similar results. In the bolted joint tests, where the pixel size was highest, the airbrush technique was used. In the complete contact tests with higher magnification (smaller pixel size), the plain ground surface was used because the size of the droplets created in air brushing would have been too big for creating a proper speckle pattern [111]. Artificial movement of an image was made in Matlab and the motion was calculated by the software resulting in a small difference. Uncertainties due to lighting and camera noise were also studied. It would be useful to directly compare the displacements during fretting loading with those of another displacement measurement device, and this warrants further study.

3 Modelling

Both the complete contact and bolted joint contact setup was modelled using ABAQUS FE-programme 6.10 - 6.13 [90] to study contact quantities in greater detail and also to predict fretting fatigue cracking. Smooth contact surfaces were assumed and wear was not taken into account. Implicit finite element modelling was used here, i.e., after each load increment equilibrium of internal structure forces is enforced with external loads.

3.1 Complete contact model

The FE-model includes the parts shown in Figure 8. The contact is relatively wide, so a two-dimensional plane strain model was created. In addition, the crack nucleation point was in the middle zone of the contact edge in the experiments. In DIC measurements, however, the side surface was measured and the plane strain model is an approximation. 3D FEM analysis of the complete contact warrants further study. As the specimen is experiencing bending, incompatible mode elements were used [90]. Linear elements are more reliable in frictional contact [90], thus, CPE4I elements were used. The mesh size at the contact edge ranged between 15 µm and about 40 µm.

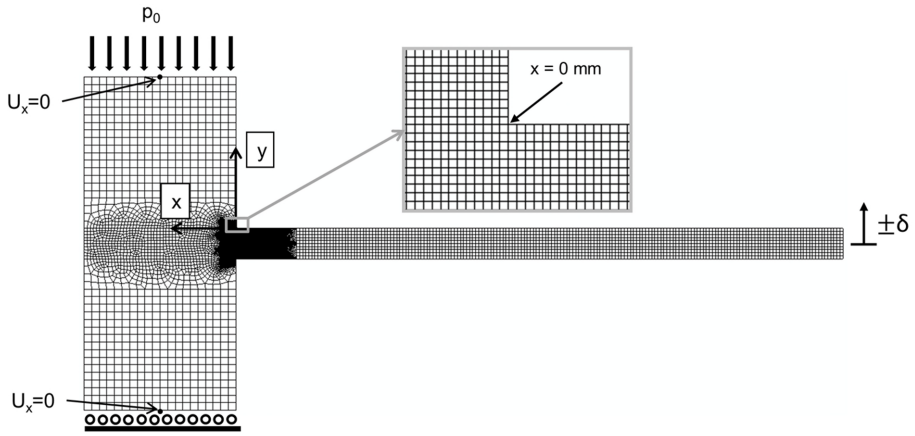

Figure 8. The FE-model used in Publication III (adapted, with the origin changed).

Contact pressure in the test contact is created by applying a normal load (or pressure load) on the upper block. The bottom end of the lower block is fixed in the *y*-direction and *x*-displacements are restricted at the nodes at the lower and upper block. In Publication V, a spring was used at the upper side of the block to take into account rotation due to the transverse loading. Transverse loading of the specimen is created by displacing the tip of the free end of the specimen, as in the experiments.

The contact tangential behavior was described using either Lagrange multiplier or the penalty method with an elastic slip value of 0.005 μm. The elastic slip value used is small enough not to have a major effect on the results. Normal direction was described either using the Lagrange multiplier or the Augmented Lagrange method with default stiffness. The Coulomb friction model was adopted and constant COF was assumed along the contact surface. At least three load cycles were run to reach steady-state contact conditions. Both automatic and manual incrementation was used to divide the loads.

An isotropic material hardening model was used in Publication III as it is expected in the complete contact case and experiments also indicate plasticity. Flicek et al. analysed the contact edge in terms of plasticity and concluded that in the tests presented in Publication I, the plasticity at the edge is within small scale yielding [117]. Findley fatigue criterion was used to predict fretting fatigue cracking on the basis of previous experience [114]. Findley criterion was applied as a cracking risk, where the Findley cracking risk value over 1 suggests that failure will occur with a certain probability. TCD was applied by directly calculating Findley values at some distance below the contact interface that is of a similar scale of material microstructure and material defect size [10].

3.2 Bolted joint model

The three dimensional model of the bolted contact was assembled. The displacements of the side surfaces of the specimens measured by DIC were compared to corresponding displacements of the 3D model. However, slip and other contact quantities in the fretting area was extracted using the FEM. In the model, the lower end of the bottom block was fixed. A spring at the top end of the upper block takes into account the rotation of the test device which is caused by the transverse loading. The transverse load was applied at the specimens' free tips. The bolt, nut and spacers were attached, i.e., tied together. The mesh of the bolted joint setup is shown in Figure 9. Due to symmetry, only one half of the test device was modelled.

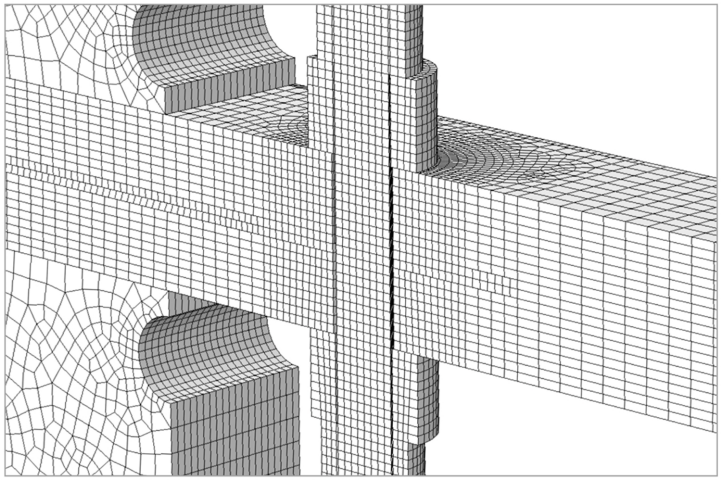

Figure 9. The mesh of the bolted joint model (Publication VI).

The element size was 1 mm in the contact area and the element type used was C3D8I. The master-slave contact algorithm was applied with surface-to-surface contact discretization and finite sliding contact condition. Penalty friction with elastic slip value of 0.05 μm was used together with the Coulomb friction model. The Augmented Lagrange method was used in normal direction. Three loading cycles were performed and each cycle was divided into 50 increments.

4 Results and discussion

4.1 Overall contact characteristics

The complete contact and bolted joint contact studied are very different from each other in terms of contact geometry and loading. In the specimen free part, the stress is nominally similar, i.e., the maximum nominal bending moment acts at the contact edge (main clamping side), having also the point of maximum (nominal) bending stress, and the stress linearly decreases towards the free end. Of course, the tip clamping that transfers the transverse loading and the bolted joint slightly modify this nominal stress behavior. The contact pressure distributions during one loading cycle in both cases are shown in Figure 10.

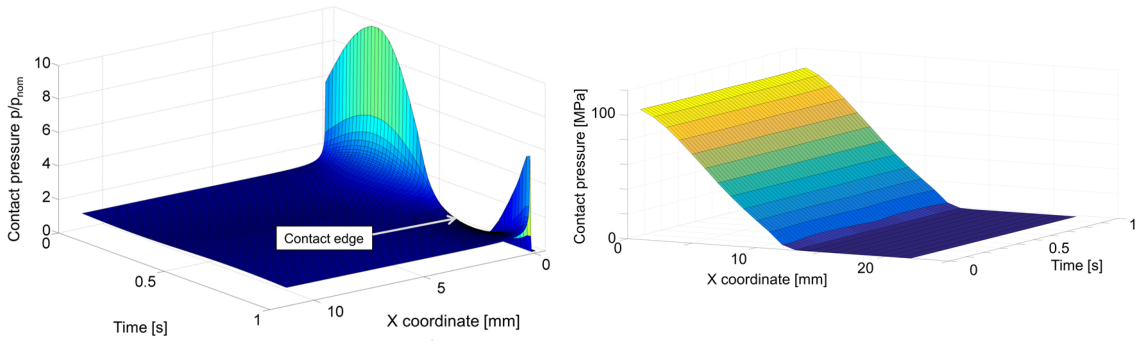

Figure 10. Contact pressure distributions during one loading cycle, complete contact (on the left, Publication V, adapted with the origin changed) and bolted joint (on the right).

In the complete contact case having asymptotic stress, a steep contact pressure gradient occurs at the contact edge when the specimen's edge is in contact with the fretting pad. The high contact pressure occurs only over a small area. During loading, the contact may open (depending on the loading parameters), i.e., the edge 'lifts off', which is illustrated in Figure 10 (on the left) at the time moment around 0.75 s. Contact opening also means that the contact is incomplete at the moment. The opening always leads to slip [29], though this slip can be small. In all the experimental tests carried out here, contact opening occurred

(numerical result). Depending on loading parameters, the complete contact under examination here can

- be completely adhered, i.e., sticking; no relative movement at any point,
- have edge slipping,
- have a contact opening at the edge and therefore, slip or
- be fully sliding, i.e., the whole contact is slipping (gross sliding).

The first three cases are relevant here. The contact tractions and stresses, slip, nominal contact area (due to the contact opening) depend on loading parameters (bulk loading and normal load) and COF. At the point of cracking, the contact pressure is cyclic in the complete contact case and has a much higher maximum value (at the contact edge) compared to the bolted joint case. In the bolted joint case, the uneven contact pressure distribution does not change substantially during loading and there is no peak in contact pressure (Figure 10). Figure 11 shows the contact pressure distributions of different tests in the bolted joint experiments. Clearly, the contact size does not change with similar geometry (because of the receding contact), and the contact pressure increases when increasing the bolt preload (normal load), as would be expected. With a larger spacer, the distribution is wider and maximum pressure lower under the same normal load.

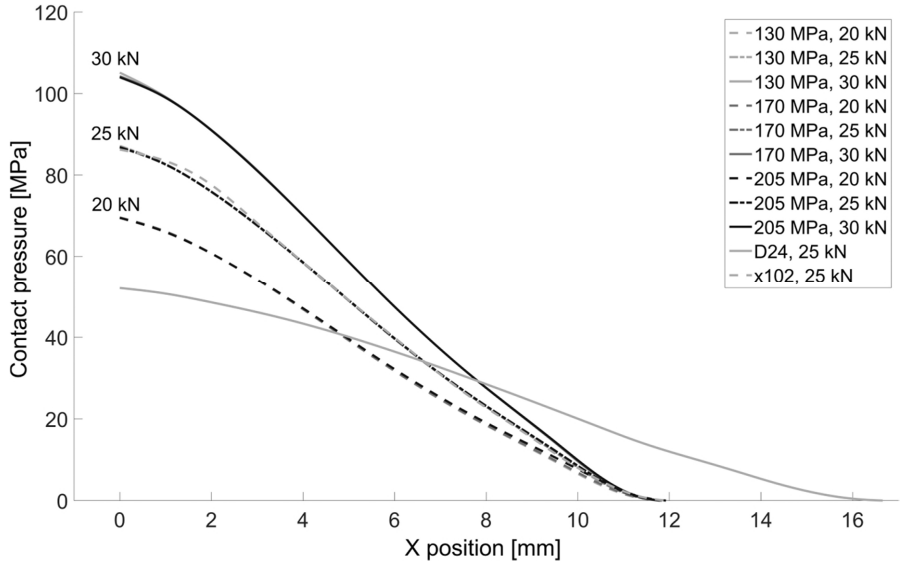

Figure 11. Contact pressure distributions of different tests in bolted joints (Publication VI).

The stress state in these cases is very different. The state of stress in complete contact is multiaxial, but in the bolted joint case here the axial (longitudinal) stress is clearly higher than other components (Publication VI), and can be approximated as somewhat uniaxial. Furthermore, there is a steep gradient in stresses in the complete contact which is not the case in the bolted contact. As shown further, slip amplitude is about a decade higher in the bolted joint case compared to slip in the untreated complete contact specimens, and the

amount of wear is also higher (in the bolted joint case). In the surface treated complete contact specimens, where the bulk loading is markedly increased compared to the untreated specimens, the amount of slip is also notably increasing.

4.2 Fatigue life

4.2.1 Complete contact

An important goal of the study was to perform experimental fatigue tests. Most of the untreated complete contact fretting fatigue (FF) and plain fatigue test results are summarized in Figure 12. The bulk (bending) stress amplitude in the specimen is shown as a function of the number of loading cycles to complete fracture. The fretting test series with a nominal contact pressure of 100 MPa, 30 MPa (both series with sharp edges) and almost complete contact (radiused contact edge, radius was 1 mm) are shown and compared to the plain fatigue results.

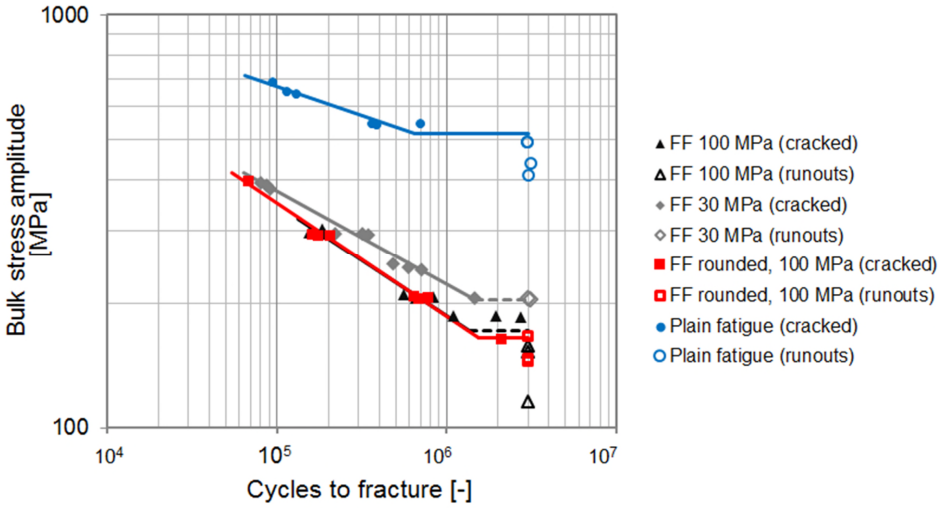

Figure 12. Sum-up of majority of the complete contact experimental fretting fatigue test results (results from Publications I, III and [118]).

A major drop in fatigue life can be clearly seen in all fretting cases. The results indicate that the lowest fatigue limit is achieved with rounded contact edge, though the difference between this and the sharp ended contact is small, if any. Fatigue life decreases as the nominal contact pressure is increased. The scatter of the results is rather small and the results indicate good repeatability and validity of the test procedure. However, to improve the statistical reliability of the results more testing would be needed, especially to determine more accurately the difference between the sharp ended and rounded edge contacts.

The effect of fretting increases significantly with a greater number of cycles. The ‘knock down’ factor is at a fretting fatigue limit level of around 2.5 - 3 but at higher stress levels it is

much lower. Extrapolation of the results reveals that fatigue life around 3000 cycles is the same for both plain and fretting fatigue. At the stress level of the plain fatigue limit, plain fatigue life is about 22 times greater than the fretting fatigue lifetime.

Figure 13 shows calculated Findley cracking risk values (Mod) with different contact pressures (using COF 0.8) and the experimental fatigue limits in the sharp ended case.

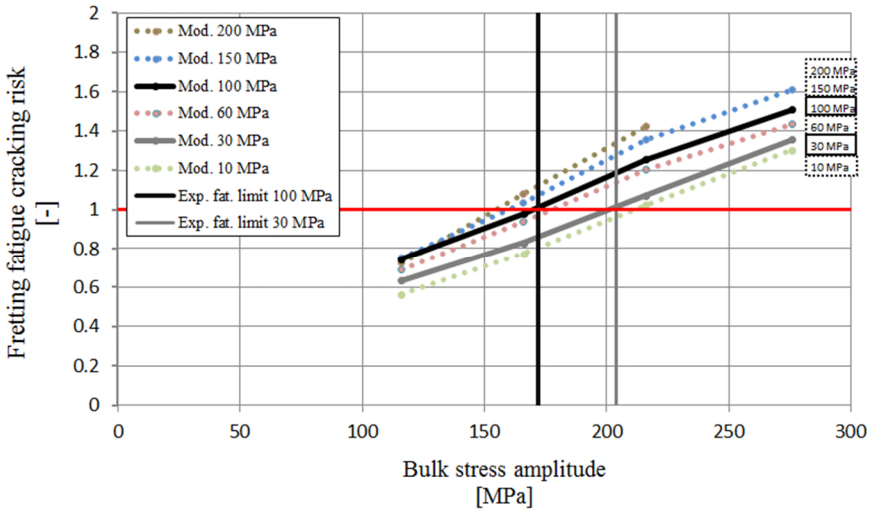

Figure 13. Cracking risks with different nominal contact pressures.

Cracking risk values increase with the increase in nominal contact pressure (normal load). This suggests that the decrease in fatigue life can be 'simple' because of increased stresses due to increased normal loading. As noted earlier, the standard for interference fits guides to use sufficiently high contact pressure to prevent slip. However, the results show that an increase in nominal contact pressure will increase the cracking risk, although the effect is more pronounced at higher stress levels (above the fatigue limit). Figure 14 shows the calculated cracking risks in sharp and rounded edge cases.

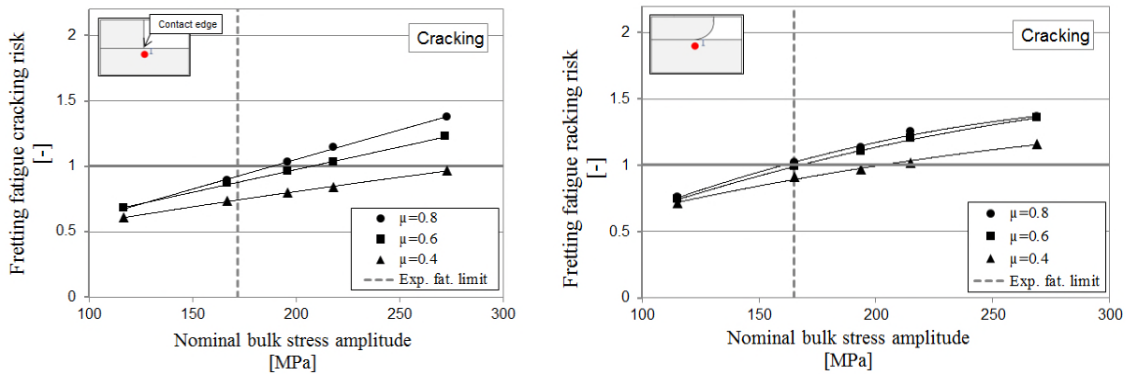

Figure 14. Cracking risks in sharp (left) and rounded (right) edge cases (Publication III).

According to the experimental (Figure 12) and numerical results, the rounded contact edge used did not increase the fatigue limit as would be expected. This is consistent with other studies having axial bulk loading [61,119,120]. In this case, the numerical results show that high peak stresses and contact tractions exist in both cases, as shown in Figure 15.

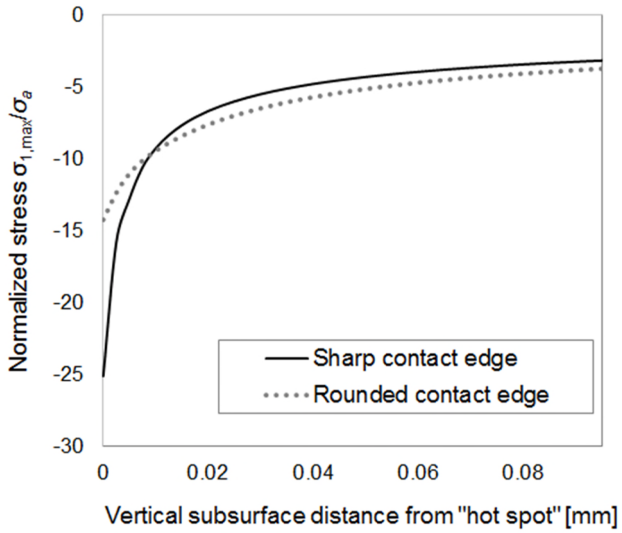

Figure 15. Maximum in plane principal stress (normalized) as a function of vertical subsurface distance.

Figure 15 shows the maximum (in plane) principal stress normalized with bulk stress amplitude as a function of distance in vertical direction (perpendicular to the contact surface) from the “hot spot”, i.e., the point of maximum stress, in both sharp and rounded ended cases. This result is calculated with a FEM model having the element size at the contact edge of 2.5 µm, elastic material model and a coefficient of friction 0.6. Although the highest stress at the surface is for the sharp ended specimen, at some distance the stress is higher for the rounded edge. The sharp ended contact has a notably steeper gradient close to the contact surface. In the modelling results, a COF around 0.6 - 0.8 is needed for the results to match the experiments, though higher a COF does not markedly affect the results, whereas a lower COF significantly reduces the cracking risk. The results agree with the literature in that some kind of averaging is needed to match the results to the experiments.

In the fretting specimens, the cracks were nucleated evenly whether on the upper or the lower side of the specimen (Publications I and III), though often the cracks had also been nucleated on the both sides. Typically, these cracks met approximately at the centre line of the specimen. In the untreated specimens, the cracks were nucleated at the contact edge (though in some tests with 30 MPa nominal contact pressure cracking occurred a small distance inside the contact). Cracking occurred mainly in the central region in the lateral direction. In the nitrided specimens (having the highest bulk loadings), however, the main crack leading to complete fracture typically nucleated a small distance inside the contact. The plain fatigue specimens cracked at the point of maximum bending stress (outside the

clamping contact). The scanning electron microscope (SEM) images in Figure 16 show cracking surfaces and a crack nucleation point at the contact edge of an untreated specimen (on the left).

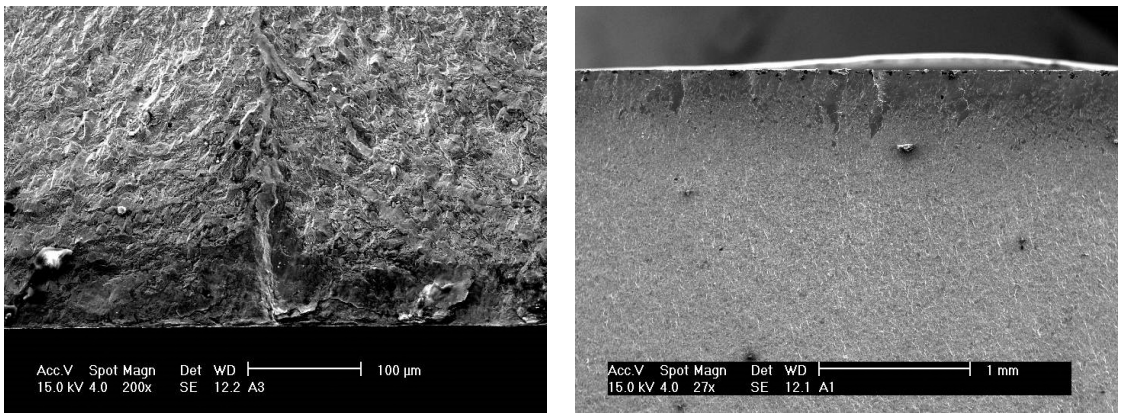

Figure 16. Cracking surfaces and a crack nucleation point at the contact surface.

Typically, multiple cracks nucleated and coalesced into larger cracks leading to complete fracture. After nucleation and some growth, the cracks propagated perpendicular to the calculated maximum principal stress. Figure 17 shows a cross section of the specimen.

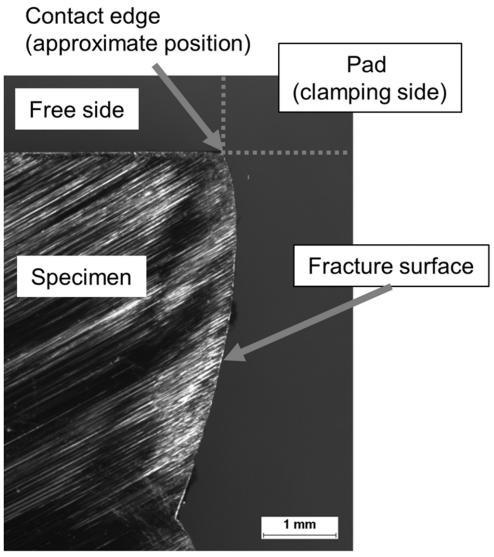

Figure 17. Cross-section of a fractured specimen.

Figure 18 shows cracking risk values along a contact path for sharp and rounded contacts. The (nominal) *x*-coordinates of the contact edges are 0 and 1 mm for the complete and rounded edge case, respectively. The calculation results agree with the experimental results with regard to the cracking point. A localized peak occurs in the predicted cracking risk in both cases. The maximum value occurs at the contact edge in both cases, as did the cracking point in the experiments.

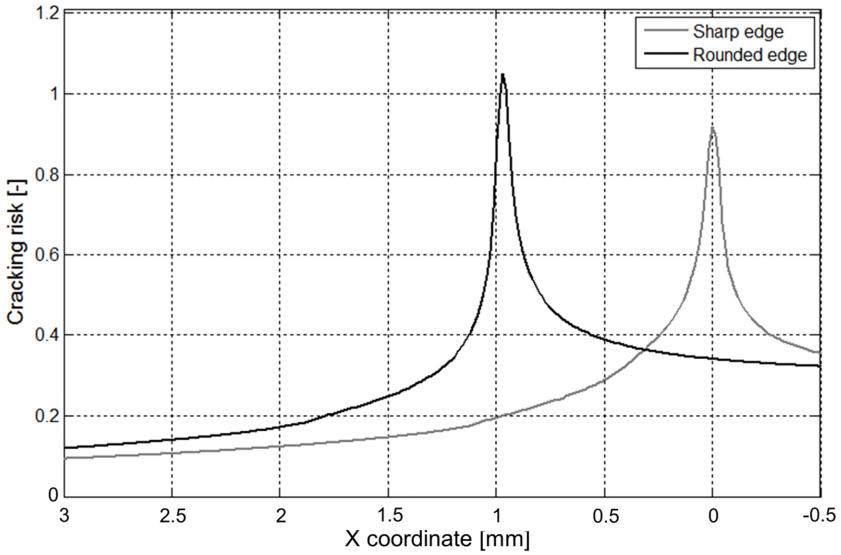

Figure 18. Cracking risk along a contact path (Publication III, adapted with origin changed).

The theory of critical distances was used with the critical distance around the material's microstructural dimensions in untreated sharp and rounded cases. The Findley values were calculated at a chosen distance 15 µm below the surface, which is a half of the critical distance as defined in [121]. Accurate determination of this critical distance was not the focus of the study; instead the main objective was to study both experimentally and numerically the relative differences between the sharp and rounded geometries and determine the failure location. The determination of the critical distance based on fracture mechanics and fatigue experiments [121] and following calculations for comparison warrant further study.

4.2.2 Effect of surface treatment

The effect of nitriding and shot peening on fretting and plain fatigue behavior was also studied (Publication VII). The experimental results are compared to the untreated test results from Publication I. The results achieved for the nitrided fretting specimens are shown in Figure 19.

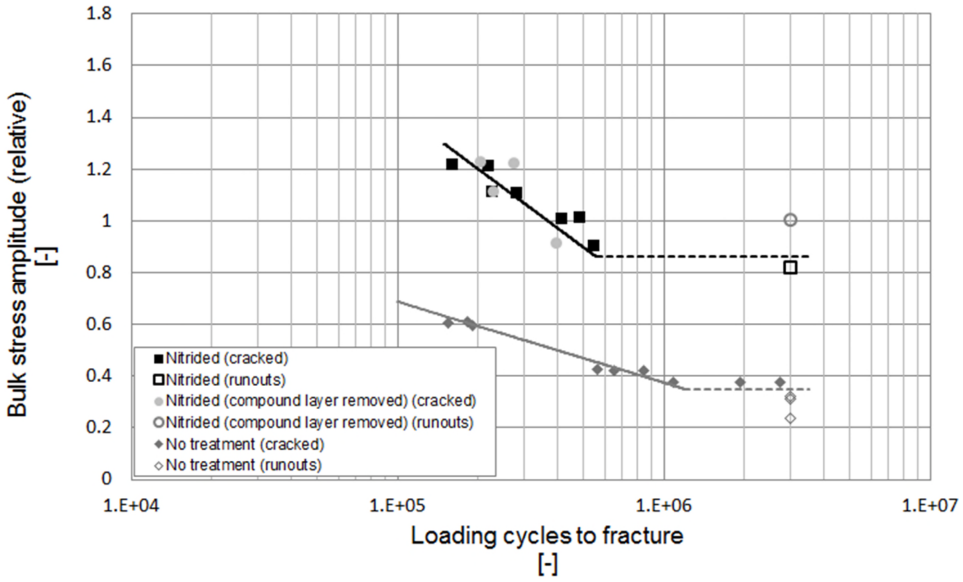

Figure 19. Test results of nitrided fretting specimens (Publication VII).

The specimen bulk stress amplitudes are scaled to the nominal plain fatigue limit. The nitriding process markedly increases fretting fatigue life. The fretting fatigue limit increased by 150 %. In addition, the plain fatigue limit was increased by about 25 %. A compound layer is created as a by-product of nitriding. The removal of the layer did not show any effect on the results. Figure 20 show the results for the shot peened fretting test specimens.

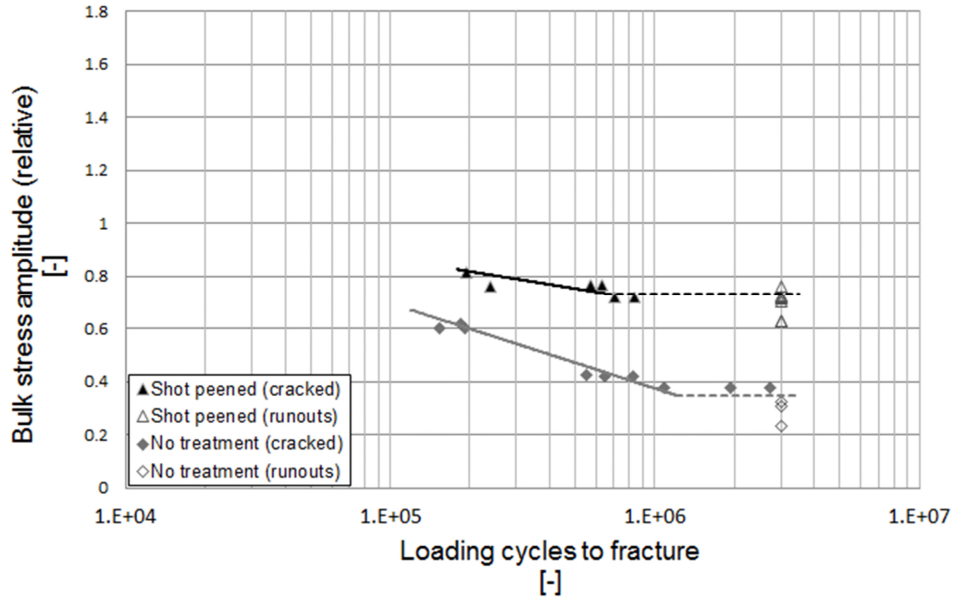

Figure 20. Test results of shot peened fretting specimens (Publication VII).

Here also the fretting fatigue lives increase noticeably. The fretting fatigue limit increased 110 %. The plain fatigue limit was increased by about 10 %. Nitriding increased the fatigue lives even more. The nitrided specimens may have had a lower COF [122], thus reducing

the risk of fretting cracking which can prolong fatigue life. However, as similar fatigue lives were achieved with the compound layer and the layer removed, this may not be the case. A major difference in surface roughness exists between the specimens, but the effect of this remains somewhat unclear. The fretting movement also notably relaxed the residual stresses during testing in shot peened specimens (Publication VII). However, the relaxation in nitrided specimens due to fretting remain unclear and this warrants further study. The results show that shot peening and nitriding are advantageous with regard to fretting and plain fatigue with quenched and tempered steel.

The test device and the results presented in Publication I aroused interest among the fretting community [60] and initiated a response that forms the basis of Publication II. In Publication I, the fatigue test results were compared in the traditional way by comparing the nominal bending stress values between fretting and plain fatigue. One disadvantage is that the results in this case are not easily interpreted [60] and such they present the experimental fretting fatigue results of Publication I in the form of the stress intensity factors, thus allowing a broader interpretation of the results. Findley values, for example, can be used to ‘transfer’ results, as has been done in the literature. However, it is not clear how accurately this can be done between rather different test results. For example, between the complete contact, where fretting wear is minor and in the bolted joint case, where the fretting damage is much greater. Presumably the effect of wear should be taken into account in the modelling.

4.2.3 Bolted joints

Fretting fatigue tests were carried out with different bulk (bending) loadings and bolt preloads. Most of the experimental results are presented in Figure 21, where a surface is fitted to the test points.

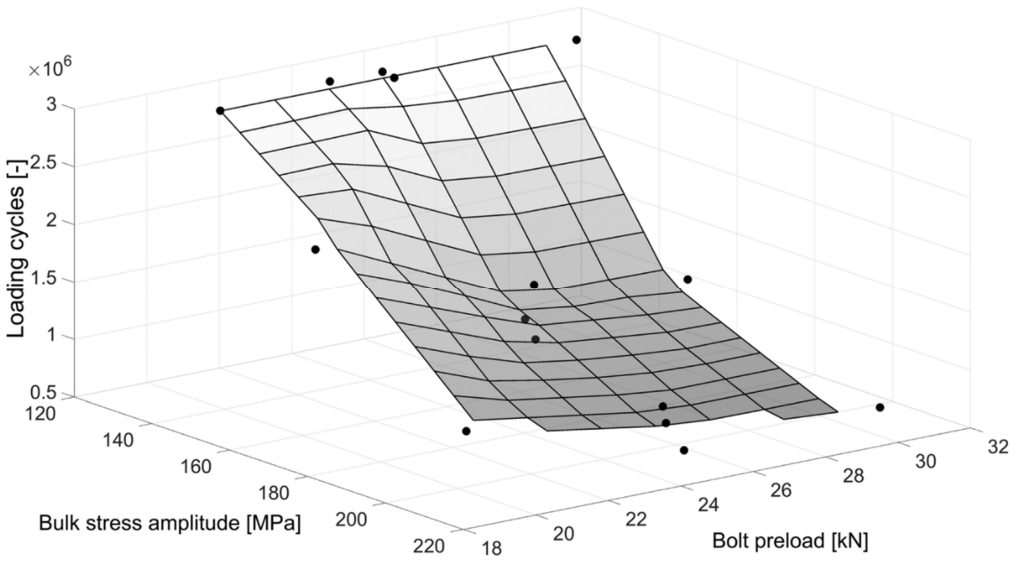

Figure 21. Experimental fretting fatigue test results in bolted joints (Publication VI).

The graph shows clearly that fatigue life decreases as the bulk stress amplitude increases and also that fatigue life is reduced by increasing the normal load in contact, i.e., bolt preload. The bulk stress is reported at the center of the hole (scaled from the strain gauge measurement), as presented in Figure 1 in Publication VI. True axial stress amplitudes (within the limits and assumptions of the model) were calculated approximately at the point of maximum axial stress and presented in an *S-N* form (Publication VI). Axial stress is longitudinal, i.e., normal stress parallel to the surface. The fatigue limit (around 180 MPa) achieved is relatively small compared to the plain fatigue limit of 517 MPa. Fatigue life decreased as the normal load (preload) was increased, which is also reflected in the series with the larger spacer, where lower nominal contact pressure was achieved by increasing the nominal contact area while also keeping the normal load unchanged.

Cracks that led to complete fracture were fretting-induced rather than the result of the stress concentration of the bolt hole. Findley fails to predict cracking in the bolted joint case. For example, in the 166 MPa / 30 kN case, where the experimental specimen failed, the cracking risk value is about 0.4 (even though the COF used in the model was 1.0). This suggest that surface modification and damage has a marked effect on fatigue cracking and should be taken into account. The distribution of the Findley cracking risk is somewhat wide as is the axial stress having maximum value approximately at the same point.

A ‘design’ map was reproduced using the calculated axial stress, slip (calculated) and fatigue lives (experiments). This kind of map can be useful for a designer. However, simplifications were made in the model and to draw more accurate maps of conditions having complex loading (non-proportional loading and multiaxial stress state), some fatigue criterion should be used (possibly together with wear simulation) instead of the single stress component presented here.

4.3 Comparison between DIC and FEM displacement fields

Because DIC is a full field method, it seems likely that the results could usefully be compared to the FEM results. Figure 22 presents a comparison between DIC (top) and FEM (bottom) of measured and calculated displacements at the complete contact edge area. The upper part is the pad and the lower part the specimen; the contact interface between these parts can be clearly seen due to the relative movement between them. The displacement fields for DIC and FEM show similar behavior, with certain COF in the model. The maximum displacement of the specimen exists at the contact edge. DIC appears to be a promising method to validate finite element models, and not only contact models.

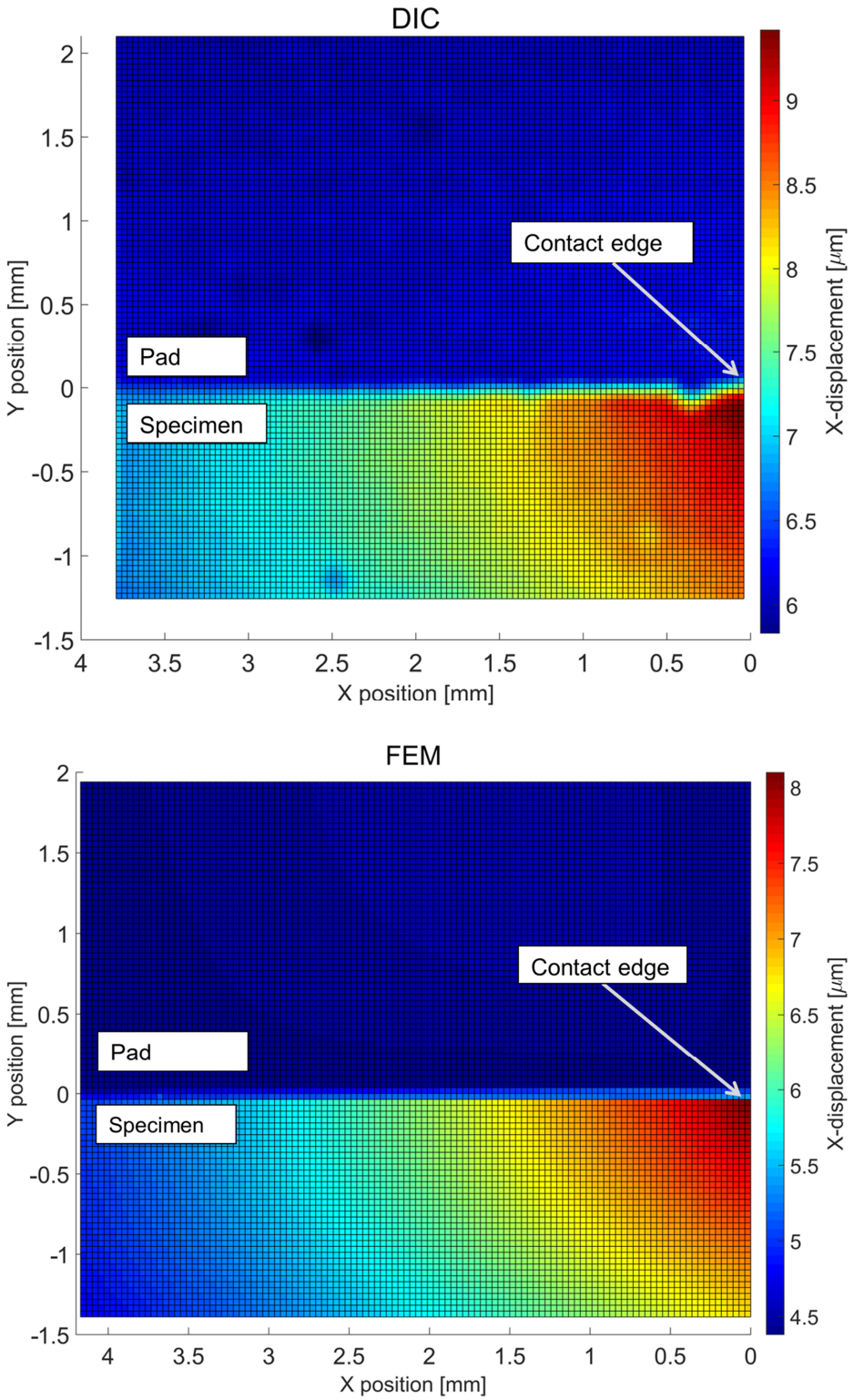

Figure 22. Comparison of *x*-displacements in the complete contact case (Publication V, adapted with the origin changed).

4.4 Relative displacement fields close to the contact interface

The DIC method was applied in both the complete contact and bolted joint case to measure the local displacement field (Publications IV and VI). Relative tangential displacements (slip) between a flat fretting pad (or another test specimen in the bolted joint setup) and a cyclically loaded flat fretting specimen was determined using the displacements measured close to the contact interface. In the complete contact case, these measured displacements were compared with the 2D approximation (FEM). In the bolted joint case, measured displacements were compared with the 3D FEM model but slip in the fretting regime (hole area) was extracted using the (3D) FEM. Figure 23 shows the relative tangential displacements during fretting fatigue tests in complete contact and bolted joint cases.

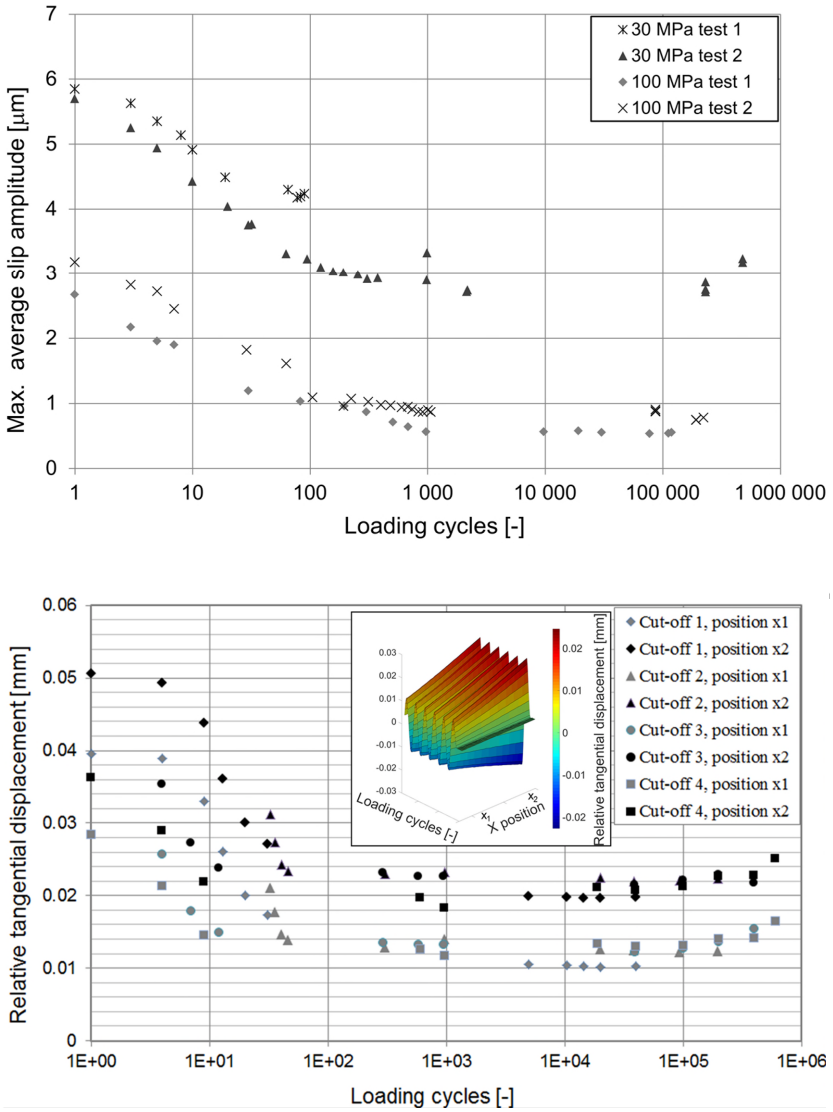

Figure 23. Relative tangential displacements during tests, complete contact (above, Publication IV) and bolted joint (below, Publication VI).

Clearly, slip amplitude decreases and flattens out during testing. The slip decreases markedly during testing as a result of increasing the COF. The relative displacement amplitude is higher in the bolted joint case, but obviously this depends on the operating parameters. The stabilization of the results occurs around 1000 loading cycles, which is in line with general observations.

4.5 Evaluation of coefficient of friction

The coefficient of friction was estimated by combining the DIC and FEM results. The relation between different COFs and displacements was determined in the FE-model (Publication V), and by comparing the displacements between DIC and FEM, the COF during fatigue tests was evaluated. The side faces were measured with DIC, but plane strain approximation was made in the complete contact model. The COF was determined by comparing slip amplitudes, slip regime lengths and accumulated slip amplitudes. The steady-state COF values were found to range between 0.55 - 0.8.

Figure 24 shows the evaluated coefficients of friction (maximum slip amplitudes compared) during fretting fatigue tests in the complete contact case.

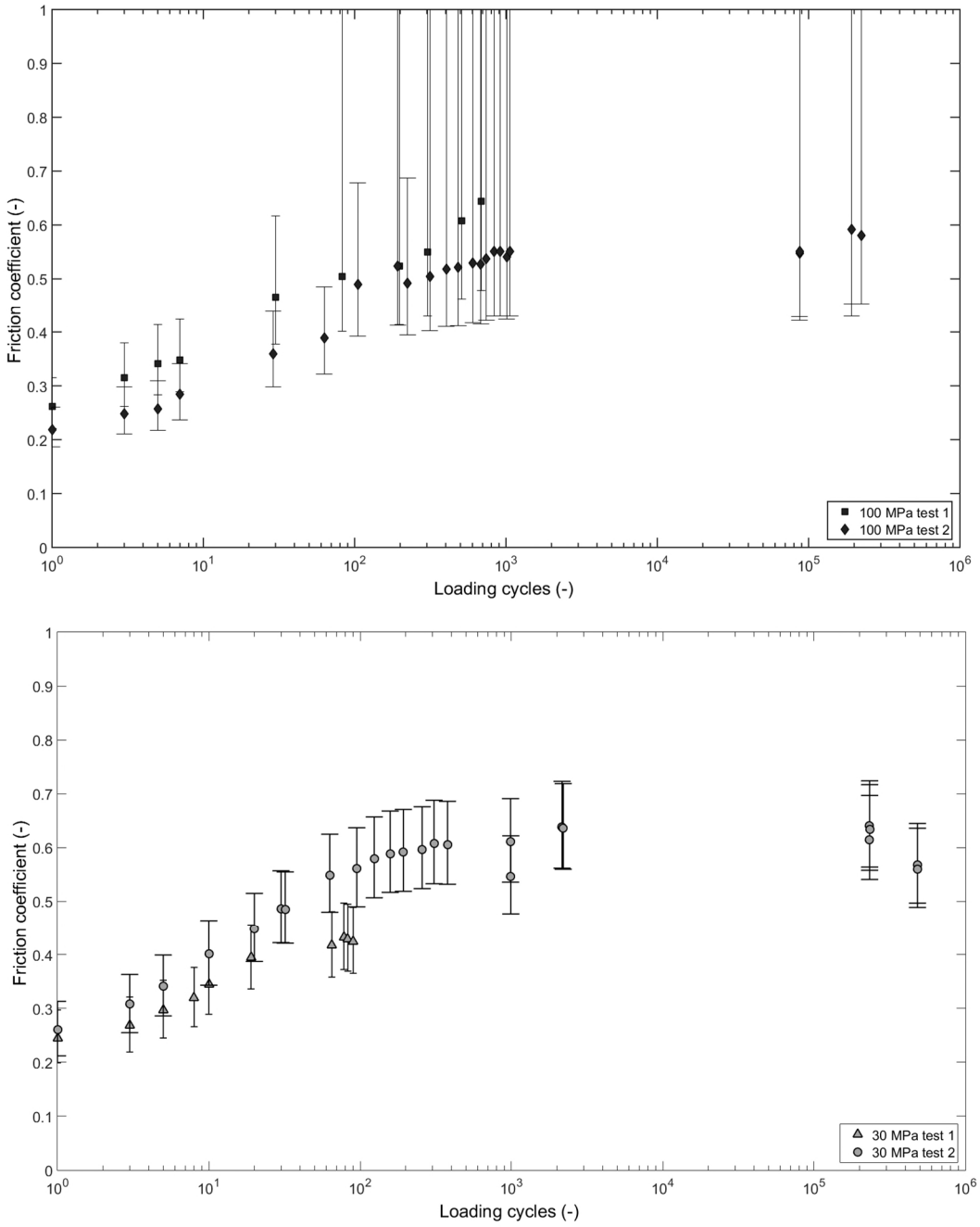

Figure 24. Evaluated coefficients of friction during fretting fatigue tests (Publication V).

The COFs start growing from about 0.2 - 0.3 and stabilized at around 0.5 - 0.6. Due to the small relative displacements in the 100 MPa case, the results are very sensitive to variation of the displacements. The error bars shown are calculated by assuming variations of ±0.5 μm in the measured displacements. COFs over ~0.5 have a very large range of variation and, clearly, COFs above ~0.6 cannot be determined due to an almost sticking contact. In the lower contact pressure case (30 MPa), where the relative displacements are higher, the error bars are acceptable. Accumulated slip was shown to be somewhat sensitive to COF,

thus making it a potential method to evaluate the COF. In the bolted joint case, similar methodology was used and COFs around 0.8 - 1.0 were achieved.

For the same material as used here, steady state coefficients of friction in gross sliding of around 0.8 have been measured in an another test device [27]. In this respect, the values achieved are therefore reasonable. The procedure presented was not intended to be an accurate method for determining COF and further validation is needed for this. However, the different ways to evaluate the COF showed similar kinds of behavior. In the complete contact, the contacting (fretting) pad geometry could be modified to allow the measurement of tangential force, as in ‘bridge’ type fretting devices though at the expense of modified contact geometry. This would allow the determination of the COF from the Q/P relation in gross sliding.

4.6 Partial slip regime length

As discussed in the introduction, relative tangential displacement is typically measured at a certain distance from the contact interface, thus including bulk compliances. Additionally, only one value is reported due to single-point determination. This relative displacement, possibly numerically corrected to take into account compliances, is then referred to as slip. Strictly speaking, to determine actual slip, the relative displacements should be measured exactly at the contact interface. Currently, this is very difficult to achieve and needs further study. In the complete contact case, slip was determined as a relative displacement between the fretting specimen and pad, about 150 μm away from the contact interface. All the tests here in the complete contact case were carried out in partial slip conditions. Slip distribution, i.e., the micrometer-level slip amplitude and the size of the slip region, was determined at specified time intervals during a fretting fatigue test to study the evolution of these parameters (Publication IV). Figure 25 presents the measured cyclic slip distributions in the 100 MPa case (upper figure) and the corresponding calculated results (lower figure).

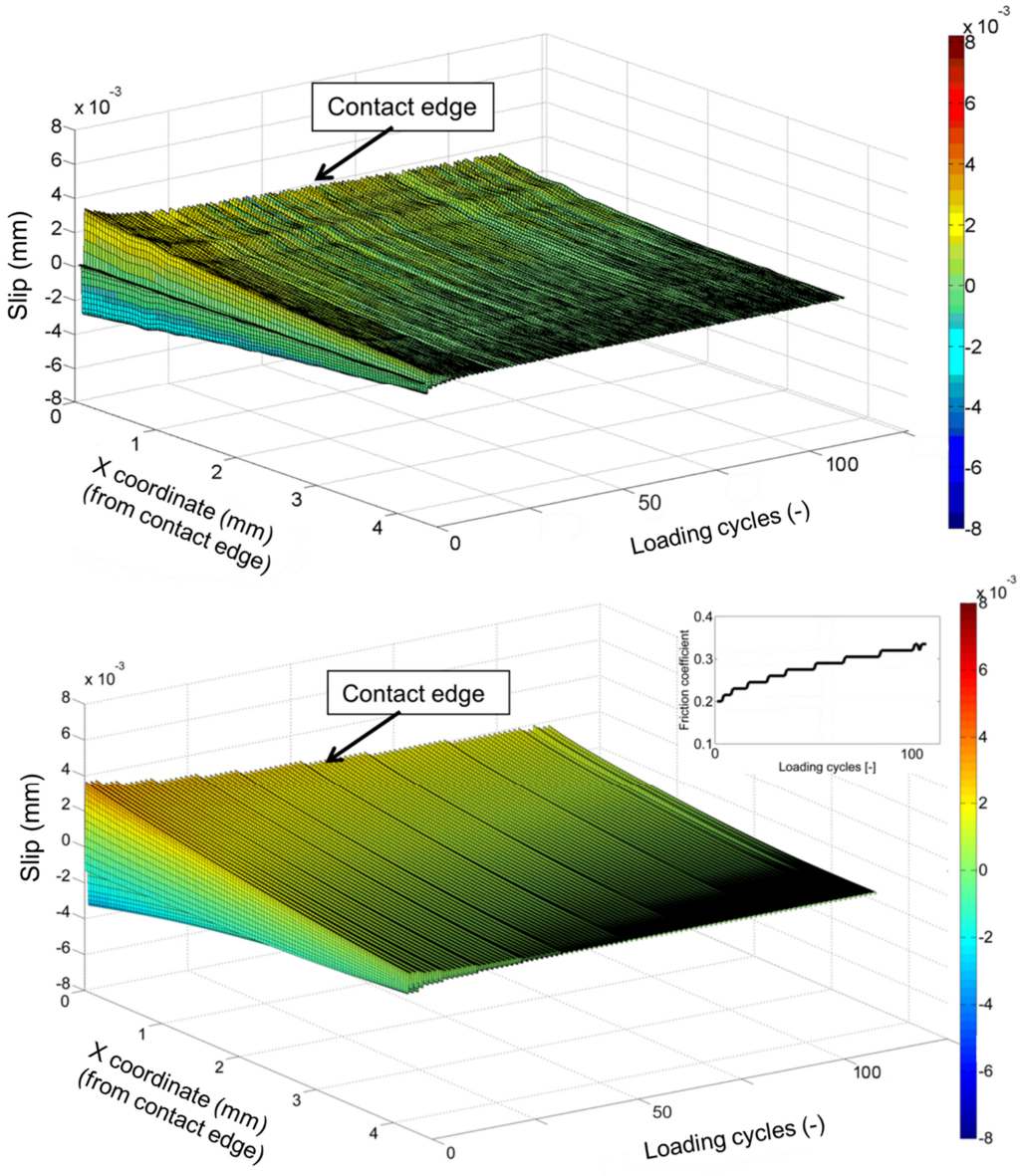

Figure 25. Cyclic relative displacement field, DIC (upper), FEM (lower) (Publication V).

Clearly, the length of the slip region decreases during loading cycles, which is to be expected due to the increasing COF. Using the simple Coulomb friction model (uniformly distributed over the slipping and sticking contact areas) and a plane strain model, the slip behavior (slip amplitude and slip regime length) can be repeated relatively well. In the lower contact pressure case, the COF increases more rapidly. One explanation is the effect of surface modification, which might be expected to be higher in the lower contact pressure case where slip is higher. The evolution of the slip regime length during testing is shown in Figure 26. Part of the results had to be extrapolated because the slip region was larger than the field of view (FOV).

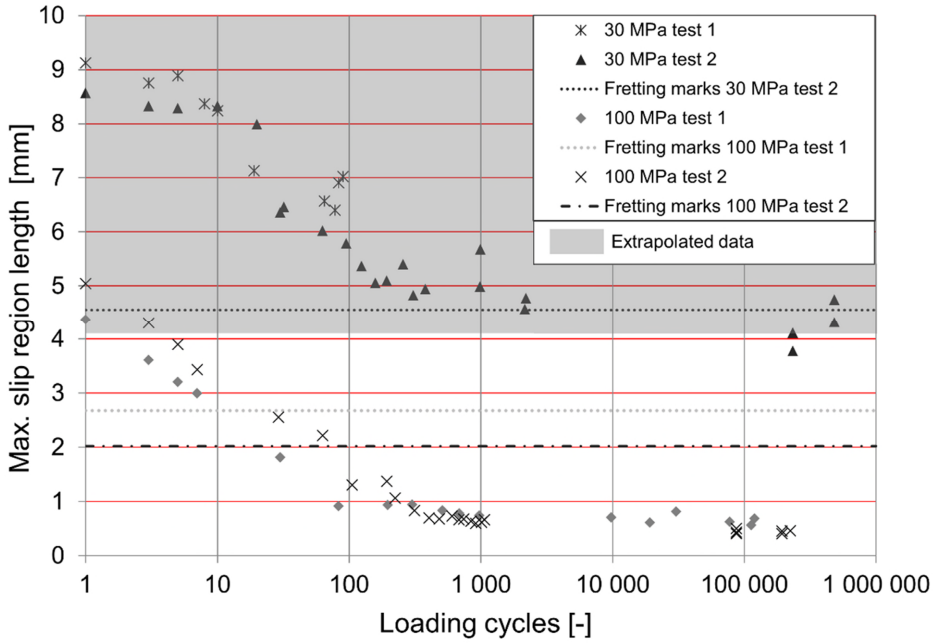

Figure 26. Slip regime length during fretting fatigue tests (Publication IV).

Extrapolation was mainly used in the 30 MPa case. With the current setup, the full fit of the slip region into the FOV can only be achieved with parameters that lead to relatively small slip amplitude. The length of slip region clearly decreases during loading cycles. A notable drop occurs after about 100 cycles and it stabilizes around 1000 cycles (in line with the stabilization of slip amplitude).

The method to determine the distribution of the cyclic relative displacement field using the Digital Image Correlation method shows much potential, though further experimental work is still needed to fully validate the method and to measure the interface more closely. An estimation of the actual slip at the contact interface can be achieved by extrapolating the results. Despite the approximations of the methods (primarily with the 2D model and constant COF along the contact surface) there is a similar pattern of behavior seen in both numerical and experimental results.

4.7 Fretting wear and scars

Fretting marks were observed in every test, although in some cases (with low bulk loading) the marks were minor. It is clearly evident that the wear marks are created by fretting and the surface topography is modified. In the complete contact tests the amount of wear was typically low or moderate (Publications I, III). In the bolted joints (Publication VI), severe wear and material transfer were observed. Figure 27 shows a typical fretting scar in the complete contact case.

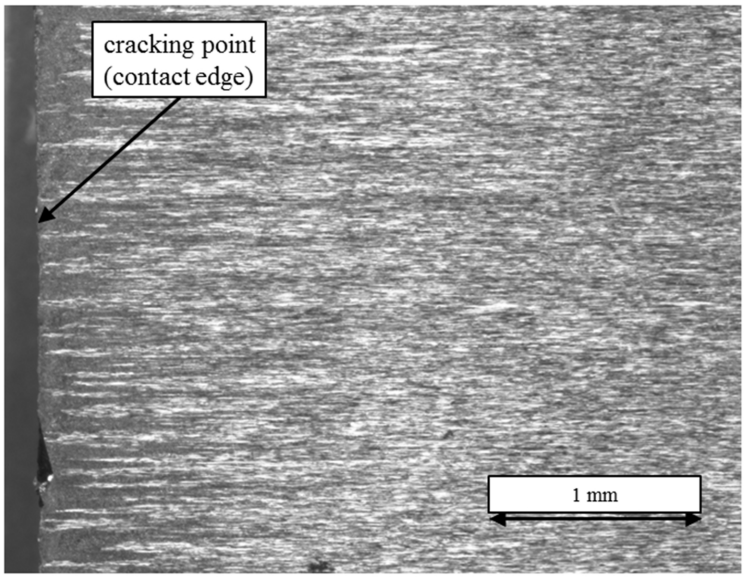

Figure 27. Typical fretting scar in the complete contact tests (Publication I).

Here fretting marks (scars) can be seen about two millimetres from the contact edge. Close to the edge, under higher slip and tractions, the scars are more evident. Moving away from the edge, the unchanged surface area increases and the marks become less obvious. The wear marks have roughly similar dimensions for different specimens, although more severe wear domains are evident in specimens that had higher bulk loading. In the surface treated specimens, fretting scars, and thus slip regime length, were obviously longer because of higher bulk loading.

In bolted joints, Figure 28, the point of severe damage and cracking occurs away from the hole. The position of the cracks was clearly linked to the vicinity of the most severe fretting scar. Random contact spots seemed to have small cracks already visible under microscopic examination, which may start or continue to grow if there is enough bulk loading. Asymmetric fretting scars can be explained on the basis of the principal fretting quantities, namely, traction, stress and slip.

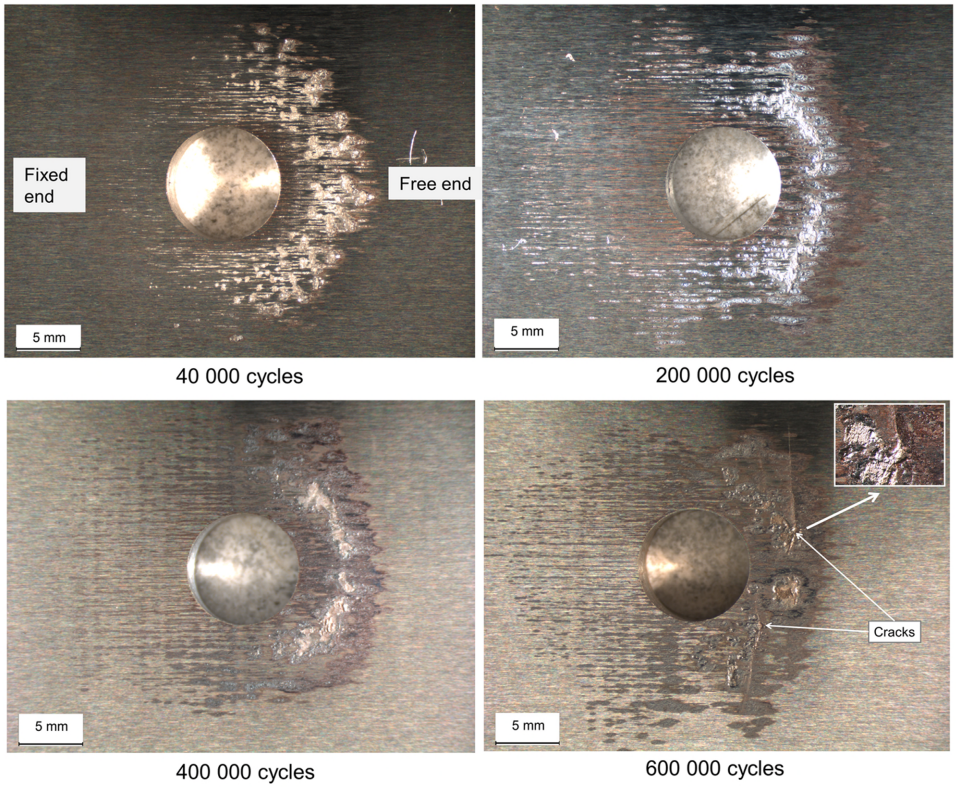

Figure 28. Typical fretting scars in bolted joint tests (Publication VI).

The transition of the macroscopic cracking leading to complete fracture from the geometrical stress concentration (hole) can be explained by the high COF since the increase in the COF moves the point of maximum stress away from the area of the hole to the merely flat-flat area (Figure 29), as the experiments also show.

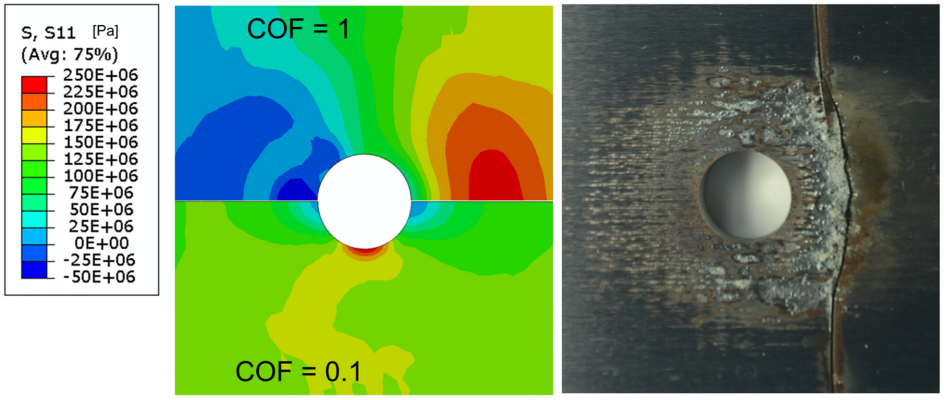

Figure 29. Stress in the specimen with two notable different coefficients of friction (Publication VI).

An important observation was that the fretting scar distribution does not properly correlate with either contact pressure or slip distribution, but it does correlate with the frictional energy distribution. The point of maximum dissipated frictional energy corresponds relatively well with the point of severe wear, Figure 30.

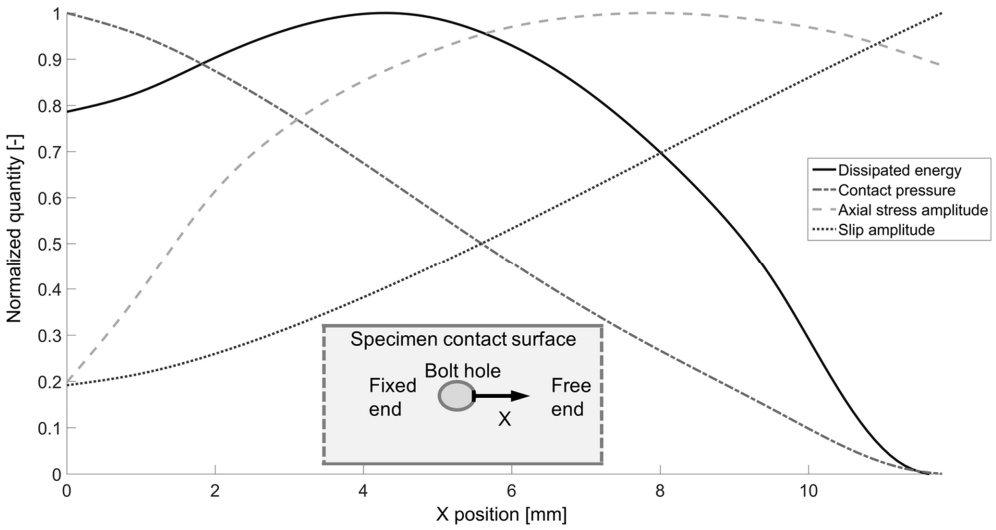

Figure 30. Distributions of different quantities along contact length (adapted from Publication VI).

The cracking point in the experiments occurs on the bulk loading side (right side) of the area of severe damage and the calculations also show this. It seems quite logical that the macroscopic cracks leading to complete fracture are created at the point of maximum stress in the presence of a fretting-degraded surface, where fretting had nucleated cracks that grow due to the bulk loading. To utilize and 'transfer' the results even further, the contact quantities (dissipated energy) could be determined at the cracking points and wear area. The values could be employed elsewhere as threshold values for fretting damage and crack nucleation.

4.8 Practical implications

Useful fretting fatigue data for different operating and design parameters, both at a scientific and practical level were presented for a widely used material (quenched and tempered steel) in machine elements such as shafts. Some of the results can be used directly at the design stage of machines, though the data can also be further used for a deeper analysis. With regard to press fits (shaft-hub connections, for example), of which the complete contact test device is a '2D simulation' (i.e., when there is stress peak at the contact edge (hub edge) and relatively low slip), useful results were achieved in the experiments. The fatigue life results were measured with different load levels, i.e., the stress in the specimens (shaft) and normal load (preload of an interference fit) and with two contact geometries. Both of the surface treatments studied increased fatigue life and have been implemented in practice and the results are of practical value. With regard to the bolted joint tests, the test geometry and loadings directly emulate actual bolt contacts. The results achieved showed how fretting can adversely decrease the fatigue life of bolted joints and how different parameters affect the fretting behavior of bolted joints. In both the complete and bolted contacts, the

increase in normal load led to a decrease in fatigue life. The point of maximum dissipated frictional energy corresponded to the areas of fretting damage and cracking. It is also worth noting that the increase in cyclic bulk loading (and in fretting loading) led to decreased fatigue life.

4.9 Recommendations for further research

Many of the recommendations were mentioned in the text and some of these are revisited here. From the experimental perspective, DIC measurements could be improved in order to determine displacements closer to the contact interface. DIC could be also be used for in situ crack detection and three dimensional (3D) DIC could be applied for gaining extra data. Measurement repeatability and the accuracy of the absolute slip values determined with DIC are important subjects and warrant further investigation and study. With regard to fretting scars and cracking, the bolted joints specimens were inspected only at a general level. Deeper microscopic and fractographic analysis of cracks and fretting scars would provide additional information on fretting crack nucleation. Considering real connections, such as shaft-hub connections, these are typically under lubrication, at least initially, when the surfaces are lubricated for assembly and for corrosion prevention. The effect of lubrication, therefore, is another area for study with potential practical value. Only self-mated, quenched and tempered steel was used in the study; testing of material pairs where the material of the other surface differs requires further investigation.

With regards to modelling, a constant COF, both spatially and temporarily, was utilized. The effect of using a variable COF could also be studied as well as non-Coulomb friction [27]. In addition, wear and/or surface topography should be taken into account, especially in the bolted joint case, if a more profound analysis is needed. The method used to evaluate the COF based on displacement measured should be validated using simultaneous COF measurement. As for the surface treatment tests and corresponding modelling, residual stress measurements (Publication VII) showed that grinding can create a large amount of residual stresses. Here again, this would be an area that needs to be taken into account in the modelling process, though compressive residual stress can be taken as an additional safety factor in the calculations. The effect of surface treatment on the fretting fatigue and wear behavior of bolted specimens is another area for further examination. Detailed stress analysis of the experimental results would derive even more value from the experiments. Further understanding and practical benefit can be achieved both in complete and bolted contacts by applying fracture mechanics to crack growth. This is because the major part of fretting fatigue life typically occurs during crack propagation. In addition, fracture mechanics can be used to determine whether cracks will propagate or cease.

5 Conclusions

Fretting fatigue is a damage mechanism occurring in practical connections in machine components. In fretting, the contacting surfaces are under cyclic relative movement that can lead not only to surface damage but also seriously decrease fatigue life due to the clear tendency of fretting to nucleate cracks. The cracks can continue to grow as a result of the cyclic loads in a component, leading to premature failure. A major challenge is that there is still no universal fretting fatigue model to predict fretting cracking. This thesis has studied fretting fatigue in complete and bolted connections. Actual complete contacts can be found in practice in shaft-hub connections (press fits), for example, and bolted joints are often used to clamp parts together in assemblies. The material used in the study was self-mated quenched and tempered steel, which is a widely used material in heavy loaded connections in machines. The effect of various design parameters and fretting palliatives on the fretting fatigue behavior was studied. The Digital Image Correlation method was applied to both contacts in order to measure relative displacement fields. The Finite Element Method was applied to study the contacts in greater detail. Smooth surfaces were assumed in the modelling and wear was not taken into account. Fretting cracking risk values were calculated using the Findley multiaxial fatigue criterion. The Theory of Critical Distances was employed in the complete contact case to average stresses due to the steep stress gradients.

A complete contact fretting test device was developed having a large nominal contact area and transverse (bending) loading. The device emulates conditions which can often be found in practice, for example, in power transmission components. Because of this the experiments address actual contact conditions in machines in practice. The test device was also used with minor modifications to study bolted joints. A large number of fretting fatigue tests were made in complete contact with different operating conditions (specimen bulk loading and nominal contact pressure) and contact geometries. Several fretting fatigue test series were carried out in bolted joints using different operating (bolt preload, specimen bulk loading) and design parameters. The complete contact fretting test device that was developed aroused much interest in the fretting community and the ensuing exchange of correspondence mostly discussed the generalization of the results.

Essential design parameters mostly had a notable effect on fretting fatigue behavior in complete and bolted connections, which emphasizes that fretting is important to take into account. Fretting seriously decreased the fatigue life in both types of contact. Fretting damage and cracking were observed with relatively low nominal bulk loadings. In the complete contact case, the fretting fatigue limit was about 30 % of the plain fatigue limit in terms of nominal loading. The modelling results agreed with the experiments in terms of cracking prediction and contact quantities. Slight rounding of the sharp ended contact edge did not provide any improvement compared to the sharp ended case. In both types of contact, fatigue life decreased when the cyclic loading of the test specimen was increased and the increase in contact normal load (contact preload) decreased fatigue life. In complete contact tests, the cracking point was at the contact edge area. Contact conditions prevented the bolted joint from failing at the geometrical stress concentration (bolt hole), but the specimens failed as a result of fretting instead. By increasing the coefficient of friction in the bolted joint case's model, the point of cracking shifted away from the hole area. The area of fretting damage and cracking point corresponded to the distribution of frictional energy dissipation. Fretting damage was observed in every test and at a relatively early stage in the loading history. The Findley criterion (within the limits and assumptions of the model) failed to predict cracking in the bolted joint case but did so in the complete contact case when 'averaging' of stresses was taken into account. The coefficient of friction had a significant effect on the fretting fatigue cracking risk due to the increased frictional stresses. An increase in the coefficient of friction also reduces contact slip. In the complete contact case, surface treatments led to a major increase in the fretting fatigue lives. Compressive residual stresses created by shot peening and nitriding increased the fretting fatigue limit 110 % and 150 %, respectively. Fretting caused stress relaxation at the contact surface of the treated specimens. Some of the results can be directly exploited at the design stage of components but the data gained can be used in further analyses.

The Digital Image Correlation method was applied in both types of contact to measure relative displacements close to the contact interface to minimize bulk compliances. This made it possible to determine the cyclic relative displacement (slip) field. A small pixel size was needed to gain an adequate spatial resolution of the displacements and a microscope was employed for the purpose. The relative displacements were found to decrease noticeably during fretting fatigue testing in response to the increasing coefficient of friction. DIC and FEM methods were successfully compared in terms of relative displacements. DIC provides full-field displacements and has potential to FE-model validation.

References

[1] Schivje J. Fatigue of Structures and Materials. 2nd ed. Springer Netherlands; 2009.

[2] Dobrominski JM. Variables of Fretting Process: Are There 50 of Them? In: Attia MH, Waterhouse RB, editors. Stand. Frett. Fatigue Test Methods Equipment, ASTM STP 1159, Philadelphia: American Society for Testing and Materials; 1992, p. 60–66.

[3] Hutchings IM. Tribology: Friction and Wear of Engineering Materials. 1st ed. London: Edward Arnold; 1992.

[4] Holmberg K, Andersson P, Erdemir A. Global energy consumption due to friction in passenger cars. Tribol Int 2012;47:221–234.

[5] Bhushan B. Principles and Applications of Tribology. 2nd ed. New York: John Wiley & Sons; 2013.

[6] Dowson D. History of Tribology. 1st ed. London: Longman Group Limited; 1979.

[7] Hills DA, Nowell D. Mechanics of Fretting Fatigue. Dordrecht: Kluwer Academic Publishers; 1994.

[8] Socie DF, Marquis GB. Multiaxial Fatigue. Warrendale: Society of Automotive Engineers, Inc; 1999.

[9] Suresh S. Fatigue of Materials. 2nd ed. Cambridge: Cambridge University Press; 1998.

[10] Rabb R. Todennäköisyysteoriaan pohjautuva väsymisanalyysi. Helsinki: BoD - Books On Demand; 2013.

[11] Farrahi GH, Tirehdast M, Abad EMK, Parsa S, Motakefpoor M. Failure analysis of a gas turbine compressor. Eng Fail Anal 2011;18:474–484.

[12] Waterhouse RB. Fretting fatigue. London: Applied Science Publishers; 1981.

[13] Lindley TC. Fretting fatigue in engineering alloys. Int J Fatigue 1998;19:39–49.

[14] Waterhouse RB. A Historical Introduction to Fretting Fatigue. In: Attia MH, Waterhouse RB, editors. Stand. Frett. Fatigue Test Methods Equipment, ASTM STP 1159, Philadelphia: American Society for Testing and Materials; 1992, p. 8–9.

[15] Hurricks PL. The mechanism of fretting - A review. Wear 1970;15:389–409.

[16] Jin O, Mall S. Effects of slip on fretting behavior: experiments and analyses. Wear 2004;256:671–684.

[17] Pape JA, Neu RW. A comparative study of the fretting fatigue behavior of 4340 steel and PH 13-8 Mo stainless steel. Int J Fatigue 2007;29:2219–2229.

[18] Araujo JA, Nowell D, Vivacqua RC. The use of multiaxial fatigue models to predict

fretting fatigue life of components subjected to different contact stress fields. Fatigue Fract Eng Mater Struct 2004;27:967–978.

[19] Araújo JA, Nowell D. Analysis of pad size effects in fretting fatigue using short crack arrest methodologies. Int J Fatigue 1999;21:947–956.

[20] Fellows LJ, Nowell D, Hills DA. On the initiation of fretting fatigue cracks. Wear 1997;205:120–129.

[21] Zhou ZR, Vincent L. Mixed fretting regime. Wear 1995;181–183:531–536.

[22] Sabelkin V, Mall S. Relative Slip on Contact Surface under Partial Slip Fretting Fatigue Condition. Strain 2006;42:11–20.

[23] Iyer K, Mall S. Analyses of Contact Pressure and Stress Amplitude Effects on Fretting Fatigue Life. J Eng Mater Technol 2001;123:85–93.

[24] Nakazawa K, Maruyama N, Hanawa T. Effect of contact pressure on fretting fatigue of austenitic stainless steel. Tribol Int 2003;36:79–85.

[25] McColl IR, Ding J, Leen SB. Finite element simulation and experimental validation of fretting wear. Wear 2004;256:1114–1127.

[26] Mulvihill DM, Kartal ME, Olver AV, Nowell D, Hills DA. Investigation of non-Coulomb friction behaviour in reciprocating sliding. Wear 2011;271:802–816.

[27] Hintikka J, Lehtovaara A, Mäntylä A. Fretting-induced friction and wear in large flat-on-flat contact with quenched and tempered steel. Tribol Int 2015;92:191–202.

[28] Mugadu A, Hills DA, Nowell D. Modifications to a fretting-fatigue testing apparatus based upon an analysis of contact stresses at complete and nearly complete contacts. Wear 2002;252:475–483.

[29] Hills DA, Paynter RJH, Dini D. An overview of the quantification of fretting fatigue lives of complete contacts. Eng Fract Mech 2012;80:3–12.

[30] Smith EH. Mechanical Engineers Reference Book. 12th ed. Oxford: Butterworth-Heinemann Ltd; 1998.

[31] Vingsbo O, Söderberg S. On fretting maps. Wear 1988;126:131–147.

[32] Fouvry S, Kapsa P, Vincent L. Quantification of fretting damage. Wear 1996;200:186–205.

[33] Lee H, Jin O, Mall S. Fretting fatigue behavior of Ti-6Al-4V with dissimilar mating materials. Int J Fatigue 2004;26:393–402.

[34] Bertini L, Santus C. Fretting fatigue tests on shrink-fit specimens and investigations into the strength enhancement induced by deep rolling. Int J Fatigue 2015;81:179–190.

[35] Fouvry S, Kapsa P, Zahouani H, Vincent L. Wear analysis in fretting of hard coatings through a dissipated energy concept. Wear 1997;203–204:393–403.

[36] Zhou ZR, Fayeulle S, Vincent L. Cracking behaviour of various aluminium alloys during fretting wear. Wear 1992;155:317–330.

[37] Fouvry S, Kubiak K. Introduction of a fretting-fatigue mapping concept: Development of a dual crack nucleation - crack propagation approach to formalize fretting-fatigue damage. Int J Fatigue 2009;31:250–262.

[38] Hills DA, Nowell D. What features are needed in a fretting fatigue test? Tribol Int 2009;42:1316–1323.

[39] Juuma T. Torsional fretting fatigue strength of a shrink-fitted shaft. Wear 1999;231:310–318.

[40] Alfredsson B. Fretting fatigue of a shrink-fit pin subjected to rotating bending: Experiments and simulations. Int J Fatigue 2009;31:1559–1570.

[41] Attia HM, Waterhouse R, editors. Standardization of Fretting Fatigue Test Methods and Equipment, ASTM STP 1159. Philadelphia: American Society for Testing and Materials; 1992.

[42] Arora P, Jacob M, Salit M, Ahmed E, Saleem M, Edi P. Experimental evaluation of fretting fatigue test apparatus. Int J Fatigue 2007;29:941–952.

[43] Rossino LS, Castro FC, Bose Filho WW, Araújo JA. Issues on the mean stress effect in fretting fatigue of a 7050-T7451 Al alloy posed by new experimental data. Int J Fatigue 2009;31:2041–2048.

[44] Sabsabi M, Giner E, Fuenmayor FJ. Experimental fatigue testing of a fretting complete contact and numerical life correlation using X-FEM. Int J Fatigue 2011;33:811–822.

[45] Peng JF, Song C, Shen MX, Zheng JF, Zhou ZR, Zhu MH. An experimental study on bending fretting fatigue characteristics of 316L austenitic stainless steel. Tribol Int 2011;44:1417–1426.

[46] Benhamena A, Talha A, Benseddiq N, Amrouche A, Mesmacque G, Benguediab M. Effect of clamping force on fretting fatigue behaviour of bolted assemblies: Case of couple steel–aluminium. Mater Sci Eng A 2010;527:6413–6421.

[47] Chakherlou TN, Oskouei RH, Vogwell J. Experimental and numerical investigation of the effect of clamping force on the fatigue behaviour of bolted plates. Eng Fail Anal 2008;15:563–574.

[48] Benhamena A, Amrouche A, Talha A, Benseddiq N. Effect of contact forces on fretting fatigue behavior of bolted plates: Numerical and experimental analysis. Tribol Int 2012;48:237–245.

[49] Chakherlou TN, Razavi MJ, Aghdam AB, Abazadeh B. An experimental investigation of the bolt clamping force and friction effect on the fatigue behavior of aluminum alloy 2024-T3 double shear lap joint. Mater Des 2011;32:4641–4649.

[50] Walvekar AA, Leonard BD, Sadeghi F, Jalalahmadi B, Bolander N. An experimental study and fatigue damage model for fretting fatigue. Tribol Int 2014;79:183–196.

[51] Jin O, Mall S. Effects of independent pad displacement on fretting fatigue behavior of Ti–6Al–4V. Wear 2002;253:585–596.

[52] Wittkowsky BU, Birch PR, Dominguez J, Suresh S. An apparatus for quantitative fretting fatigue testing. Fatigue Fract Eng Mater Struct 1999;22:307–320.

[53] Ferrero J, Yettou E, Barrau J, Rivallant S. Analysis of a dry friction problem under small displacements: application to a bolted joint. Wear 2004;256:1135–1143.

[54] Sabelkin V, Mall S. Investigation into relative slip during fretting fatigue under partial slip contact condition. Fatigue Fract Eng Mater Struct 2005;28:809–824.

[55] Johnson KL. Contact Mechanics. Cambridge: Cambridge University Press; 1985.

[56] Fouvry S, Kapsa P, Vincent L. Analysis of sliding behaviour for fretting loadings: determination of transition criteria. Wear 1995;185:35–46.

[57] Madge JJ, Leen SB, McColl IR, Shipway PH. Contact-evolution based prediction of fretting fatigue life: Effect of slip amplitude. Wear 2007;262:1159–1170.

[58] Fouvry S, Duó P, Perruchaut P. A quantitative approach of Ti-6Al-4V fretting damage: Friction, wear and crack nucleation. Wear 2004;257:916–929.

[59] Nesladek M, Spaniel M, Jurenka J, Ruzicka J, Kuzelka J. Fretting fatigue - Experimental and numerical approaches. Int J Fatigue 2012;44:61–73.

[60] Hills DA, Flicek RC, Dini D. A discussion of: Development of a complete contact fretting test device by J Juoksukangas et al. Proc Inst Mech Eng Part J J Eng Tribol 2014;228:123–126.

[61] Mall S, Naboulsi S, Namjoshi SA. Contact geometry effects on fretting fatigue crack initiation behaviour of Ti–6Al–4V. Tribol - Mater Surfaces Interfaces 2008;2:25–32.

[62] Merhej R, Fouvry S. Contact size effect on fretting wear behaviour: application to an AISI 52100/AISI 52100 interface. Lubr Sci 2009;21:83–102.

[63] Costa JD, Ferreira JM, Ramalho AL. Fatigue and fretting fatigue of ion-nitrided 34CrNiMo6 steel. Theor Appl Fract Mech 2001;35:69–79.

[64] Mutoh Y, Tanaka K. Fretting fatigue in several steels and a cast iron. Wear 1988;125:175–191.

[65] Chan PC, Thornley JC. Common Features of Fretting-Fatigue Cracking in Steels. J Fail Anal Prev 2002;2:85–90.

[66] Leidich E, Maiwald A, Vidner J. A proposal for a fretting wear criterion for coated systems with complete contact based on accumulated friction energy density. Wear 2013;297:903–910.

[67] Cadario A, Alfredsson B. Influence of residual stresses from shot peening on fretting fatigue crack growth. Fatigue Fract Eng Mater Struct 2007;30:947–963.

[68] Li CX, Sun Y, Bell T. Shot peening of plasma nitrided steel for fretting fatigue strength enhancement. Mater Sci Technol 2000;16:1067–1072.

[69] Allen C, Li CX, Bell T, Sun Y. The effect of fretting on the fatigue behaviour of plasma nitrided stainless steels. Wear 2003;254:1106–1112.

[70] Torres MAS, Voorwald HJC. An evaluation of shot peening, residual stress and stress relaxation on the fatigue life of AISI 4340 steel. Int J Fatigue 2002;24:877–886.

[71] Thaitirarot A, Hills DA, Dini D. Contact mechanics of frictional lap joints. J Strain Anal Eng Des 2013;48:321–329.

[72] Ciavarella M, Hills DA, Monno G. The influence of rounded edges on indentation by a flat punch. Proc Inst Mech Eng Part C J Mech Eng Sci 1998;212:319–328.

[73] Giannakopoulos AE, Lindley TC, Suresh S, Chenut C. Similarities of stress concentrations in contact at round punches and fatigue at notches: implications to fretting fatigue crack initiation. Fatigue Fract Eng Mater Struct 2000;23:561–571.

[74] Giannakopoulos AE, Lindley TC, Suresh S. Aspects of equivalence between contact mechanics and fracture mechanics: theoretical connections and a life-prediction methodology for fretting-fatigue. Acta Mater 1998;46:2955–2968.

[75] Hills DA, Thaitirarot A, Barber JR, Dini D. Correlation of fretting fatigue experimental results using an asymptotic approach. Int J Fatigue 2012;43:62–75.

[76] Flicek RC, Hills DA, Dini D. Sharp edged contacts subject to fretting: A description of corner behaviour. Int J Fatigue 2015;71:26–34.

[77] Swalla DR, Neu RW. Influence of coefficient of friction on fretting fatigue crack nucleation prediction. Tribol Int 2001;34:493–503.

[78] Crisfield MA. Non-linear Finite Element Analysis of Solids and Structures. John Wiley & Sons; 2000.

[79] Bohorquez L, Dominguez J. Characterization of the contact between a punch and a half-infinite substrate in a fretting situation. Int J Mech Sci 2007;49:608–621.

[80] Yang B, Chu M, Menq C. Stick–slip–separation analysis and non-linear stiffness and damping characterization of friction contacts having variable normal load. J Sound Vib 1998;210:461–481.

[81] Kim HS, Mall S. Investigation into three-dimensional effects of finite contact width on fretting fatigue. Finite Elem Anal Des 2005;41:1140–1159.

[82] Rajasekaran R, Nowell D. On the finite element analysis of contacting bodies using submodelling. J Strain Anal Eng Des 2005;40:95–106.

[83] Talemi RH, Wahab MA. Finite Element Analysis of Localized Plasticity in Al 2024-T3 Subjected to Fretting Fatigue. Tribol Trans 2012;55:805–814.

[84] Giner E, Sukumar N, Denia FD, Fuenmayor FJ. Extended finite element method for fretting fatigue crack propagation. Int J Solids Struct 2008;45:5675–5687.

[85] Madge JJ, Leen SB, Shipway PH. The critical role of fretting wear in the analysis of fretting fatigue. Wear 2007;263:542–551.

[86] Mall S, Jain VK, Fadag HA. Effects of Shot-Peening on Fretting Fatigue Crack Growth Behavior in Ti-6Al-4V. Strain 2011;47:e305–e318.

[87] Rammohan YS, Murthy H. Three dimensional finite element analysis of partial slip contacts subjected to combined loading. Finite Elem Anal Des 2012;56:9–19.

[88] Bernardo AT, Araujo JA, Mamiya EN. Proposition of a finite element-based approach to compute the size effect in fretting fatigue. Tribol Int 2006;39:1123–1130.

[89] Leen SB, Richardson IJ, McColl IR, Williams EJ, Hyde TR. Macroscopic fretting variables in a splined coupling under combined torque and axial load. J Strain Anal Eng Des 2001;36:481–497.

[90] Abaqus Theory Manual 6.13-EF, Dassault Systèmes 2013.

[91] Wriggers P. Computational Contact Mechanics. 2nd ed. Springer; 2006.

[92] Lanoue F, Vadean A, Sanschagrin B. Finite element analysis and contact modelling considerations of interference fits for fretting fatigue strength calculations. Simul Model Pract Theory 2009;17:1587–1602.

[93] Lykins CD, Mall S, Jain V. An evaluation of parameters for predicting fretting fatigue crack initiation. Int J Fatigue 2000;22:703–716.

[94] Lykins CD, Mall S, Jain VK. Combined experimental – numerical investigation of fretting fatigue crack initiation. Int J Fatigue 2001;23:703–711.

[95] Namjoshi SA, Mall S, Jain VK, Jin O. Fretting fatigue crack initiation mechanism in Ti-6Al-4V. Fatigue Fract Eng Mater Struct 2002;25:955–964.

[96] Ruiz C, Boddington PHB, Chen KC. An investigation of fatigue and fretting in a dovetail joint. Exp Mech 1984;24:208–217.

[97] Ding J, Houghton D, Williams EJ, Leen SB. Simple parameters to predict effect of surface damage on fretting fatigue. Int J Fatigue 2011;33:332–342.

[98] Wei DS, Yuan SH, Wang YR. Failure analysis of dovetail assemblies under fretting load. Eng Fail Anal 2012;26:381–396.

[99] Mutoh Y, Xu JQ. Fracture mechanics approach to fretting fatigue and problems to be solved. Tribol Int 2003;36:99–107.

[100] Araujo JA, Nowell D. The effect of rapidly varying contact stress fields on fretting fatigue. Int J Fatigue 2002;24:763–775.

[101] Naboulsi S, Mall S. Fretting fatigue crack initiation behavior using process volume approach and finite element analysis. Tribol Int 2003;36:121–131.

[102] Fouvry S, Kapsa P, Vincent L. A Multiaxial Fatigue Analysis of Fretting Contact Taking Into Account the Size Effect. In: Hoeppner DW, Chandrasekaran V, Elliott CB, editors. Frett. fatigue Curr. Technol. Pract. ASTM STP 1367, West Conshohocken, PA, USA: American Society for Testing and Materials; 2000, p. 167–182.

[103] Taylor D. Geometrical effects in fatigue: a unifying theoretical model. Int J Fatigue

1999;21:413–420.

[104] Araujo JA, Susmel L, Taylor D, Ferro JCT, Mamiya EN. On the use of the Theory of Critical Distances and the Modified Wöhler Curve Method to estimate fretting fatigue strength of cylindrical contacts. Int J Fatigue 2007;29:95–107.

[105] Hosford WF. Mechanical Behavior of Materials. Cambridge University Press; 2005.

[106] Tsai CT, Mall S. Elasto-plastic finite element analysis of fretting stresses in pre-stressed strip in contact with cylindrical pad. Finite Elem Anal Des 2000;36:171–187.

[107] Cruzado A, Leen SB, Urchegui MA, Gómez X. Finite element simulation of fretting wear and fatigue in thin steel wires. Int J Fatigue 2013;55:7–21.

[108] Benhamena A, Laïd Aminallah, Baltach A, Aid A, Benguediab M, Amrouche A, et al. The Fretting Fatigue Behavior of Bolted Assemblies. In: Öchsner A, Silva LFM, Altenbach H, editors. Des. Comput. Mod. Eng. Mater., Springer; 2014, p. 187–204.

[109] SFS 5595. Kutistus- ja puristusliitos. Laskentaperusteet ja muotoiluohjeet. (In Finnish). Suomen Standardoimisliitto SFS; 1989.

[110] Brown KH, Morrow C, Durbin S, Baca A. Guideline for Bolted Joint Design and Analysis: Version 1.0. Sandia Report, SAND2008-0371 2008:47.

[111] Sutton MA, Orteu J-J, Schreier HW. Image Correlation for Shape, Motion and Deformation Measurements. New York: Springer; 2009.

[112] Kartal ME, Mulvihill DM, Nowell D, Hills DA. Determination of the Frictional Properties of Titanium and Nickel Alloys Using the Digital Image Correlation Method. Exp Mech 2011;51:359–371.

[113] De Pauw J, De Waele W, Hojjati-Talemi R, De Baets P. On the use of digital image correlation for slip measurement during coupon scale fretting fatigue experiments. Int J Solids Struct 2014;51:3058–3066.

[114] Lehtovaara A, Rabb R, Pasanen A. Modelling and evaluation of the fretting fatigue cracking risk in smooth spherical contacts. Tribol Int 2011;44:1526–1534.

[115] Infinity long-distance microscope K2/SC. Infinity Photo-Optical Company. Boulder, CO, USA 2011.

[116] Lavision. Davis 8.2 Commercial DIC equipment and software 2014.

[117] Flicek RC, Ramesh R, Hills DA. A complete frictional contact: The transition from normal load to sliding. Int J Eng Sci 2015;92:18–27.

[118] Juoksukangas J, Lehtovaara A, Mäntylä A. Effect of contact pressure on fretting fatigue life in complete contacts. Proc. Seventh Int. Symp. Frett. Fatigue (ISFF7). Oxford Univ. Oxford, UK, 2013, p. 2.

[119] Hutson AL, Nicholas T, Goodman R. Fretting fatigue of Ti – 6Al – 4V under flat-on-flat contact. Int J Fatigue 1999;21:663–669.

[120] Francis M, Van Ngan L, Henri C, Ngan NH. Stress concentration of shrink fit

assembly using finite element method. In: Miao L, editor. Proc. IASTED Asian Conf. Model. Simul., Anaheim: ACTA Press; 2007, p. 67–70.

[121] Taylor D. The Theory of Critical Distances: A New Perspective in Fracture Mechanics. 1st ed. Oxford: Elsevier; 2007.

[122] Kubiak K, Fouvry S, Wendler BG. Comparison of Shot Peening and Nitriding Surface Treatments Under Complex Fretting Loadings. Mater Sci Forum 2006;513:105–118.

ORIGINAL PUBLICATIONS

Publication I

Development of a complete contact fretting test device

by

J. Juoksukangas, A. Lehtovaara and A. Mäntylä

Proc. IMechE, Part J: J. Engineering Tribology, 227(6), 2013, 570–578,
doi:10.1177/1350650112466162

Development of a complete contact fretting test device

J. Juoksukangas[1*], A. Lehtovaara[1] and A. Mantyla[2]

[1]Department of Mechanics and Design, Tampere University of Technology, P.O. Box 589, 33101 Tampere, Finland

[2]Research & Development, Wartsila Finland Oy, P.O.Box 244, 65101 Vaasa, Finland

*Corresponding author, e-mail: janne.juoksukangas@tut.fi

ABSTRACT

Fretting fatigue is a potential risk for serious and unexpected damage in modern machine components. A test device has been developed for evaluating fretting fatigue and wear in complete and almost complete contacts with asymptotic edge effects. The device developed also allows plain fatigue testing. The fretting loading can be fully reversing or may fluctuate and it can be adjusted continuously. Macroscopic crack nucleation and growth are followed using strain gauge measurements. A series of fretting fatigue tests and a reference series of plain fatigue tests were carried out with EN 10083-1-34CrNiMo6+QT steel. The fatigue life in the fretting series with a sharp, flat-ended pad was notably lower compared to the plain fatigue life, resulting in a strength reduction factor of 3.

Keywords: fretting fatigue, fretting test device, complete contact

Notation

a	Half-width of a punch
k	Slope exponent of *S-N* curve
K_t	Stress concentration factor
N	Loading cycles
N_{af}	Number of cycles at the point when S-N curve reaches the fatigue limit
N_1	Number of cycles to macroscopic crack nucleation
N_2	Number of cycles to complete fracture
P	Normal load
p	Contact pressure
R	Load ratio
S	Stress
Sa	Arithmetic mean surface roughness
σ_a	Bulk stress amplitude
σ_{af}	Fatigue limit

1. INTRODUCTION

Fretting refers to small amplitude tangential movement between two contacting bodies. The micrometer level oscillating movement can cause wear of the bodies (fretting wear) and decrease fatigue life (fretting fatigue). Fretting exists typically in bonded contacts which are designed to be nominally static, e.g., interference fits and bolt joints. The movement between the bodies can be produced by, for example, vibration. Fretting fatigue can lead to serious and unpredictable damage because fatigue cracking can develop imperceptibly within bodies inside a machine element. A comprehensive review of the fretting phenomenon and related contact mechanics is given in [1–2].

Contacts can be divided into complete and incomplete contact. Complete contact means that the contact area is independent of the applied normal loading. An asymptotic contact pressure $p(x)$ can be found in complete contacts, as shown in Figure 1, where a square-ended punch with a half-width a, is pressed in the y-direction onto an elastic flat plane by a normal load P.

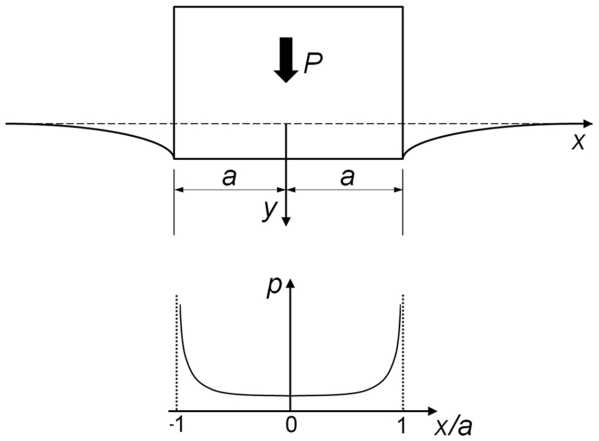

Figure 1. Schematics of a complete contact having an asymptotic contact pressure distribution.

Analytical solutions for physical quantities in complete contacts are limited, but can be found in the case presented in Figure 1, if the punch is rigid and the counter plane is elastic half-space, when, theoretically, stresses are singular at the contact edges [2]. Although the solution is easy to apply, it does not take into account, for example, rounding of the edge, material plasticity, or elasticity of the punch. More complex studies generally involve numerical modeling. However, when using the finite element method, for example, very fine meshes have to be used to capture the steep stress gradients and this leads to time-consuming and expensive calculations.

In the past, attention has been paid to analysis of almost complete contacts, which include a flat portion with rounding at the contact edge, so that the contact size is almost independent of the applied loading [3]. Rounding relieves the theoretical infinite pressure at the edge, though there can still be high stress concentration and slip between the bodies. In practice, a designer normally removes sharp edges, for example, by means of a rounding or a chamfer, thus creating almost complete contact. Wear can also round the edges, either during manufacture or in use. Solutions for contact tractions and subsurface stresses for an almost complete contact, when the edge is rounded and both of the bodies are elastic, are given in [4]. In the past decade, an asymptotic method has been used to characterize complete and almost complete contacts, e.g., [5]. The idea is to present the local stress state, close to the contact edge (crack nucleation regime), by a generalized stress intensity factor. In [6], the stress intensity factors have been found for a contact having similar geometry and boundary conditions to that in the test device developed here.

Experimental fretting tests are important in providing actual fretting data as well as for verifying fretting models. The typical fretting test devices are presented in [1]. In the test arrangements for complete contacts with a pad against a specimen, the axially applied cyclic bulk loading in the specimen can be used to create tangential loading in the contact. These devices are, typically, based on a normal fatigue testing machine, e.g., [7–9], with the addition of a fixed pad holding frame. A disadvantage can be the moderate control of the relative displacement in the contact. Alternatively, to allow separate control of the loading quantities, the holding frame of the pads is used to apply both the normal and tangential loading (shear traction and slip) in the contact [10]. In some cases, the cyclic bulk loading of the specimen is produced by a bending load, such as in [11–12]. Hertzian type test arrangements having incomplete contact are common when singular stress states at the edges and misalignment problems need to be avoided, e.g., [13–14]. Experiments in real applications are still needed for final validation of the modelling results. However, real application tests should be minimized by

modelling and laboratory tests because they are slow and very expensive.

Little attention has been given to the fretting fatigue behaviour of quenched and tempered 34CrNiMo6 steel, which is a commonly used material in heavy load conditions, where the contact surfaces have to transfer high tractions. This material is used, for example, in medium speed diesel engines in components such as connecting rods, camshafts and crankshafts, where the load conditions pose a potential risk of fretting. Most of these joints are nominally plane-to-plane contacts involving cases with edge singularity. Fretting fatigue and wear in incomplete contacts, also with this material, have been successfully evaluated with a sphere-on-flat fretting test device developed in-house [15]. The new test device broadens testing possibilities to take account of the larger contact areas and asymptotic edge effects involved in complete and almost complete contact.

This study focuses on the development of the fretting test device for complete and almost complete contacts. The device allows characterization, for example, of the effect of different contact geometries, materials and operating parameters on fretting fatigue and wear. The design and the characteristics of the test device are examined in detail. In addition, the results of experimental fretting fatigue life with quenched and tempered steel are presented and compared to the plain fatigue results. They are also measured with the same developed device.

2. EXPERIMENTAL

The objective was to develop a compact test device based on complete contact, allowing the evaluation of the effect of different parameters on the fretting response in a controlled environment and also enabling a number of tests to be performed in a relatively short time. For comparison purposes, it should also be possible to conduct plain fatigue tests with the same device. The design and characteristics of the test device developed are described below.

2.1 Test device

The main parts of the test device are a cantilever test specimen and two pads, which create the test contact, and also the applications for normal, tangential, and bulk loadings. A general view of the test device developed is shown in Figure. 2.

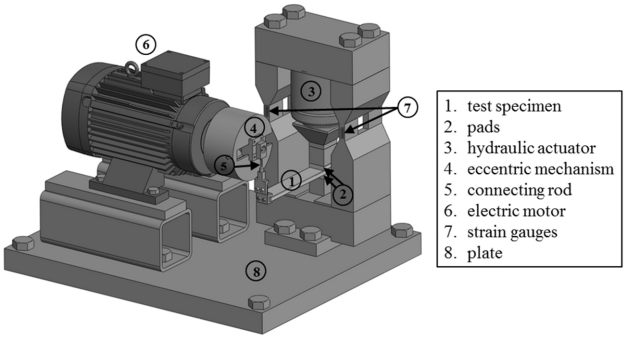

Figure 2. The developed complete contact fretting test device.

The normal load is created by a hydraulic actuator, which clamps the pads and the specimen together. An eccentric mechanism bends the specimen at the free end, creating bulk (bending) stresses in the specimen and tangential loading (shear traction, slip) in the contact. The parts are mounted on a thick steel plate. All non-movable parts were designed to be heavy and rigid to avoid excessive deformation and vibration. The loading path is closed to prevent the transfer of forces or moments generated by the device to the surroundings.

The fretting contacts are formed by the flat specimen clamped between the two flat-ended pads, as shown in Figure 3. An asymptotic contact pressure distribution is created having a pressure peak at the contact edge. A pure normal load is applied by the hydraulic actuator without tangential forces, which eliminates external shear tractions when a normal load is applied. The normal load can be adjusted continuously up to 600 kN, equivalent to an average contact pressure of 300 MPa. The

steel blocks next to the pads are long and narrow so as to guarantee smooth (average) pressure distribution in the test contacts. With complete contacts, it is important to avoid misalignment since this can have a major effect on stress distribution [10].

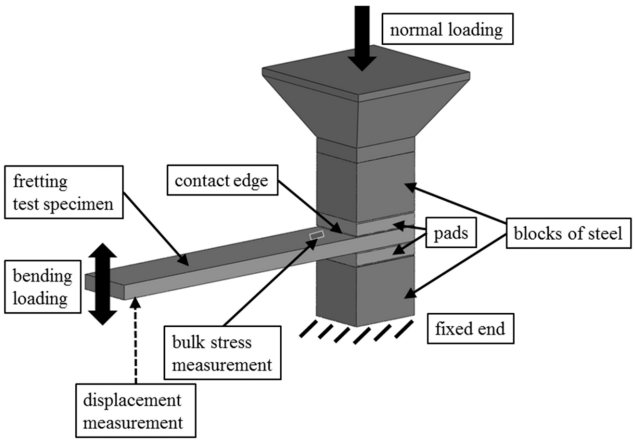

Figure 3. Test contact configuration.

The cyclic loading at the free end of the specimen is created by the eccentric mechanism, as shown in Figure 2. The connecting rod, the lower end of which moves the test specimen tip up and down, is attached to a slider at its upper end. The slider is further connected via a dovetail joint to a crank disc, which is rotated by the motor. The motor is connected to an inverter to allow flexible control of the motor speed. The bottom end of the connecting rod is connected to the specimen via a flexible joint, which prevents clearances and minimizes external moments on the specimen. The dovetail joint allows continuous adjustment of the bending load (bulk stress amplitude) by varying the amount of eccentricity. The mean bulk stress can also be continuously adjusted by varying the length of the connecting rod. The loading of the specimen can therefore be fully reversing or pulsating. The bulk loading has a maximum frequency of 50 Hz and bulk (nominal bending) stresses up to 1000 MPa can be achieved with normal steel. A modal analysis of the device was performed and one suitable driving frequency was found to be 41 Hz, which is high enough to conduct a single test in a day. This frequency was chosen for the subsequent experiments. The test device is fitted with an automatic control system to permit long periods of unmonitored and unsupervised testing.

2.2 Test specimens

The test device can perform fretting fatigue experiments of complete and almost complete contacts with asymptotic contact edge effects. The measurement of plain fatigue can be also carried out by using a plain fatigue test specimen. In plain fatigue experiments, the contact has no effect on the fatigue process. Plain fatigue tests can be used as a reference for fretting tests. The fretting and plain fatigue test specimens are shown in Figure 4.

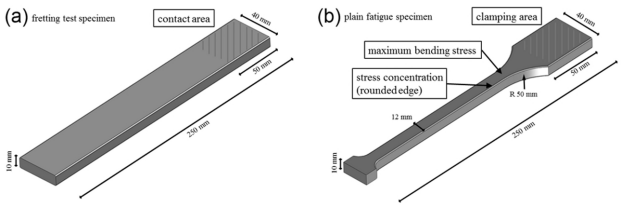

Figure 4. Fretting test specimen (a) and the plain fatigue specimen (b).

The fretting test specimen has a length of 250 mm, a width of 40 mm and a thickness of 10 mm. The edges of the long sides have a rounding of 1 mm. The pads, shown in Figure 3, have a length of 50 mm, a width of 40 mm, a thickness of 10 mm and a small chamfer along the side edges. Almost complete contacts can be evaluated by rounding the contact edge of the pads. These parts forming the test contacts have simple geometries to enable easy and accurate manufacture. The surface finish of the test parts can be chosen according to the needs of a particular test series. In addition, specimens having a surface treatment, e.g., shot peening or a coating, can be tested without any modification to the test device.

In the plain fatigue specimen, the width of the free surface is reduced to a value of 12 mm to move the point of maximum bending stress and hence, the cracking point clearly away from the fixed end, as

shown in Figure 4 (b). In the plain fatigue case, the normal load (contact pressure) is only used to clamp the specimen and it has no effect on the plain fatigue results. This average contact pressure should be high enough, such as 100 MPa, to sufficiently clamp the specimen and the pads together. The test arrangement is otherwise the same in both types of test. A 3D FE-analysis was used to calculate the stress concentration factor, K_t, for the plain fatigue specimen in bending. A K_t value of 1.05 was found for the corners of the specimen, as shown in Figure 4 (b). Fatigue cracking will likely occur there and so attention should be paid to careful polishing of the corners and also the plane surfaces, to minimize surface effects.

2.3 Measurement system

The bulk loading of the specimen and the normal load (average contact pressure) are the main parameters measured. A strain gauge is attached to every specimen to obtain accurately the bulk stress amplitude and the mean stress created by the bending load; see Figure 3. In the fretting specimens, the strain gauge is attached a few millimeters away from the contact edge. Therefore, the measured values are scaled to the contact edge, i.e., the point of maximum bending stress, using the proportion of the lengths. Obviously, the contact stresses are neglected. The scaled values are used in the results reported here. In the plain fatigue specimens, the strain gauge is attached at the point of maximum stress, which takes place in the longitudinal direction 34 mm from the fixed end, Figure 4 (b). This measured value multiplied by the calculated stress concentration factor K_t is used in the reported results. In both cases, the strain gauge also indicates the number of cycles for macroscopic crack nucleation point, as shown below. A laser sensor at the free end of the specimen measures the displacement of the specimen, Figure 3. The displacement signal is used to stop the device if the specimen breaks. The stress values derived from this data can be used to verify the strain gauge values.

The average contact pressure is calculated from the measured normal load and the contact area. The normal load is measured by strain gauges connected to the corners of the normal loading frame (Figure 2) and also from the hydraulic pressure. In addition to the nominal (average) contact pressure, the four-point strain gauge measurement shows the uniformity of the average contact pressure. If the strain values at all four corners of the frame are equal, the nominal pressure distribution in the contact can be assumed to be smooth. All the measurement sensors are regularly calibrated. The laser sensor is calibrated with a dial gauge and both of the normal load measurement methods using an external force sensor. All the measured data are collected onto a computer for further analysis purposes.

The number of load cycles for the macroscopic crack nucleation point is estimated from the data of the strain gauge on the specimen, which is located near the crack nucleation point in both specimens. The growing crack releases the local stresses, which at some point are reflected in the strain gauge data. Figure 5 shows a typical bulk stress envelope graph of a cracked fretting specimen during a test having a fully reversed loading (load ratio R = -1). The bulk stress amplitude is shown as a function of loading cycles. The bulk stress amplitude is 299 MPa.

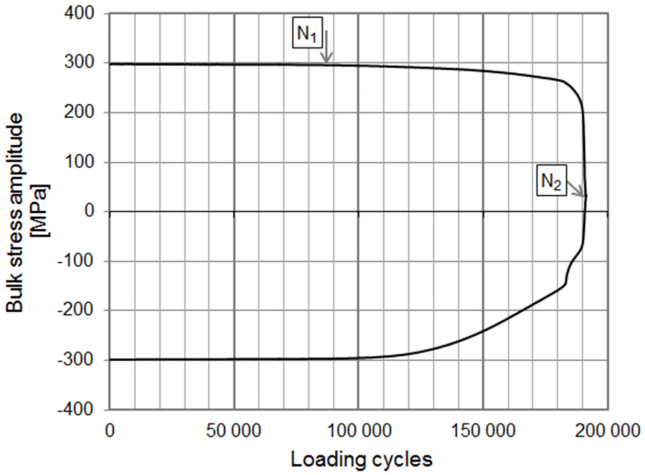

Figure 5. Envelope of the bulk stress amplitude during a test.

Figure 5 shows that there is a decrease on both sides of the measured bulk stress before complete fracture occurs after 191 000 cycles, when the bulk stress is reduced to zero. The specimen was cracked on both upper and lower sides. The macroscopic crack nucleation point, N_1, is defined by a 0.5% decrease in the bulk stress amplitude. It is estimated that the crack should be at least several tenths of a millimeter in depth before it is observed with this method. The upper side of the stress envelope has reached the N_1 limit after 87 000 cycles, indicating that the specimen has cracked. Similarly, the macroscopic crack nucleation point for the lower side is 107 000 cycles. The smaller N_1 value is used in the reported results. Value N_2 is the total number of cycles required for complete fracture.

2.4 Test series

A fretting fatigue life test series with 12 points and four stress levels was performed. A plain fatigue series with 10 points and three stress levels was performed to determine the fatigue strength of the material. In plain fatigue tests, contact issues are not involved in the fatigue process. The test material for the specimen and pads was quenched and tempered steel EN 10083-1-34CrNiMo6+QT. The ultimate strength of the material is 1031 MPa and the 0.2% yield strength is 927 MPa. Brinell hardness value HBW is 321. In both types of test, a fully reversed bending loading was applied at a frequency of 41 Hz. Three million cycles was set as the upper test limit, which means approximately 20 hours of testing. The sampling frequency was 2000 Hz for the strain gauge and laser measurements and 50 Hz for the other measurements. Prior to the tests, the specimen and pads were carefully cleaned with solvent. The tests were conducted at normal room temperature and humidity.

In the fretting tests, the specimens and pads were ground longitudinally. The front face of the pads was also ground to make the contact edge sharp and to gain uniform edge qualities for the pads. Obviously, there will be always present some radius at the contact edge. Contact edges were measured by an optical microscope and an estimate for the radius was found to be around 20 µm. The specimens were also measured before testing with an optical profilometer. The analyzed surface area was 4.9 × 3.8 mm^2, with a 6.72 µm sampling period. The arithmetic mean surface roughness, S_a, was 0.3 µm, and this was the same for both the specimens and the pads. The constant average contact pressure was 100 MPa and the bulk (bending) stress amplitude of the specimen, measured and scaled to the contact edge, ranged from 116 MPa to 303 MPa.

In the plain fatigue tests, stress levels from 408 MPa to 685 MPa were used. The plain fatigue specimens were also ground longitudinally and had a mean S_a value of 0.2 µm. The corners of the free surface were polished. In the plain fatigue tests, an average contact pressure of approximately 100 MPa was used, although it does not have an effect on the results if a sufficient value is used to clamp the parts tightly together.

3. RESULTS

3.1 Crack nucleation point

After the tests, the specimens were inspected visually and some with an optical microscope and scanning electron microscopy (SEM). In the fretting specimens, the cracks were invariably nucleated at the contact edge and propagated approximately normal to the contact surface. The cracks were nucleated evenly either on the upper or the lower side of the specimen. Often the cracks had been nucleated on the both sides of the specimen, as shown on the left in Figure 6, where the cracks meet approximately at the centre line. The envelope of the bulk stress showing the number of cycles for the macroscopic crack nucleation of this specimen was shown in Figure 5. A cracked surface of a plain fatigue specimen is shown on the right in Figure 6.

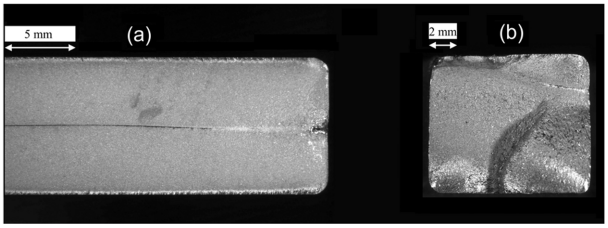

Figure 6. Fracture surfaces of a fretting specimen (a) and a plain fatigue specimen (b).

In the fretting specimens, cracks have been nucleated in the central region of the contact edge in the lateral direction. There were no cracks clearly nucleated from the corners. Typically, several initial cracks were nucleated along the contact edge and coalesced into these larger cracks. Depending on the geometry of the contacting bodies, the ends of the contact edge can generate a stress concentration and, hence, an increased cracking risk. The geometry used in this study and in part of the experimental tests in [16] causes local stress concentration at the corners of the contact edge, but in neither case did it seem to affect the crack nucleation mechanism. In the plain fatigue specimens, however, cracks were often nucleated at the corners of the specimen and in the longitudinal direction, roughly at the point of maximum bending stress.

3.2 Fatigue life

The results of the both test series are presented here in the form of *S-N* curves. The measured bulk (bending) stress amplitude in the specimen is plotted against the number of cycles required for complete fracture (N_2) as well as the number for macroscopic crack nucleation (N_1). In the fretting fatigue tests, the measured stress value is scaled to the contact edge and in the plain fatigue tests the measured value is multiplied by the calculated stress concentration factor. The fatigue limit in the fretting and plain fatigue series is determined by treating the test points around the fatigue limit as a staircase test points, even though the number of test points in this case was low [17–18]. The mean fatigue limit is obtained by application of the maximum likelihood method. The least squares method was used to draw the finite lifetime line. Figure 7 shows the bulk stress amplitude against the number cycles required for complete fracture (S-N_2) for both test series. The equation for the curve fitting is also shown. It has the following form:

$$\sigma_a = \frac{\sigma_{af}}{\left(\frac{N}{N_{af}}\right)^{1/k}} \quad (1)$$

where σ_a is the bulk stress amplitude when the number of load cycles is N. The fatigue limit is σ_{af} and N_{af} is the number of cycles at the point when the *S-N* curve reaches the fatigue limit. The slope exponent of the curve is k.

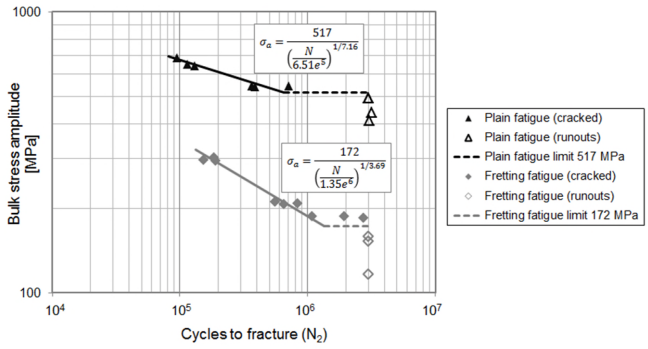

Figure 7. Fretting fatigue and plain fatigue test results (N_2).

The points at three million cycles are run outs, where the specimens have not been cracked. In both series, the lifetime decreases as the bulk stress amplitude increases. A fatigue limit of 517 MPa was achieved in the plain fatigue tests, which is about half the measured ultimate strength of the test material. A fatigue limit of 172 MPa was achieved in the fretting tests, showing a marked decrease in fatigue strength. The scatter of the results is small, suggesting good repeatability of the tests.

Similarly, the bulk stress amplitude against the number of cycles for macroscopic crack nucleation point (S-N_1) for both series is shown in Figure 8. The N_1-point for one of the test points at a stress level of 544 MPa is not available due to a strain-gauge failure. There are two test points at the stress level of 493 MPa.

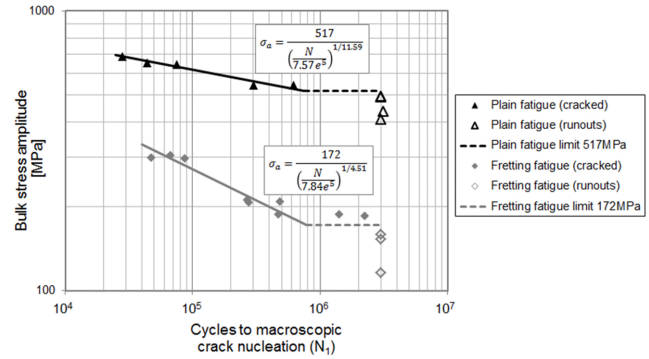

Figure 8. Fretting fatigue and plain fatigue test results (N_1).

In both series, there is a shift to the left in finite lifetime points compared to the corresponding N_2 values. Otherwise, the shapes of the curves are similar. The scatter of the results is small in this case, which suggests that the mechanism and location of macroscopic crack nucleation remain virtually constant. To conclude, the results show a major impact of fretting and edge singularity on the lifetime of the specimens. The resulting strength reduction factor achieved in these tests is three. In addition, the results indicate good repeatability of the tests with both analysis methods (N_1 and N_2).

In future tests, the crack shape and size at the macroscopic crack nucleation point will be determined by stopping the device when the bulk stress starts to decrease. The determination of this macroscopic crack nucleation point and crack growth widens the scope of the device for verifying fretting fatigue life models. In addition, the measurement of relative displacement will be realized in future work, which is important in terms of fretting wear. Also being considered is the development of a way or a device to measure the bulk stress in the specimen without a strain gauge.

3.3 Wear scars

Figure 9 shows an example of a fretting scar at the central region of a fretting specimen.

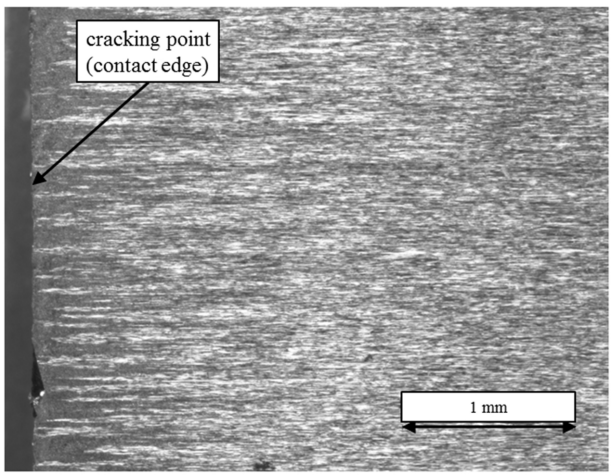

Figure 9. Fretting scar on a specimen.

The contact edge point, i.e. the cracking point, is on the left. The fretting marks can be seen almost two millimeters from the contact edge. Near the edge,

the machining marks have been worn away completely, meaning that wear depth is of a similar magnitude to surface roughness. Moving away from the edge, the unchanged surface area increases. The wear marks have roughly similar dimensions for different specimens, although more severe wear domains are observed in specimens that had higher bulk loading.

4. CONCLUSIONS

A test device has been developed for evaluating fretting fatigue and wear at complete and almost complete contacts with asymptotic edge effects. The device developed also allows plain fatigue testing. The device has uniform nominal contact pressure, which can be measured. The cyclic bending load of the specimen introduces tangential loading into the contact. The bending load can be fully reversing or fluctuating and it can be adjusted continuously. Macroscopic crack nucleation and growth are recorded by strain gauge measurements. A loading frequency of up to 50 Hz results in relatively short testing times.

A fretting fatigue test series and a reference plain fatigue test series were carried out using quenched and tempered EN 10083-1-34CrNiMo6+QT steel. In the fretting tests, the average contact pressure was kept constant and the bulk stress varied. The fatigue lives in the fretting series with a sharp, flat-edged pad were notably lower compared to the plain fatigue results, leading to a strength reduction factor of three. In addition, the results indicate good repeatability of the fatigue tests.

The analysis of the fretting scars revealed that local slip can occur at about two millimeters away from the contact edge and that the maximum wear depth is similar to the maximum peak-to-valley height of the initial profile.

FUNDING

This work was supported by Wartsila Finland Oy, Metso Paper Oy and Tekes (Finnish Funding Agency for Technology and Innovation).

ACKNOWLEDGEMENTS

The work has been done within FIMECC Ltd and its DEMAPP program. The authors wish to thank Janne Kortelainen, MSc, Juhani Vestola, MSc, Christian Lonnqvist, MSc, and Olli Nuutila, LicSc, for their work in developing the test device. Jussi Laurila, LicSc, is acknowledged for support in the fracture surface analysis.

REFERENCES

1. Hills DA and Nowell D. *Mechanics of Fretting Fatigue*. Dordrecht: Kluwer Academic Publishers, 1994.
2. Johnson KL. *Contact Mechanics*. Cambridge, UK: Cambridge University Press, 1985.
3. Hills DA and Mugadu A. An overview of progress in the study of fretting fatigue. *J Strain Anal Eng Des* 2002; 37(6): 591–601.
4. Ciavarella M, Hills DA and Monno G. The influence of rounded edges on indentation by a flat punch. *P I Mech Eng C-J Mec* 1998; 212(4): 319–328.
5. Mugadu A, Hills DA and Limmer L. An asymptotic approach to crack initiation in fretting fatigue of complete contacts. *J Mech Phys Solids* 2002; 50(3): 531–547.
6. Hills DA, Paynter RJH and Dini D. An overview of the quantification of fretting fatigue lives of complete contacts. *Eng Fract Mech* 2012; 80: 3–12.
7. Arora PR, Jacob MSD, Salit MS, et al. Experimental evaluation of fretting fatigue test apparatus. *Int J Fatigue* 2007; 29(5): 941–952.
8. Wittkowsky BU, Birch PR, Dominguez J, et al. An apparatus for quantitative fretting fatigue testing. *Fatigue Fract Eng Mater Struct* 1999; 22(4): 307–320.
9. Sabsabi M, Giner E and Fuenmayor FJ. Experimental fatigue testing of a fretting complete contact and numerical life correlation

using X-FEM. *Int J Fatigue* 2011; 33(6): 811–822.

10. Mugadu A, Hills DA and Nowell D. Modifications to a fretting-fatigue testing apparatus based upon an analysis of contact stresses at complete and nearly complete contacts. *Wear* 2002; 252(5–6): 475–483.
11. Peng JF, Song C, Shen MX, et al. An experimental study on bending fretting fatigue characteristics of 316L austenitic stainless steel. *Tribol Int* 2011; 44(11): 1417–1426.
12. Alfredsson B. Fretting fatigue of a shrink-fit pin subjected to rotating bending: Experiments and simulations. *Int J Fatigue* 2009; 31(10): 1559–1570.
13. Fridrici V, Fouvry S and Kapsa Ph. Fretting wear behavior of a Cu–Ni–In plasma coating. *Surf Coat Technol* 2003; 163–164: 429–434.
14. Zheng JF, Yang S, Shen MX, et al. Study on rotational fretting wear under a ball-on-concave contact configüration. *Wear* 2011; 271(9–10): 1552–1562.
15. Pasanen A, Jarvisalo S, Lehtovaara A, et al. Development of a test device for the evaluation of fretting in point contact. *Lubr Sci* 2009; 21(2): 41–52.
16. Dini D. *Studies in Fretting Fatigue With Particular Application to Almost Complete Contacts*. PhD Thesis, Christ Church, University of Oxford, Trinity Term, 2004.
17. Dixon WJ and Mood AM. A Method for Obtaining and Analyzing Sensitivity Data. *J Am Stat Assoc* 1948; 43: 108–126.
18. Rabb BR. *Fatigue Testing and Its Statistical Evaluation into Design Rules*. PhD Thesis, Tampere University of Technology, Publications 253, 1999.

Publication II

Response to discussion with DA Hills et al., concerning the article “Development of a complete contact fretting test device” by J Juoksukangas et al.

by

J. Juoksukangas, A. Lehtovaara and A. Mäntylä

Proc. IMechE, Part J: J. Engineering Tribology, 228(1), 2014, 127–128,
doi:10.1177/1350650113500947

Response to discussion with DA Hills et al., concerning the article "Development of a complete contact fretting test device" by J Juoksukangas et al.

J. Juoksukangas[1]*, A. Lehtovaara[1] and A. Mantyla[2]

[1]Department of Engineering Design, Tampere University of Technology, Finland
[2]Research & Development, Wartsila Finland Oy, Finland
*Corresponding author: Janne Juoksukangas, email: janne.juoksukangas@tut.fi

1. INTRODUCTION

The authors are grateful for the valuable comments concerning the developed complete contact fretting test device. In the original article[1], the primary goal was to introduce the design, instrumentation and proper functionality of the test device. In addition, the results of the first fretting and plain fatigue tests are shown in basic form. In the discussion paper[2] the respondents suggest that the experimental data could be processed more comprehensively and propose an asymptotic stress analysis. The proposed method is, in this respect, a welcome extension to the original article.

In the original article, the fretting fatigue test results are compared to the plain fatigue test results using the nominal bending stress value in the specimen. Although in the plain fatigue tests this nominal stress value can be used to describe the state of stress in the crack nucleation regime, in the fretting tests the case is very different due to the complex stress state at the contact edge, as pointed out in the discussion paper. Nevertheless, this classical way of representing the results is commonly used in mechanical engineering. As noted by the respondents, a disadvantage is that the results in this case may not be easily interpreted and generalized.

2. ASYMPTOTIC STRESS ANALYSIS

The respondents propose an asymptotic stress analysis method to interpret data from the test device. Such a method was also mentioned by the authors in the original article. Not only can the stress state at the crack nucleation regime be found by using this method, but the crack nucleation conditions can also be quantified and used further for similar geometries. The authors calculate that contact separation has occurred in each fretting test, which inevitably means that slip has also occurred between the surfaces, despite of the friction coefficient. Indeed, fretting marks caused by slip were found in all the test specimens. However, as the respondents note, slip can also be created when the contact is fully closed but the coefficient of friction is lower than the given value $g^{I}_{r\theta} = 0.543$.

In the asymptotic analysis of the discussion paper, it is assumed that the mode *I* stress intensity controls the crack nucleation. The fretting test results from the original paper are presented in the form of a $\Delta K_I - N_I$ curve and the fatigue limit is found in terms of the stress intensity factor, which is a very interesting outcome. Only the macroscopic crack nucleation test data (from Figure 8) is used. It should be emphasized that the crack already has a macroscopic length, and its recognition depends on the measurement system

used. Calibration of the system is a future plan, as noted in the original article.

In terms of universalizing the results to different loading conditions, a disadvantage of the current procedure may be that ΔK_I does not take into account the effect of the static clamping load p_0. With the developed test device, it has been shown[3] that the fretting fatigue limit increases by about 15 % when using a contact pressure value of 30 MPa, compared to the value of 100 MPa. These results suggest, therefore, that the clamping load should be taken into account if the results are to be transferred over different loading conditions, i.e., contact pressure values. The respondents acknowledge, however, that more advanced investigation lies beyond the scope of the discussion paper.

Use of the asymptotic method seems to be an effective way of quantifying fretting or notch fatigue crack nucleation. After numerical calculation of the stress intensity factors, the method is fast to apply. At present, it seems that experimental fretting test data with the same material but at least with different loading conditions is needed to validate the asymptotic method as a crack nucleation tool.

3. CONCLUSIONS

The respondents propose an asymptotic stress analysis method to interpret data from the developed fretting test device and show impressive outcomes. They present the original fretting fatigue test results in the form of a ΔK_I –N curve and the fatigue limit is found in terms of the stress intensity factor, which is also used for different geometries. The present version of the proposed method could benefit from implementing the effect of static clamping load on ΔK_I. More tests with the same material and different loading conditions are proposed for validating the use of asymptotics, which presently seems to be an effective and powerful method.

ACKNOWLEDGEMENTS

This study has been carried out within FIMECC Ltd (Finnish Metals and Engineering Competence Cluster) and its DEMAPP program. The authors are grateful for the financial support provided by Wartsila Finland Oy, Metso Paper Oy and Tekes (Finnish Funding Agency for Technology and Innovation). In addition, the doctoral program in Concurrent Mechanical Engineering (CME) and the Academy of Finland are acknowledged.

REFERENCES

1. Juoksukangas J, Lehtovaara A and Mantyla A. Development of a complete contact fretting test device. *Proc. IMechE, Part J: J. Engineering Tribology* 2012; 227(6): 570–578.
2. Hills DA, Flicek RC and Dini D. A discussion of: Development of a complete contact fretting test device by J. Juoksukangas, A. Lehtovaara and A. Mantyla. *Proc. IMechE, Part J: J. Engineering Tribology* 2013.
3. Juoksukangas J, Lehtovaara A and Mantyla A. Effect of contact pressure on fretting fatigue life in complete contacts. *Proceedings of the Seventh International Symposium on Fretting Fatigue* (ISFF7). Oxford University, Oxford, UK, 2013, 2 p.

Publication III

The effect of contact edge geometry on fretting fatigue behavior in complete contacts

by

J. Juoksukangas, A. Lehtovaara and A. Mäntylä

Wear, 308(1–2), 2013, 206–212, doi:10.1016/j.wear.2013.06.013

Wear 308 (2013) 206–212

Contents lists available at ScienceDirect

Wear

journal homepage: www.elsevier.com/locate/wear

The effect of contact edge geometry on fretting fatigue behavior in complete contacts

Janne Juoksukangas [a,*], Arto Lehtovaara [a], Antti Mäntylä [b]

[a] Engineering Design, Tampere University of Technology, P.O. Box 589, 33101 Tampere, Finland
[b] Research & Development, Wärtsilä Finland Oy, P.O. Box 244, 65101 Vaasa, Finland

ARTICLE INFO

Article history:
Received 5 December 2012
Received in revised form
24 May 2013
Accepted 17 June 2013
Available online 20 July 2013

Keywords:
Fretting fatigue
Complete contact
Cracking risk
Contact edge geometry

ABSTRACT

The effect of contact edge geometry on the fretting fatigue behavior of a complete contact was studied with 34CrNiMo6 quenched and tempered steel. The contact geometries employed were sharp and rounded square-ended pads against a plane surface. A 2D elasto-plastic finite element model of the contact setup was used to calculate fretting cracking risk for these geometries using the Findley multiaxial fatigue criterion and the theory of critical distances. A series of experimental fretting fatigue tests was carried out with two corresponding geometries and loadings using an in-house complete contact fretting test device. It was found that the slightly rounded contact edge has a somewhat higher risk of cracking than the sharp contact edge. This agrees with the experimental results. The effect of the friction coefficient on the cracking risk was also studied. In addition, fretting wear scars from the experimental test specimens were evaluated.

1. Introduction

Fretting refers to small amplitude tangential motion between contacting bodies. The micrometer-level oscillating movement can cause wear of the bodies (fretting wear) and decrease the fatigue life (fretting fatigue). Fretting typically occurs in contacts such as interference fits and bolt joints, which are designed to be nominally static. The movement between the bodies can, for example, be produced by vibration. Fretting fatigue can lead to serious and unpredictable damage because fatigue cracks may nucleate in contacts inside a machine element. The fretting phenomenon and related contact mechanics are explained in Refs [1,2].

Contacts can be divided into complete and incomplete contacts. Complete contact means that the nominal contact area is independent of the normal loading applied, whereas in the case of incomplete contact, the contact area depends on the normal loading. An example of an incomplete contact would be a cylinder pressed against a plane. A complete contact can be created, for example, if a square-ended punch is pressed against a flat plane. The resulting contact pressure distribution is asymptotic with a steep stress gradient at the contact edges. Until recently, attention has focused on the analysis of almost complete contacts which include a flat portion with rounding at the contact edge so that the nominal contact size is almost independent of the applied loading. Rounding relieves (theoretical) infinite stresses at the edge, though there can still be high stress concentration and slip between the bodies. In practice, a designer normally removes sharp edges, for example, by rounding or chamfering, thus creating almost complete contact. Wear can also round the edges either during manufacture or in use.

An asymptotic analysis of a complete contact can be carried out to determine the stress state at the contact edge, i.e., the crack nucleation regime. This has been done for a similar test configuration used here in Ref. [3]. Formulations for contact tractions and internal stresses for an almost complete contact, when the edge is rounded and both of the bodies are elastic, are given in [4]. To accurately take account of parameters such as specific contact geometry and material plasticity, numerical methods are usually needed. However, when using, for example, the finite element method (FEM) in complete contact modeling, very fine meshes have to be employed to capture the steep stress gradients. This may involve time-consuming and expensive calculations as well as possible convergence problems.

Traditional multiaxial fatigue models have been applied to fretting fatigue. Fouvry et al. [5,6] found that fretting fatigue predictions with a multiaxial fatigue criterion were systematically too conservative and better results were achieved when the stresses were averaged over a small structural volume. The size of this volume was linked to a material's microstructure (grain size). Araujo and Nowell [7] have successfully used averaging methods to correct critical plane calculations with experimental data. They found that the averaging dimension corresponds to the

* Corresponding author. Tel.: +358 3 311511; fax: +358 3 31152307.
E-mail address: janne.juoksukangas@tut.fi (J. Juoksukangas).

0043-1648/$ - see front matter © 2013 Elsevier B.V. All rights reserved.
http://dx.doi.org/10.1016/j.wear.2013.06.013

grain size of the material used, though they note that the dimension may not necessarily be a material constant. The theory of critical distances [8] has also been applied to fretting fatigue, e.g., [9]. Similar approaches, where the internal stress state below a contact surface is used, have been also employed [10,11]. Finally, the use of discrete elements in the finite element method implicitly leads to an averaging of stresses.

Research into the role that contact edge geometry plays in fretting fatigue has typically been based on a punch-on-flat configuration with axial bulk loading. For example, in Ref. [12] it was found that a punch with small rounding (radius 0.4 mm) has a longer fatigue life than a large (radius 3.2 mm) one. In Ref. [13] fretting fatigue life with a flat pad was longer than that with a flat and rounded pad with rounding of 2 mm. In an FE-study of a shrink-fit assembly, Francis et al. [14] found that when the contact edge was rounded, stresses increased as the rounding increased and hence rounding of the contact edge of such an assembly was not recommended.

The objective of this study was to evaluate fretting fatigue behavior in complete and almost complete contacts. The risks of fretting fatigue were calculated for contacts having different contact edge geometries and were compared with the corresponding experimental results obtained with an in-house complete contact fretting test device.

2. Experimental test device

The contact setup of the in-house complete contact fretting test device includes a cantilever fretting test specimen, two pads and two blocks of steel as shown in Fig. 1. A detailed description of the test device and test procedure is given in [15]. Only a brief overview of the experiments is given here.

The specimen and the pads, which create the two test contacts, are clamped together by a normal load (constant nominal contact pressure). Cyclic bulk loading of the specimen is created by deflecting the specimen tip. This bending creates a fretting regime close to the contact edge, where relative movement (slip) is created between the pad and specimen. The test specimen has a length of 250 mm, a width of 40 mm and a thickness of 10 mm. The pads have a length of 50 mm, a width of 40 mm and a thickness of 10 mm. The non-moving parts of the test device are heavy and the design is stiff to prevent excessive deformation and vibration.

In the present tests, the material used in the specimen and the pads was EN 10083-1-34CrNiMo6+QT. Both the sharp and rounded edge specimens and pads were ground longitudinally, which produced an arithmetic mean surface roughness (Sa) of 0.3 μm. This was measured with a Wyko NT1100 optical profilometer. The analyzed surface area was 4.9×3.8 mm^2, with a 6.72 μm sampling period. The front face of the complete contact pads was also ground to form a sharp contact edge and to give the pads uniform edge qualities. For the almost complete contact pads, the contact edge was rounded. The rounding was milled and carefully ground and polished by hand. The geometry of each rounding was inspected with an optical microscope to confirm the quality. New specimens and pads were introduced in every test.

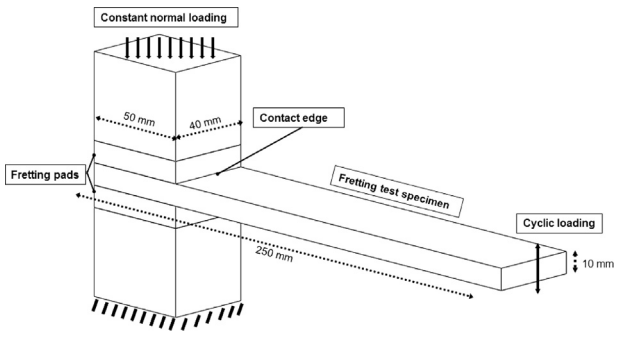

Fig. 1. A schematic view of the test contact setup, showing only parts around the fretting contact.

3. Modeling

The contact setup of the complete contact fretting test device was modeled using ABAQUS FE-program 6.10 [16]. The FE-model includes the test specimen, two pads and two blocks of steel, as shown in Fig. 2 for the sharp-edged case.

A two-dimensional plain strain model was created. This is a reasonable choice because, in the experiments, the crack nucleation point was found to be in the middle zone of the contact edge. Linear, four node CPE4I elements were employed in the model. The mesh is very fine at the contact edges with an element size of 15 μm × 15 μm, which is the same order of magnitude as the grain size of the steel used. Several elements of the same size were used around the contact edge, covering the entire slip area. Contact pressure is created by applying a normal load to the top of the upper block, while the lower end of the block is fixed in the y-direction. The midpoints of the bottom block end and the upper block end are fixed in the x-direction. Bulk loading of the specimen is created by displacement-controlled loading at the tip of the free end of the specimen. A similar bending moment acts in the contact edge points, denoted $x=50$ mm in the sharp-edged case and $x=49$ mm in the rounded-edge case.

For the almost complete contact model, the contact edge was rounded to have a specific radius of curvature, mainly 1 mm. The other dimensions were the same. The mesh was similar to the sharp-edged case, i.e., the element size at the edge is 15 μm and the mesh of the specimen is the same in both models. The finite element model for the rounded edge is shown in Fig. 3. The figure also schematically shows elastic deformations at the contact edge. When normal load is applied, the point of nominal (initial) contact edge, a (which is the width of the flat part of the pad), moves to point b.

The contact surface interaction between the specimen and pads was defined in Abaqus by a master-slave algorithm, in which the specimen was the master surface. The Coulomb friction model was used to describe the frictional behavior of the contacting surfaces. The contact is sticking, i.e., there is no relative tangential movement between the surfaces until the shear traction is equal to a critical value, τ_{crit}, Eq. 1.

$$\tau_{crit} = \mu p \tag{1}$$

This critical value is achieved by multiplying the contact pressure p by the coefficient of friction μ. The Lagrange friction

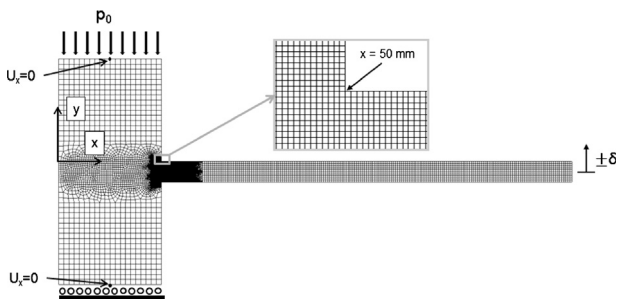

Fig. 2. FE-model of the sharp-ended contact.

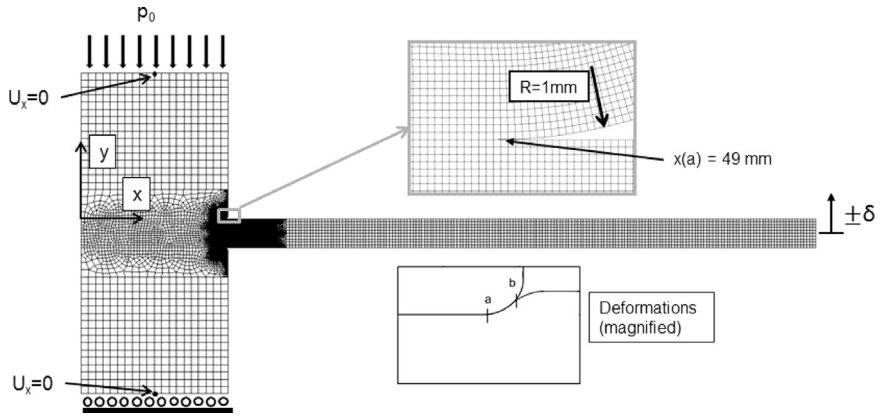

Fig. 3. FE-model of the contact having a rounded edge.

formulation was used to determine the tangential behavior of the contact, which is the most accurate generally used algorithm to describe the stick-slip behavior. The material used was EN 10083-1-34CrNiMo6+QT having an elastic modulus of 206 GPa and Poisson's ratio of 0.28. The ultimate strength of the material is 1030 MPa and the 0.2% yield strength is 930 MPa. An elasto-plastic material model with isotropic hardening was used. The stress–strain relationship after 890 MPa is described by the power law equation:

$$\sigma = 1160MPa * \varepsilon^{0.62} + 890MPa \quad (2)$$

In the equation, σ and ε are true stress and true plastic strain, respectively. Symmetric behavior was assumed for both tension and compression sides. Plastic deformations at the contact edge were limited to a local area and therefore the stress-based multiaxial Findley fatigue criterion is used to calculate the risks of fretting fatigue cracking [17]:

$$d = \max\left[\frac{\tau_a(t) + k_F\sigma_n(t)}{f_F}\right] \quad (3)$$

where $\tau_a(t)$ is the shear stress amplitude and σ_n is the normal stress in the critical plane. The constants f_F and k_F are material parameters for which values of 380 MPa and 0.29 were used, respectively. These values were obtained from separate experiments for the same steel grade, although with slightly different properties compared to the actual steel used here. However, it is expected that the possible error in the f_F value due to this mismatch could be 10% at maximum. Value d is the maximum cracking risk. A cracking risk value above one suggests that failure is likely to occur with some probability. The nodal stress components from the two extreme cases (tip down and tip up) were captured for use in the cracking risk calculation. The Findley cracking risk values were calculated in a Matlab environment [18]. Python codes were written to allow automated FE-runs, by setting only input values for different tests. Output values, mainly the cracking risk values, are automatically calculated and tabulated.

Cracking risks were calculated with several bulk load levels and friction coefficients. In this study, the nominal contact pressure was 100 MPa in all the cases. At the beginning of the analysis the pads and the specimen were clamped together by the applied normal load with a friction coefficient of 0.2. The bulk loading of the specimen was then executed with a specific friction coefficient value. A single loading cycle comprises a down and up movement of the specimen. Five load cycles were performed to represent steady-state contact conditions, i.e., tractions and slip. However, in most of the calculation cases two or three cycles would have been sufficient. Friction coefficient values of 0.4, 0.6, and 0.8 were used to represent steady-state conditions. A wide range of friction coefficient values was used because it is known that fretting can dramatically change frictional behavior. Normally, in steel to steel contact the friction coefficient is initially around 0.2, but this increases to higher values as fretting occurs, i.e., the number of load cycles increases in the contact. Typical friction coefficient values around 0.6 have been experimentally measured and used in calculations relating to complete and almost complete contacts, e.g., [13,19]. Somewhat similar nominal bulk stress amplitudes at the contact edge were used in the specimen as in the experiments.

The theory of critical distances (TCD) was utilized in the cracking risk calculations [8]. Cracking risks were determined by the stress state defined at a distance below the surface, i.e., using the point method. Due to the lack of a parameter needed to calculate the critical distance according to the theory [8], a distance of 15 μm below the surface was chosen instead. The distance reflects the level of grain size, though this is not determined precisely. The critical distance has often been linked to the material microstructure, i.e., scale of grain size, as discussed earlier. The TCD method has the advantage that the material behavior can be elastic at that depth or at least the highest plasticity is relieved. The use of any miscalculated (non-converged) surface stress values can also be avoided.

4. Results and discussion

4.1. Experimental fretting fatigue results

The fretting fatigue tests were conducted using the in-house complete contact fretting test device. Twelve tests both with the sharp edge and rounded edge specimens were performed. The results for the sharp contact edge are presented in Ref. [15]. Nominal contact pressure was 100 MPa. This average contact pressure is determined by dividing the applied normal load by the nominal contact area. This was done without taking into account the deformations in the rounded edge case. Nominal bulk (bending) stresses at the contact edge varied from 116 MPa to 395 MPa. The slight increase in the 'free' length of rounded test specimen due to the rounding was taken into account in the tests. Five main bulk stress levels were used in the both tests. The tests were carried out with fully reversed loading ($R=-1$) and the cut-off limit was three million cycles.

The results for both types of test are shown in Fig. 4, where the maximum nominal bulk (bending) stress amplitude of each test specimen is plotted as a function of the amount of loading cycles to fracture. The fatigue limits for sharp and rounded edges were determined by reproducing a staircase test and the limits were

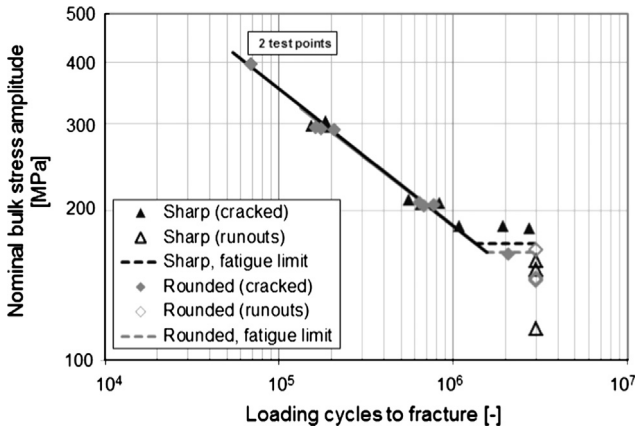

Fig. 4. Experimental fretting fatigue results for sharp and rounded contact edge cases.

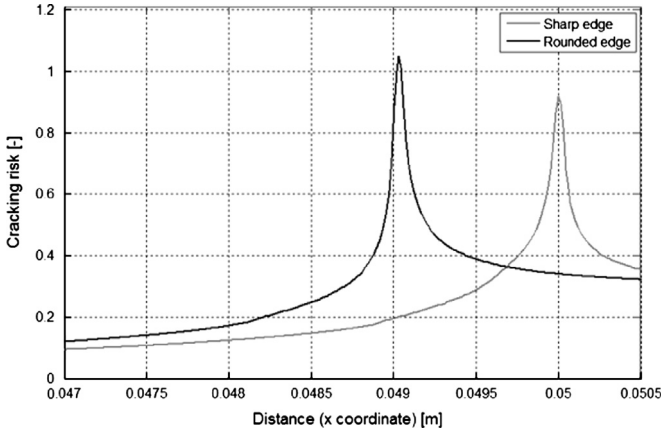

Fig. 5. Examples of the cracking risk curves along the *x*-direction near the contact edge.

obtained by application of the maximum likelihood method [20,21].

The figure shows that very similar fatigue lives are achieved in the finite regime and the fatigue limits are also at similar levels. In the detailed analysis, the sharp-ended contact has a slightly higher fatigue limit than the rounded one. In the sharp edge case, a fatigue limit of 172 MPa was achieved and for the rounded edge, this limit was 165 MPa. However, more tests would be needed to improve the statistical reliability of the results. In both cases fretting scars were observed in every test specimen indicating that there has been relative movement (slip) between the fretting specimen and pad.

4.2. Modeling results

Examples of the fretting fatigue cracking risk curves at a contact edge are shown in Fig. 5 for both sharp and rounded edge cases. The friction coefficient used was 0.6 and the nominal bulk stresses are close to the experimental fretting fatigue limits.

In the sharp edged case, the maximum cracking risk occurs at the contact edge, where a steep peak exists. In the rounded edge case, a similar kind of behavior is observed. The point of maximum cracking risk moves slightly from the nominal contact edge position ($x=49$ mm), due to elastic deformations. The contact edge was also the location where the specimens mainly cracked in the experiments, though there were a few specimens in both series where cracking appeared some tenths of a millimeter inside the contact (from the contact edge). Cracking risk maps for both the sharp edge and rounded edge cases are presented in Figs. 6 and 7, respectively. The maximum cracking risk of a test is plotted against the nominal bulk stress amplitude at the contact edge (excluding contact stresses). The gray vertical line is the fretting fatigue limit achieved in the experiments.

Figs. 6 and 7 show that both contacts display very similar cracking risk behavior. Detailed inspection reveals that the rounded edge has a slightly higher cracking risk around the fatigue limit than the sharp edge. This agrees with the experimental results, where the fatigue limit achieved with a rounded edge was slightly lower than with a sharp-edge contact. The results also show that, when using a friction coefficient in the range of 0.6–0.8, the calculated Findley cracking risk in both cases has a value close to one, with the nominal bulk stress amplitude value corresponding to the fatigue limit obtained in the experiments. Cracking risks with the lowest value of friction coefficient are too small. The values used for the calculation distance and coefficient of friction appear realistic, as discussed earlier. Increasing the friction coefficient has the effect of increasing the cracking risk and the trend is

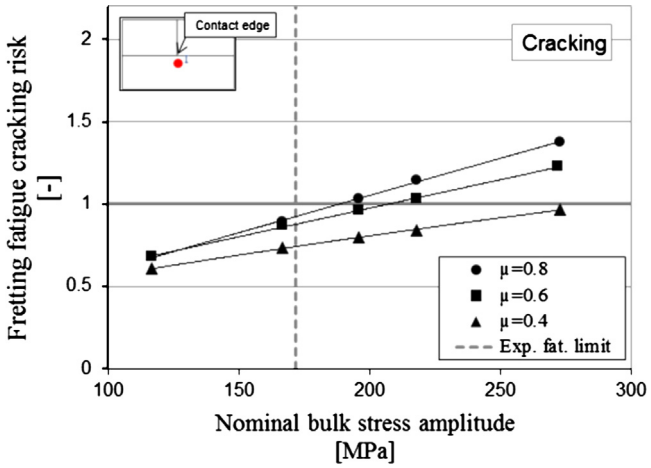

Fig. 6. Cracking risks compared to the experimental results (sharp contact edge).

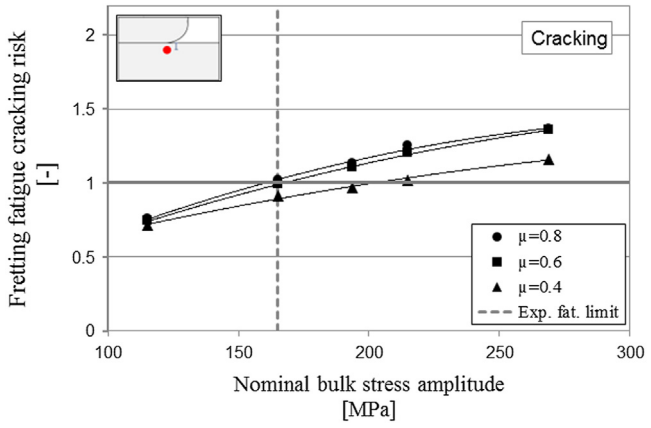

Fig. 7. Cracking risks compared to the experimental results (rounded contact edge).

the same in all the calculated cases. However, the cracking risk seems to become less sensitive to friction when the bulk stress amplitude is low. With the lowest value of bulk stress and with friction coefficient values of 0.6 and 0.8, the cracking risk values are close to each other. The amount of slip is very small and the contacts can already remain stuck during loading. If the contacts

are stuck, there is no relative movement between the parts at the contact edge (or elsewhere) and, fretting damage cannot be expected, i.e., it becomes a plain fatigue case with a notch effect [3].

The cracking risk has a fairly linear relationship relative to the bulk stress around the fatigue limit. With higher cracking risks, the slight concave shape in the values is attributable to plasticity. The accuracy of the results may be reduced here because a stress-based criterion was used and isotropic material hardening behavior was assumed. However, the main focus of interest in this study was crack nucleation and at the bulk load levels around the fatigue limits, the amount of plasticity is small or non-existent (at the calculation distance). Figs. 8 and 9 show the cracking risk behavior at the surface, i.e., at "hot-spots" to study the effect of the calculation depth on the results. These values are only rough approximations due to the calculation accuracy of the surface stress values.

Unsurprisingly, the figures show that the cracking risk values are higher at the surface than in the subsurface. With friction coefficient values of 0.6 and 0.8, the cracking risks are already well over one but, again, the rounded edge has a slightly higher cracking risk than the sharp edge at load levels around the fatigue limit. The calculation depth chosen does not seem to change this result. The effect of the friction coefficient on the cracking risk is greater at the surface than in the subsurface. This supports the generally known fact that friction-induced shear traction has its greatest impact at the surface or just below.

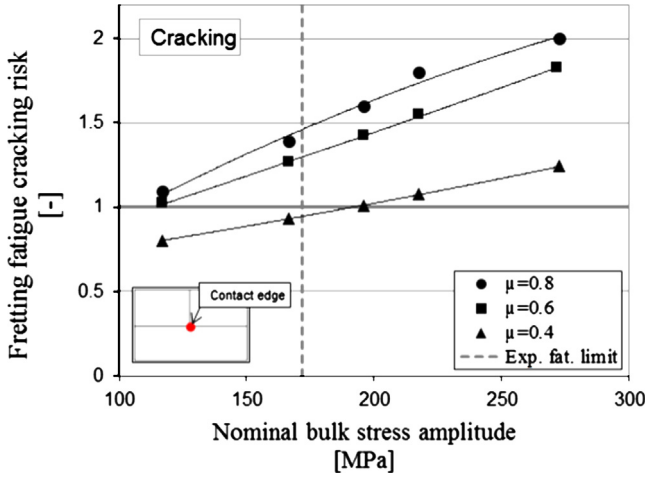

Fig. 8. Surface cracking risks (sharp contact edge).

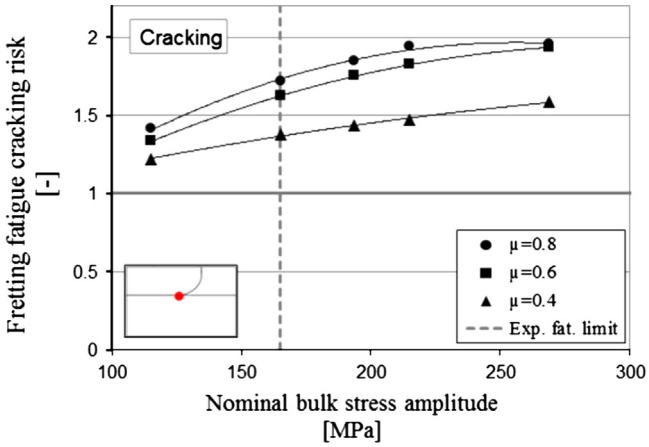

Fig. 9. Surface cracking risks (rounded contact edge).

Overall, high peak values and steep gradients in contact tractions and internal stresses are observed in both cases. In the rounded edge case, the contact edge and further contact tractions are located deeper in the material. Together with the geometrical shape, this causes stiffer contact behavior and more pronounced local deflection than in the sharp-ended case, which can lead to even higher stresses in the specimen. Secondly, at the contact opening side, i.e., when bending the specimen 'away' from the contact corner, the sharp-edged contact tends to open more easily in terms of increased bulk loading. When the contact opens, there are no contact tractions occurring at the opening point. At bulk load levels around the fatigue limit, the rounded specimen is still in contact with the fretting pads, though sliding, so that contact tractions exist and further affect the internal stresses. However, if the pads are modeled as rigid with the elastic material behavior assumed in the specimen, the contact tractions and cracking risk would be greater in the sharp-edged case. The elasticity of both contacting parts changes this arrangement.

Additionally, by using FE, the radius of the contact edge was varied so as to study more extensive the effect of the rounding size on cracking risk. Radiuses of 2 mm and 5 mm were studied and compared to the reference case ($R=1$ mm). The bulk loading of the specimen in each case was adjusted such that the nominal bulk stress amplitude at the contact edge was 165 MPa. The friction coefficient was 0.6. Similar model parameters, e.g., mesh densities and the cracking risk calculation method were used with the different geometries. It was observed that these different roundings had only a minor effect on the cracking risk values. Moreover, the differences were at the level of the calculation accuracy.

The plain bending fatigue limit of 517 MPa was measured for the material used in [15], with the same test device. Therefore, the fatigue life of the sharp and rounded edge specimens was significantly reduced by the clamping contact with fretting and stress concentration effects. The fretting fatigue limits are only about 30% of the plain fatigue limit with the used material pair.

4.3. Contact surface wear

Fretting wear scars from both types of test specimen were inspected with an optical microscope and also with an optical profilometer. Fig. 10 show fretting scars of a sharp and a rounded specimen after about 200,000 loading cycles, having a nominal bulk stress amplitude close to 300 MPa.

The cracking point, located at the contact edge is shown on the right. The horizontal direction in the figure is the longitudinal (slip) direction in the specimens. Severe fretting marks are observed near the contact edge where machining marks have been completely removed. At the contact edge, under high contact tractions, scars are observed over the entire width, but after approximately 0.25 mm there are also unchanged areas. This length seems to have some correspondence to the steady state slip lengths achieved from the numerical model, when a friction coefficient of 0.8 is used. If the friction coefficient rises to the top value relatively quickly, say 10,000 cycles, which is typical in fretting contacts, then the contact is subjected to a high degree of friction for a major part of its life. This would be in line with the observed severe fretting scars close to the contact edge and the milder scar further away from the contact edge, which reflects a lower friction coefficient and a reduced number of load cycles. In these figures, the fretting marks cover an area about 2 mm away from the edge. The scar length depends on the nominal contact pressure (which is constant here) and the bulk stress. Generally, it was observed that increasing the bulk stress amplitude had the effect of increasing the length of the fretting mark. Maximum slip

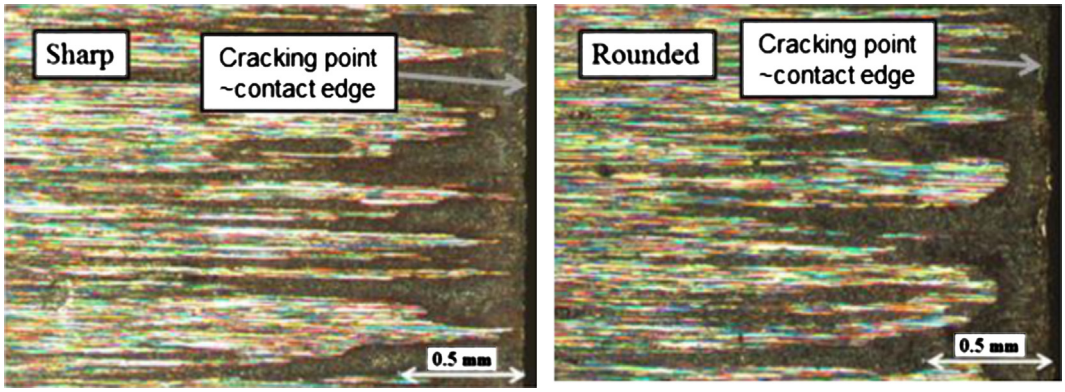

Fig. 10. Fretting scars from both types of specimen.

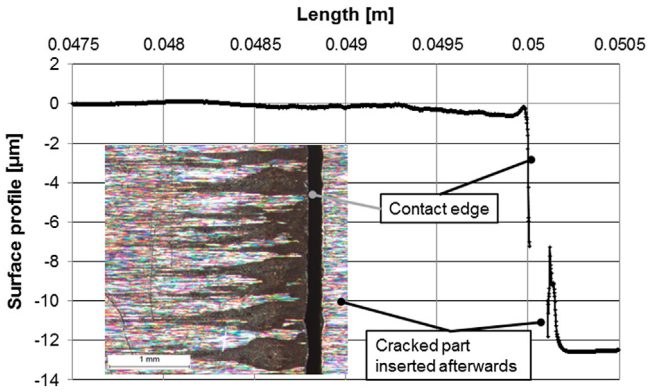

Fig. 11. Average surface profile in the *x*-direction of a sharp specimen close to the contact edge.

lengths during loading history achieved from the FE-model compared reasonably well to the experimental fretting scar lengths. However, the calculated slip lengths are heavily dependent on the chosen friction coefficient.

Fig. 11 shows an example of a surface profile of a sharp-ended experimental specimen close to the contact edge, together with the corresponding microscope profile. The bulk stress was 302 MPa and the number of load cycles was 190,000. The surface area analyzed was 4×3 mm^2, with a 1.65 μm sampling period.

The contact edge is on the right side. The cracked part (free end) of the specimen was also inserted next to the contact part of the specimen under the microscope and profilometer, which is the reason for the slight offset. The main focus, however, is on the contact part of the specimen. The surface profile presented in the figure is an average of all measured profiles in the *x*-direction across the width. There has been some wear, albeit very small, almost two millimeters away from the edge. Both sharp and rounded edges showed similar behavior in this respect. It was observed that material could have also been transferred between the specimen and pads, which indicates adhesion between the parts. However, the change in the profile is in the order of surface roughness, so the amount of wear and material transfer is very small. In many cases, it was difficult to detect any wear at all. A peak in the surface profile is shown outside the contact edge, at the free end of the specimen. This is assumed to have been created as a result of plastic deformation of the material, which can also be seen in the FE-model.

Smooth surfaces were assumed in the calculations. Surface roughness, which always occurs in practice, increases cracking risk at local surface asperities. However, the surface roughness or wear should not play a major role when comparing the cracking risks of sharp edge and rounded contacts in this case. In addition, the surface roughness of the test specimens was relatively minor.

5. Conclusions

The effect of the contact edge geometry on fretting fatigue behavior of a complete contact was studied with 34CrNiMo6 quenched and tempered steel. A 2D elasto-plastic finite element model of the contact configuration was used to calculate cracking risks for complete and almost complete contact geometries using the Findley multi-axial fatigue criterion. Experimental fretting fatigue tests were carried out with corresponding geometries and loadings. The calculations showed that the rounded contact edge has a slightly higher cracking risk than the sharp contact edge. This agrees with the experimental results, although more tests would be needed to improve the statistical reliability of the results. The Findley multiaxial fatigue criterion, used with the theory of critical distance, predicted the failure for both contact edge cases when a friction coefficient in the order of 0.6–0.8 was used. The used calculation distance below the surface (15 μm) is in the same order of magnitude as the grain size of the used material. The effect of the friction coefficient on the cracking risk is greatest at the surface. The dimensions and shapes of fretting scars in the experimental specimens were similar for both geometries. The clamping contact with fretting and stress concentration effects essentially decreased the fatigue life of quenched and tempered steel in comparison to plain fatigue.

Acknowledgments

This study has been carried out within FIMECC Ltd. (Finnish Metals and Engineering Competence Cluster) and its DEMAPP program. The authors are grateful for the financial support provided by the Wärtsilä Finland Oy, Metso Paper Oy and the Tekes (Finnish Funding Agency for Technology and Innovation). In addition, the Academy of Finland is acknowledged.

References

[1] D.A. Hills, D. Nowell, Mechanics of Fretting Fatigue, Kluwer Academic Publishers, Dordrecht, 1994.
[2] K.L. Johnson, Contact Mechanics, Cambridge University Press, 1985.
[3] D.A. Hills, R.J.H. Paynter, D. Dini, An overview of the quantification of fretting fatigue lives of complete contacts, Engineering Fracture Mechanics 80 (2012) 3–12.
[4] M. Ciavarella, D.A. Hills, G. Monno, The influence of rounded edges on indentation by a flat punch. Proceedings of the Institution of Mechanical Engineers, Part C: Journal of Mechanical Engineering Science 212(4) (1998) 319–327.319–328.

[5] S. Fouvry, P. Kapsa, L. Vincent, A Multiaxial Fatigue Analysis of Fretting Contact Taking Into Account the Size Effect, in: D.W. Hoeppner, V. Chandrasekaran, C.B. Elliott (Eds.), Fretting fatigue: Current Technology and Practises, ASTM STP 1367, American Society for Testing and Materials, West Conshohocken, PA, 2000.
[6] S. Fouvry, Ph. Kapsa, F. Sidoroff, L. Vincent, Identification of the characteristic length scale for fatigue cracking in fretting contacts, Journal de Physique IV 8 (1998) 159–166.
[7] J.A. Araújo and D. Nowell, The effect of rapidly varying contact stress fields on fretting fatigue, International Journal of Fatigue 24 (7), 2002, 763–775.
[8] D. Taylor, The Theory of Critical Distances, Elsevier, 2008.
[9] J. Araújo, L. Susmel, D. Taylor, J.C.T. Ferro, J.L.A. Ferreira, On the prediction of high-cycle fretting fatigue strength: theory of critical distances vs. hot-spot approach, Engineering Fracture Mechanics 75 (7) (2008) 1763–1778.
[10] D.J. White, J. Humpherson, Finite-element analysis of stresses in shafts due to interference-fit hubs, The Journal of Strain Analysis for Engineering Design 4 (2) (1969) 105–114.
[11] T. Hattori, M.A.B.A. Wahab, T. Ishida, M. Yamashita, Fretting fatigue life estimations based on the critical distance stress theory, Procedia Engineering 10 (2011) 3134–3139.
[12] A.L. Hutson, T. Nicholas, R. Goodman, Fretting fatigue of Ti–6Al–4 V under flat-on-flat contact, International Journal of Fatigue 21 (7) (1999) 663–669.
[13] S. Mall, S. Naboulsi, S.A. Namjoshi, Contact geometry effects on fretting fatigue crack initiation behaviour of Ti–6Al–4 V, Tribology - Materials, Surfaces and Interfaces 2 (1), (2008) 25–32.
[14] M. Francis, L.V. Ngan, C. Henri, N.H. Ngan, Stress concentration of shrink fit assembly using finite element method, in: Proceedings of the IASTED Asian Conference: Modelling and Simulation, October 8–10, 2007, Beijing, China.
[15] J. Juoksukangas, A. Lehtovaara and A. Mäntylä, Development of a complete contact fretting test device, Proceedings of the Institution of Mechanical Engineers, Part J: Journal of Engineering Tribology 227(6) (2012) 570–578.
[16] Abaqus Theory Manual 6.10-EF, Dassault Systèmes, 2010.
[17] D.F. Socie, G.B. Marquis, Multiaxial Fatigue, SAE Publications Group, Warrendale, 2000.
[18] A. Lehtovaara, R. Rabb, A. Pasanen, Modelling and evaluation of the fretting fatigue cracking risk in smooth spherical contacts, Tribology International 44 (11) (2011) 1526–1534.
[19] B. Alfredsson, Fretting fatigue of a shrink-fit pin subjected to rotating bending: experiments and simulations, International Journal of Fatigue 31 (10) (2009) 1559–1570.
[20] B.R. Rabb, Fatigue testing and its statistical evaluation into design rules, Dissertation, Tampere University of Technology, Publication 253, 1999.
[21] W.J. Dixon, A.M. Mood, A method for obtaining and analyzing sensitivity data, Journal of the American Statistical Association 43 (1948) 108–126.

Publication IV

Applying the digital image correlation method to fretting contact for slip measurement

by

J. Juoksukangas, A. Lehtovaara and A. Mäntylä

Proc. IMechE, Part J: J. Engineering Tribology, Published online August 20 2015, doi:10.1177/1350650115601695

Applying the digital image correlation method to fretting contact for slip measurement

J. Juoksukangas[1*], A. Lehtovaara[1], A. Mantyla[2]

[1]Group of Tribology and Machine Elements, Department of Materials Science, Tampere University of Technology, P.O. Box 589, 33101 Tampere, Finland

[2]Research & Development, Wartsila Finland Oy, P.O.Box 244, 65101 Vaasa, Finland

*Corresponding author: Janne Juoksukangas, E-mail: janne.juoksukangas@tut.fi

ABSTRACT

Fretting is a consequence of small relative oscillatory movement between contacting parts and can cause serious damage to machine components. This paper describes the implementation of digital image correlation (DIC) method to a fretting test device to measure the relative movement, i.e., slip, between the contacting parts. A complete contact fretting test device is used, in which two flat fretting pads are clamped against a cyclically loaded flat fretting specimen. The material used is quenched and tempered steel. DIC, equipped with a microscope, is employed to measure the local displacement field at the contact edge. The micrometer-level slip amplitude and the length of the slip region are determined at specific time intervals during a fretting fatigue test. Both of these quantities appear to decrease and stabilize during fretting fatigue testing. The slip decreases markedly during the initial cycles.

Keywords: fretting, complete contact, slip, digital image correlation, DIC.

1. INTRODUCTION

Fretting occurs between contacting parts that undergo small relative oscillatory movement. It can lead to damage in machine components, either by decreasing fatigue life (fretting fatigue) or by wearing the parts in contact (fretting wear). Typical machine elements vulnerable to fretting are, for example, mechanical joints having interference fits. The fretting movement can be created by loads that have to transfer through mechanical joints or by machine vibration. Together with the small tangential movement and typical high friction coefficient occurring in fretting contacts, high contact tractions are created. Complex multiaxial stress states having steep stress gradients can further lead to fatigue cracking. Fretting fatigue can lead to serious and unpredictable damage because cracks can grow undetected inside a machine element.

Commonly, contacts can be divided into incomplete and complete contact. Incomplete contact means that the contact area depends on the normal loading applied, like the Hertzian contact. In the case of complete contact, the nominal contact area is independent of the applied normal load, i.e., the contact has ‘sharp’ edges. Theoretically, this leads to singular contact traction field. Numerical methods are usually needed to

calculate contact tractions and stresses in complete contacts because analytical solutions are limited. A finite element method is often used for such purposes.

The relative movement, i.e., slip, between contacting parts and the friction coefficient are important fretting parameters. Fretting contact models are used to calculate quantities, such as slip, contact tractions and stresses in contacting bodies for fatigue life calculations. Moreover, slip is used directly in some fretting fatigue criteria. In the models, using the correct friction coefficient and slip as input values is critically important. However, experimental measurement of the friction coefficient from fretting contacts is not necessarily straightforward: neither is the measurement of the micrometer-level motion between the contacting parts. A displacement sensor, such as a linear variable differential transformer (LVDT) or an extensometer, is typically used to measure slip. However, these measure displacement only at a certain point. Moreover, it can be difficult, or impossible, to install the sensor close enough to the point of interest, i.e., the fretting contact. Data measured at a distance from the fretting contact can easily include extraneous test device compliances.

In this study, the digital image correlation (DIC) method is employed to measure displacements at the fretting contact. The main advantage of the method is that full-field displacement data is achieved. In the field of mechanical engineering, DIC is nowadays a well-known technique to determine displacements. The basic principle of the method is that images of an object are acquired during loading. Each image, divided into smaller areas (subsets), is compared to a reference image, such as the first image, and the displacements for each subset between the two images are then calculated. Obviously, the images must contain some visual information. The images must contain a non-uniform speckle pattern having sufficient contrast. Natural, e.g., grinded metal surface, or artificial, e.g., sprayed speckle pattern, surface features are used. Advantages of using DIC are that it is a non-destructive and non-contacting method. In addition, size and time scales have large ranges. Basically, a camera taking images and a software calculating the displacements are needed. In-plane displacements (2D) can be determined using one camera, but for out-of-plane measurements (3D), two cameras are needed. A comprehensive account of the method is given in Ref. (1). A review of two-dimensional DIC applications is given in Ref. (2).

Some authors have applied digital image correlation to fretting contacts. In Refs (3) and (4), the authors used DIC to determine frictional hysteresis loops and contact stiffness of almost complete contacts having rounded contact edges. These tests were mainly carried out in gross sliding conditions, i.e., the whole nominal contact area was sliding. In Ref. (5), DIC and ultra-sound techniques were compared for measuring contact stiffness. In these studies, pixel size varied from 1.02 μm to 1.8 μm and the spatial resolution of evaluated displacements was between 61 μm and 115 μm. The authors used a long-distance microscope to achieve high resolution views. The plain metal surface of the test specimen was used as the target surface for DIC. Slip amplitude measurements performed by 3D DIC (consisting of two cameras) have been compared to traditional slip measurements (clip gauge and Wittkowsky (6)) and discussed in Ref. (7). Pixel size was 12 μm and the spatial resolution of displacements, 420 μm. In Ref. (8), DIC and the finite element method were combined to calibrate the friction coefficient. Pixel size and spatial resolution were 8 μm and 100 μm, respectively. The cyclic slip amplitude at three different slip region points was shown. However, none of the studies present slip distribution along the contact surface. Additionally, DIC has been used to measure the frictional properties of a bolt joint (9) and the slip between individual wires of a strand of a wire rope (10). In general, DIC is

reported to be a usable method for displacement measurements in fretting contacts.

The objective of this study was to measure the local displacement field at the fretting contact edge of a complete contact using digital image correlation and to determine the slip distribution. The slip was determined at specific time intervals during fretting fatigue testing to study the evolution of the micrometer-level slip amplitude and the length of the slip region.

2. EXPERIMENTS

An in-house complete contact fretting test device was used in the experiments, in which flat fretting pads are clamped against a cyclically loaded flat fretting specimen. The material used was quenched and tempered steel. A DIC system, consisting of a digital camera extended with a microscope, was implemented into the device to measure the displacements.

2.1 Test device

Only a brief overview of the test device is given here. A detailed description of the device and test procedure is given in Ref. (11). The fretting contact includes a cantilever fretting test specimen and two fretting pads as shown in Figure 1.

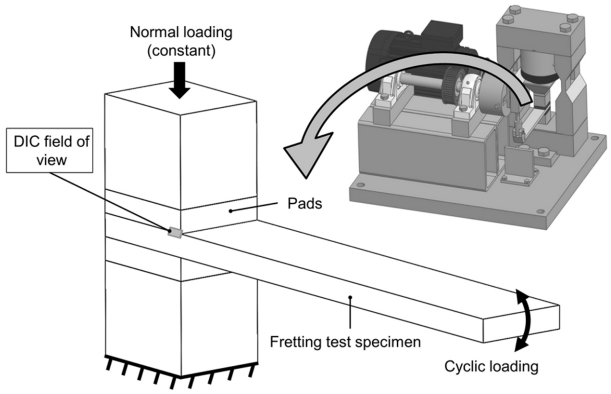

Figure 1. Schematic principle of the test device.

Two test contacts are formed by the normal load clamping the specimen and the pads together. Cyclic bulk loading of the specimen is created by deflecting the tip of the specimen. The loading is practically sinusoidal. This loading creates relative tangential movement (slip) between the pad and specimen at the contact edge. Therefore, the tests are carried out in partial slip conditions, i.e., only a part of the nominal contact area is sliding. Due to the flat pads and the flat specimen, contact traction distribution is asymptotic at the contact edge. According to a FE-study of the test setup (12), maximum slip occurs at the contact edge, and the slip gradually decreases towards (inside) the contact. The test specimen has a length of 250 mm, a width of 40 mm and a thickness of 10 mm. The pads have a length of 50 mm, a width of 40 mm and a thickness of 10 mm. The parts of the frame are heavy and the design is rigid to prevent excessive deformation and vibration.

The material of the specimen and the pads was EN 10083-1-34CrNiMo6+QT. All the test specimens and pads were made of same batch of material. Both the specimens and pads were ground longitudinally. The side faces of the specimens and pads were also ground to enable the DIC measurements. The grinding produced an arithmetic mean surface roughness S_a of 0.25 µm. This was measured with a Wyko NT1100 optical profilometer. The analyzed surface area was 4.9 × 3.8 mm^2, with a 6.72 µm sampling period. The specimens and pads were carefully cleaned with acetone before testing to emulate dry and unlubricated test conditions. The tests were conducted in a normal laboratory atmosphere, having a maximum RH of 25 %.

2.2. Digital image correlation

2D digital image correlation setup was used to measure displacements. A camera equipped with a long-distance microscope (13) was used to capture the images, as in Ref. (3). Davis DIC software (14) was used to calculate the displacements. The DIC measurement setup is shown schematically in Figure 2.

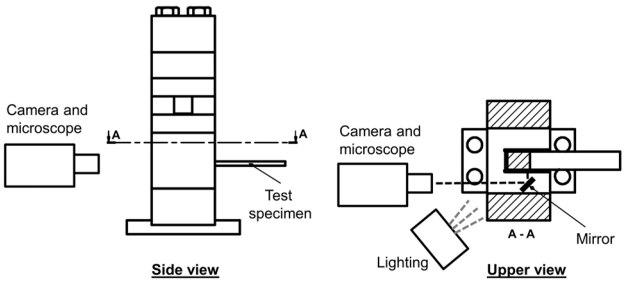

Figure 2. Principle of the DIC measurement setup.

The camera was positioned behind the device. The side face of the specimen and pad was measured using an optical mirror. The use of a mirror eliminated any need for modifications to the device. A high quality mirror was used to minimize optical distortion. The mirror was also aligned with an external gauge. Illumination was created using fibre optic lighting. The DIC setup was calibrated with a calibration plate in each experiment. A typical captured image is shown in Figure 3.

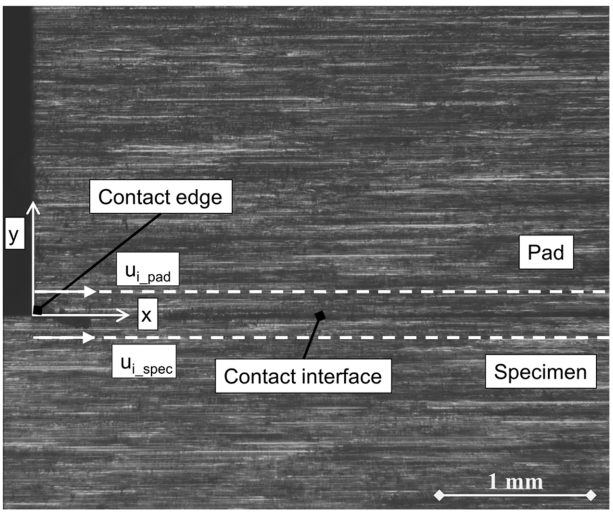

Figure 3. Typical captured image with definitions.

The plain ground metal surface of the test specimen was used as the target surface for DIC. The images were captured close to the contact edge where slip occurs, as shown in Figure 3.

Three different kinds of speckle patterns were studied in fretting environment. In these tests, slightly different DIC setup was used than in actual slip measurements. The resolution of the camera was one megapixel and one pixel equaled approximately to 5.6 µm at the surface. A microscope (13) was used to get high magnified images. Speckle patterns were made with commercial aerosol paint, air brush and also the plain ground surface was used as a target surface for DIC. In the both painting methods, the ground surface of the specimens was painted with matt black color. The displacements achieved by DIC were compared. In these images, the best accuracy was achieved with the air brush technique; however, the plain surface gave very similar results.

Measurement uncertainties and DIC verification were studied in several ways. First, an LVDT sensor was attached to the fretting test specimen for verification purposes. Displacements in *y*-direction were compared between DIC and the external sensor. Due to the lack of space, the sensor was installed about 15 mm outside the contact. A displacement of 0.1 mm was applied at that point. DIC was found to give very good agreement with the LVDT results. In this case, however, there was no contact involved. In fretting testing, an LVDT sensor cannot be attached to measure motions of the same points as DIC due to the lack of space.

Secondly, the computed displacements between two images of a static sample were compared, meaning that the images of the specimen were taken from a stationary test device. This approach can expose uncertainties due to lighting and noise from the camera and the experimental setup itself. This procedure was repeated for several sets of images and a maximum difference of 0.3 µm in *x*-displacement values was observed. The corresponding value for *y*-displacement was 0.28 µm. It should be noted that these are the maximum values observed, and in the majority of the cases these values were much smaller. Further, artificial rigid body movement was made to the captured images in Matlab and then, displacements were calculated in Davis and compared. The maximum

difference between the known displacement (made in Matlab) and the value calculated in Davis was 0.04 pixels, which is a relatively low value. Therefore, according to these accuracy studies, the measurement uncertainties in the displacements measured should be well under a micrometer. In reality, the actual uncertainties may be well below these values. In Ref. (3), one micrometer was used as an indication of uncertainty and in Ref. (4), it was 0.15 µm.

In the actual slip measurements, a 12 bit, five megapixel camera (2456 × 2058 pixels) equipped with the long-distance microscope (13) was used to capture the images. The loading frequency of the test device was decreased during DIC measurement. In addition, small loading frequency minimizes the vibrations of the test device that could complicate the measurements. The image frame rate was mostly 14 Hz, but in some cases 32 Hz was used, depending on the loading frequency of the test specimen. The field of view (i.e., measurement "window") was mainly about 4.5 mm × 3.8 mm, which gives a pixel size of about 1.83 µm at the target surface. There were minor variations in the field of view between tests. The pixel size varied between 1.60 µm - 1.86 µm at the surface between different tests. The Least Squares Matching (LSM) approach in Davis software was used to calculate the displacements. The subset size was 61 × 61 pixels and the step size, i.e., grid spacing, was 20 pixels, which equals to 20 × 1.83 µm = 36.6 µm at the surface. The slip results presented here are measured using the natural specimen surface created by grinding. The ground surface was found to provide the requisite surface features (random texture) and contrast. Even though the pattern is somewhat oriented in the *x* direction due to the grinding, the subset size is rather large and the possible horizontal trace covers only a part of the subset, the results obtained were, nonetheless, satisfactory. The usability of the plain specimen surface depends on the pixel resolution. If the pixel resolution is notably lower than the value chosen here, the pattern created by grinding may be too small and the proper pattern should be made artificially, e.g. using spraying methods. The displacement data calculated by DIC were exported to Matlab for further processing. No smoothing was used in further data processing in Matlab, except when extrapolating slip region lengths.

3. RESULTS AND DISCUSSION

Figure 4 shows calculated displacement magnitudes in a case where the displacement of the specimen tip was about 2.5 mm, corresponding to a nominal bulk (bending) stress of the test specimen of about 190 MPa at the contact edge (neglecting contact stresses). The nominal contact pressure was 100 MPa.

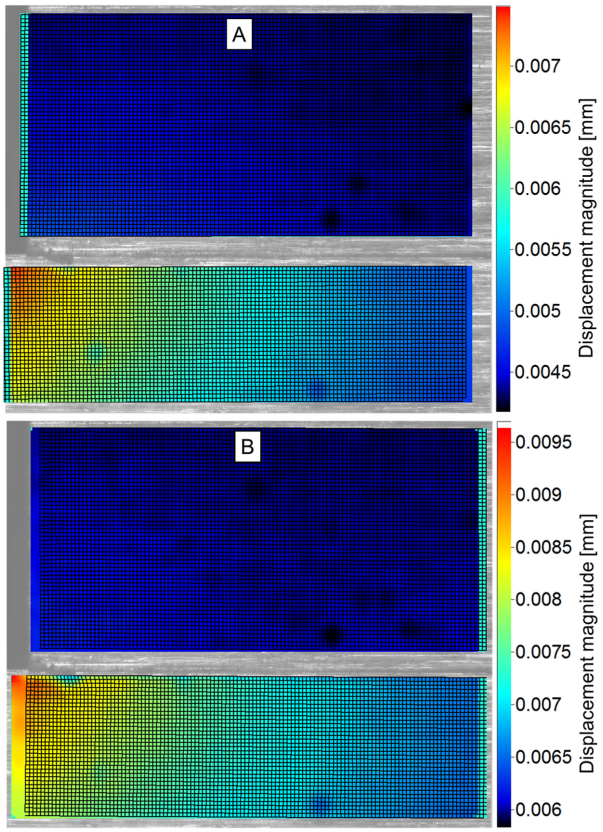

Figure 4. Examples of calculated displacements when bending the specimen down (A) and up (B).

In Figure 4, the shown displacements are scaled 15 times. In the upper figure (A), the specimen is in its lowered position (bent down) and in the lower

figure (B), the specimen is in its upper position (bent up). At the contact edge, displacements of the specimen are higher than the pad's due to the relative movement between them. The movement of the pad can be also seen. The rigid body motion of the test device at the measurement area is of the same magnitude as the slip. In the following slip measurements, the slip δ between the fretting specimen and pad is determined from the tangential displacements of the specimen (u_{i_spec}) and pad (u_{i_pad}) (see Figure 3) as follows:

$$\delta_i(t) = u_{i\_spec}(t) - u_{i\_pad}(t) \quad (1)$$

Slip is the relative tangential displacement of the pair of points (having the same x-coordinate and at the same distance from the contact interface in y-direction) in the specimen and pad, as shown in Figure 3. Obviously, actual slip is determined only on the contact surface. In practice, slip has to be determined some distance away from the contact interface. There is discontinuity in displacements at the contact interface and also there can be also distractions, e.g., fretting debris that prevents displacement calculation in these local points. Figure 5 shows the relative displacement as a function of the distance from the contact interface in y-direction. Five different points in x-direction are shown.

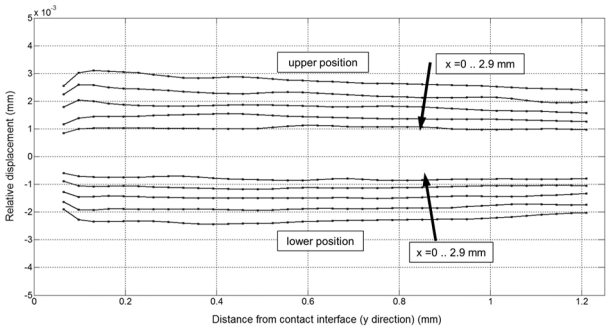

Figure 5. Relative displacement as a function of the distance from contact interface in y-direction.

Apart from the area very close to the contact, where the displacement discontinuity exists, the curves are fairly smooth. When the specimen is in its upper position (overlying curves), the relative displacement appears to decrease somewhat linearly throughout the measured length, at least close to the contact edge, i.e., x = 0. In the following results, slip is determined between points that are approximately 0.15 mm from the contact interface in y-direction, as in Ref. (8). There is some variation in this value between individual DIC measurements, depending on the division of subsets, but this has only a minor effect on the relative displacement, as the figure shows. In (4), the minimum value of this distance was somewhat below 0.1 mm.

In the results presented here, the displacement amplitude of the specimen tip was between 2.5 mm and 2.7 mm, corresponding to the maximum nominal bending stress of the test specimen of about 190 and 210 MPa, respectively. The nominal contact pressures used were 30 MPa and 100 MPa. The loading frequency was 41 Hz, but during DIC measurement the loading frequency was decreased to 0.5 Hz or 1 Hz. Decreasing the loading frequency, the vibrations of the test device are decreased and minimized. Figure 6 shows the slip during the first three cycles of a fretting fatigue test, having a nominal contact pressure of 30 MPa.

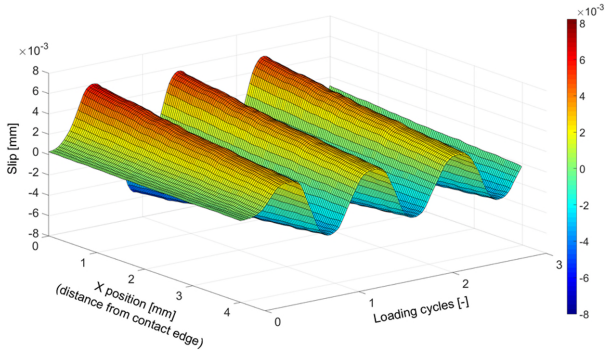

Figure 6. Slip during the first three cycles of a fatigue test (nominal contact pressure 30 MPa).

The specimen is first bent upwards. As expected, maximum slip amplitude occurs at the extreme positions of the specimen, and the slip amplitude is highest at the contact edge. In this case the slip region length is considerably wider than the field of

view. In such cases, slip region length is determined further by extrapolating the data. The slip amplitude is of similar magnitude to that measured in Ref. (8), but notably smaller than in Refs. (3,7).

Since the DIC calculation process is computationally intensive and a large amount of data is captured, it is neither useful nor even possible to capture data over the duration of a complete fatigue test. Instead, DIC measurements were taken at specific intervals during testing. It is expected that changes in displacements are slow, so the procedure is acceptable. At the start, however, there are notable changes in slip amplitudes, as can be seen in Figure 7, which shows slip in the first 31 cycles of the same fatigue test.

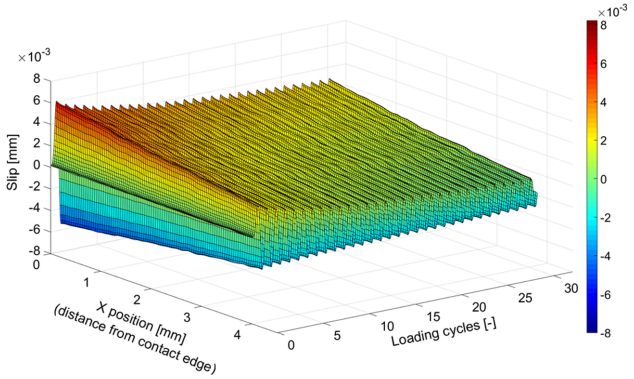

Figure 7. Slip of the first 31 cycles of a fatigue test (nom. contact pressure 30 MPa).

A major decrease in the slip amplitude occurs during the initial cycles. It is known that the friction coefficient can increase relatively rapidly during cyclic fretting loading. Slip is expected to decrease as the friction coefficient increases. Another explanation for the decrease in slip could be frictional shakedown, meaning that residual tangential tractions (from the previous cycle) minimize the likelihood of further slip (15). Besides the slip amplitude, the slip region length also decreases markedly. Apart from the first cycle, the slip at the lower position (i.e., bending the specimen downwards) is not shown in the figure. At the lower position, the contact opens with the parameters used. Strictly speaking the measured quantity at this point is not actually “slip” because the surfaces are separated at the contact edge. In this respect, the upper position is more interesting. When bending “against” the pad (the upper position), the contact is closed and the measured value represents sliding between the specimen and pad. For comparison between different normal loads, Figure 8 shows the slip distribution in the first 107 cycles of a fatigue test having nominal contact pressure of 100 MPa.

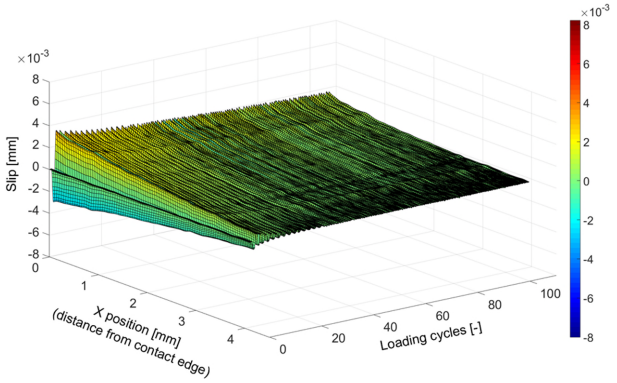

Figure 8. Slip in the first 107 cycles of a fatigue test (nom. contact pressure 100 MPa).

Similarly, slip amplitude is decreased during loading as is the length of the slip region. The slip region almost fits initially within the measurement window. The slip amplitude is lower and the slip region length smaller than in the previous results with a nominal contact pressure of 30 MPa. These effects are logical and predictable. Some noise is present in the graphs of these two loading cases. There are more measurement uncertainties in the higher contact pressure case, which is expected, as the slip is smaller and the signal-to-noise ratio is lower.

Slip distribution evolution during a fatigue test is illustrated in Figure 9. The nominal contact pressure is 30 MPa.

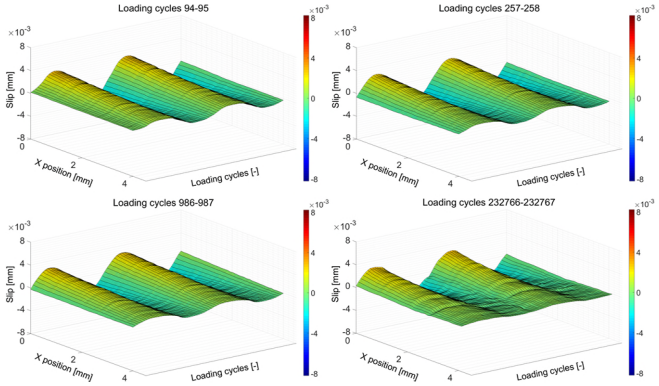

Figure 9. Slip evolution during fretting fatigue test (nom. contact pressure 30 MPa).

The slip distributions during two cycles at specific points in the fretting fatigue test are shown above (loading cycles 94 - 95, 257 - 258, 986 - 987 and 232766 - 232767). The further decrease in slip amplitude and slip region length can be seen. Figure 10 shows slip measurements in the form of 2D graphs.

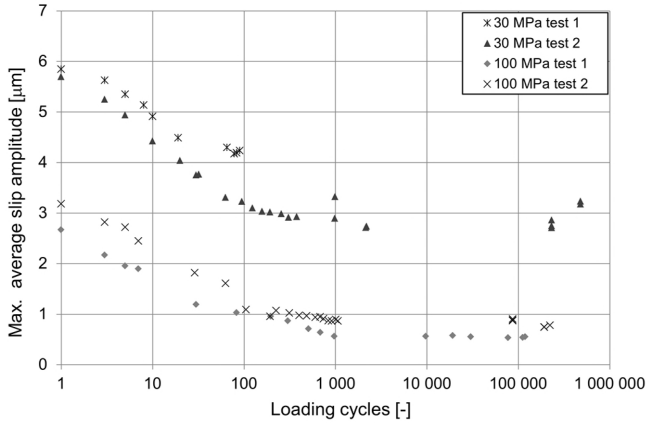

Figure 10. Slip amplitude as a function of loading cycles.

Figure 10 presents the maximum average slip amplitude of four tests plotted against the loading cycles. The maximum average slip amplitude is the mean value of the maximum slip in both directions (i.e., bending the specimen upwards and downwards) during a cycle. As shown earlier, maximum slip occurs at the contact edge, which is shown here. Results of both nominal contact pressures, i.e. 30 MPa and 100 MPa, are presented. Two tests were run for both cases to determine repeatability. Although the aim was to achieve the same nominal bulk stress in all cases, there are slight differences. This is due to the fact that the bulk stress is relatively difficult to adjust before the test without actual cyclic loading. In order to achieve slip values with constant loading already from the first cycle, no adjustment was made in this case.

In Figure 10, it is clearly seen that the slip amplitude decreases as the contact pressure increases. The slip seems to stabilize around 1000 loading cycles. There is some variation in the slip values between the tests with similar parameters. Although the minimum slip values in the 100 MPa case are within measurement accuracy, at least the trend of slip can be seen and replicated.

The slip region length was also studied as a function of loading cycles. Lengths above about four millimeters are extrapolated from the measured data. Second degree polynomial fitting was used to extrapolate the slip outside the field of view. Threshold value for the slip amplitude was 0.3 µm, i.e., lower slip values were neglected. This is due to the measurement noise. Figure 11 shows the slip region length as a function of loading cycles. The value is the mean value of the slip region length in both directions (i.e., bending the specimen upwards and downwards) during a cycle.

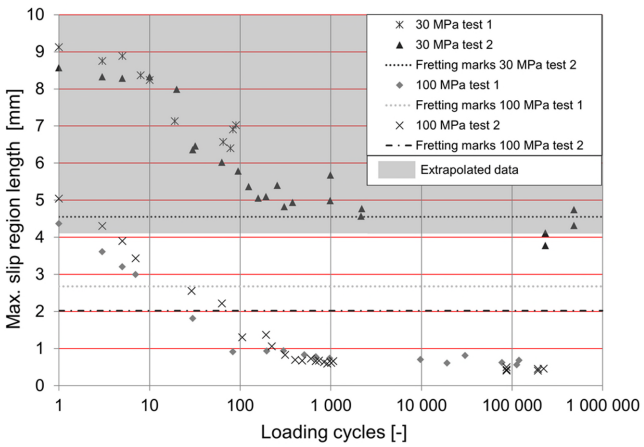

Figure 11. Slip region length as a function of loading cycles.

Correspondingly, the slip region decreases as the loading cycles increase. Again, the slip region length seems to stabilize around 1000 loading cycles. The slip region length decreases as the contact pressure increases. The figure also presents the lengths of the fretting marks of the test specimens; the length is measured using a slide gauge. Accuracy of the measurement depends on the operator and the fact that the length of the fretting mark is not constant across the specimen. The lengths shown are, therefore, somewhat tentative.

Both slip amplitude and length of the slip region decrease as the loading cycle increases. A major decrease in slip amplitude occurs during the initial cycles. In terms of the length of a typical fretting fatigue test, these values level off rather quickly. As noted earlier, it is generally recognized that the friction coefficient in fretting contact increases as the number of cycles increases. Typically, the friction coefficient reaches its upper level (around which it stays) relatively early in a fretting fatigue test. In Ref (16), a limit of 1000 cycles is set, after which the friction coefficient stabilizes. This observation supports the results here.

The relative displacements measured were a few micrometers in size. According to the DIC accuracy studies, reported slip values of fractions of a micrometer should be treated with caution since these lie at the limits of measurement accuracy. There are several reasons for these uncertainties, such as surface texture, settings of the lenses and camera, lighting and the parameters used in the calculations (DIC software). Measurement repeatability and the accuracy of absolute slip values are important subjects that warrant further investigation and study.

Digital image correlation is an applicable method for measuring small displacements related to fretting. High magnification is needed for measuring such displacements in order to achieve a reasonable degree of accuracy and spatial resolution; in practice, a microscope can be used to achieve such magnifications. These results and the measurement procedure employed here will be used for calibrating numerical fretting models and for determining the friction coefficient in this test device.

4. CONCLUSIONS

The digital image correlation (DIC) method was applied to a fretting contact to measure the local displacement field. Relative tangential movement, i.e. slip, between a flat fretting pad and a cyclically loaded flat fretting specimen was determined using the displacements measured. The material used was quenched and tempered steel and the surfaces were ground, which was used as the texture for DIC. The DIC system was equipped with a long-distance microscope capable of measuring the micrometer-level slip between the surfaces with a reasonable degree of spatial resolution and accuracy. Slip distribution, i.e., the micrometer-level slip amplitude and the size of the slip region, was determined at specified time intervals during a fretting fatigue test to study the evolution of these parameters. Both of these quantities appear to decrease and flatten out during fretting fatigue testing. The slip decreases markedly during the initial cycles. Although the relative movements are very small and high spatial resolution is needed, DIC is an applicable method to measure such displacements. The slip measurement procedure will be used to calibrate numerical fretting models and to determine the friction coefficient in the test device presented here.

ACKNOWLEDGEMENTS

This study was conducted as part of the ScarFace Research Project (Tekes decision no. 40205/12). We are grateful for the financial support provided by Tekes - the Finnish Funding Agency for

Innovation, Wartsila Finland Oy, Nome Oy, and Global Boiler Works Oy.

FUNDING

This work was supported by the Finnish Funding Agency for Innovation [grant number 40205/12], Wartsila Finland Oy, Nome Oy, and Global Boiler Works Oy.

REFERENCES

1. Sutton MA, Orteu J-J and Schreier HW. *Image Correlation for Shape, Motion and Deformation Measurements: Basic Concepts,Theory and Applications*. Springer, New York. 2009.
2. Pan B, Qian K, Xie H, et al. Two-dimensional digital image correlation for in-plane displacement and strain measurement: A review. *Meas Sci Technol* 2009; 20(6).
3. Kartal ME, Mulvihill DM, Nowell D, et al. Determination of the Frictional Properties of Titanium and Nickel Alloys Using the Digital Image Correlation Method. *Exp Mech* 2011; 51(3): 359–371.
4. Kartal ME, Mulvihill DM, Nowell D, et al. Measurements of pressure and area dependent tangential contact stiffness between rough surfaces using digital image correlation. *Tribol Int* 2011; 44(10): 1188–1198.
5. Mulvihill DM, Brunskill H, Kartal ME, et al. A Comparison of Contact Stiffness Measurements Obtained by the Digital Image Correlation and Ultrasound Techniques. *Exp Mech* 2013; 53(7): 1245–1263.
6. Wittkowsky BU, Birch PR, Dominguez J, et al. An apparatus for quantitative fretting fatigue testing. *Fatigue Fract Eng M* 1999; 22(4): 307–320.
7. De Pauw J, De Waele W, Hojjati-Talemi R, et al. On the use of digital image correlation for slip measurement during coupon scale fretting fatigúe experiments. *Int J Solids Struct*. 2014; 51(18): 3058–3066.
8. Nesladek M, Spaniel M, Jurenka J, et al. Fretting fatigue – Experimental and numerical approaches. *Int J Fatigue*. 2012; 44: 61–73.
9. Crevoisier J, Swiergiel N, Champaney L, et al. Identification of in situ Frictional Properties of Bolted Assemblies with Digital Image Correlation. *Exp Mech*. 2012; 52(6): 561–572.
10. Winkler J, Georgakis CT and Fischer G. Fretting fatigue behavior of high-strength steel monostrands under bending load. *Int J Fatigue*. 2015; 70: 13–23.
11. Juoksukangas J, Lehtovaara A and Mantyla A. Development of a complete contact fretting test device. *Proc Inst Mech Eng Part J J Eng Tribol*. 2012; 227(6): 570–578.
12. Juoksukangas J, Lehtovaara A and Mantyla A. The effect of contact edge geometry on fretting fatigue behavior in complete contacts. *Wear*. 2013; 308(1-2): 206–212.
13. Infinity long-distance microscope K2/SC. Infinity Photo-Optical Company. Boulder, CO, USA. 2011.
14. Davis 8.2 commercial DIC-software. Lavision, 2013.
15. Barber JR, Klarbring A and Ciavarella M. Shakedown in frictional contact problems for the continuum. *Comptes Rendus Mécanique*. 2008; 336(1-2): 34–41.
16. Hills D and Nowell D. *Mechanics of Fretting Fatigue*. Dordrecht: Kluwer Academic Publishers, 1994.

Publication V

A comparison of relative displacement fields between numerical predictions and experimental results in fretting contact

by

J. Juoksukangas, A. Lehtovaara and A. Mäntylä

Proc. IMechE, Part J: J. Engineering Tribology, 230(10), 2016, 1273–1287,
doi:10.1177/1350650116633573

A comparison of relative displacement fields between numerical predictions and experimental results in fretting contact

J. Juoksukangas[1*], A. Lehtovaara[1], A. Mantyla[2]

[1]Group of Tribology and Machine Elements, Department of Materials Science, Tampere University of Technology, P.O. Box 589, 33101 Tampere, Finland
[2]Research & Development, Wartsila Finland Oy, P.O.Box 244, 65101 Vaasa, Finland
*Corresponding author: Janne Juoksukangas (janne.juoksukangas@tut.fi)

ABSTRACT

In this paper, a comparison is made between calculated and measured displacements from a complete contact fretting test device. An experimental technique based on digital image correlation (DIC) was used to measure the local displacement field at the contact interface. The material of the fretting specimen and pads was quenched and tempered steel. The effect of test device compliances and rigid body movement was minimized by measuring displacements very close to the contact interface. The measured displacements were successfully compared to the computed displacements of a corresponding finite element (FE) model. The relative slip amplitude in partial slip conditions, slip distribution across the contact, length of the slip region and accumulated slip distribution, were compared. Relative slip decreases markedly with increasing normal load and friction coefficient. The friction coefficient was calibrated and determined as a function of loading cycles of fretting fatigue tests with two normal loads. The friction coefficient was found to increase at the beginning of tests and stabilize after about 1000 cycles, which is in agreement with general observations.

Keywords: Digital image correlation, finite element method, relative displacement, slip, friction coefficient

1. INTRODUCTION

Fretting is a complex phenomenon that can cause serious damage to connected parts, either in the form of wear or fatigue or both. Fretting occurs whenever there is small amplitude tangential movement (slip) between parts under normal loading. Typical practical applications are mechanical joints such as press fits. Although fretting is affected by several factors, three primary variables have been stated (1); normal load, coefficient of friction (hereafter 'COF') and relative slip amplitude between contacting parts. In terms of fretting fatigue, the partial slip contact condition is considered the most dangerous (2), that is, only a part of the contact is slipping while the rest of the contact is stuck. Fretting wear is more related to gross slip (3).

Normal load, COF and slip amplitude are dependent on each other since both the normal load and COF affect the slip (2). It is well known that COF changes by increasing the number of loading cycles (2,4). Initially, with steels, the COF may be as low

as 0.1, increasing rapidly during testing. For the same material as used here, steady state friction coefficients in gross sliding of around 0.8 have been measured in an another test device (5). Experimental quantification of COF can be rather difficult. In gross sliding, the COF is simply equal to the tangential load divided by the normal load Q/P (Coulomb friction law), whereas in partial slip conditions the COF cannot be determined in the same way due to the presence of the stick zone.

Slip amplitude is important in terms of wear analysis and is also used directly in a fretting fatigue criterion (6). Fretting wear damage has been found to increase with increasing slip amplitude (7) and the strong effect of slip on fretting fatigue life has been reported (8). The experimental measurement of slip has proven challenging. Slip amplitude is typically very low (from a few micrometers to some dozens of micrometers) and therefore liable to measurement error. Typically, LVDTs (Linear Variable Differential Transformer) and extensometers are used to measure relative tangential displacements that are referred to slip. However, such sensors are installed, for practical reasons, some distance away from the contact interface. The measurements include, therefore, test device compliances, which typically leads to higher slip magnitudes (9). For example, in (10), the slip at the contact boundary (calculated with the aid of Finite Element Method (FEM)) was one tenth of the slip measured by an extensometer at some distance away from the contact. These compliances can be excluded or minimized, for example, by using the method presented in (11) or numerical methods such as the FEM. These single-point measurements, moreover, do not provide the slip distribution along the contact surface. FE models have been used to calculate local relative slip amplitude and slip distribution and compared with global extensometer measurements (9,10,12).

Digital image correlation (DIC) is a commonly used method in solid mechanics to determine full-field displacements of loaded structures. This is an optical method which is based on the tracking of changes in images. Images are captured during loading and then processed using a DIC software. In the post-analysis, the images are divided into small subsets. Each captured image is compared to the reference image (i.e., the unloaded first image) and displacements for each subset between the current and reference image are calculated within sub-pixel accuracy. The theory and concepts of DIC are comprehensively described in (13). DIC has been applied in fretting experiments to determine frictional properties, such as, hysteresis loops and contact stiffness (14–18) and to measure tangential displacements (relative slip) (19–21). DIC has been combined with FEM to calibrate friction coefficient (17,22). In order to accurately perform microscale measurements with high resolution, relatively high magnification is needed, i.e., the pixel size at the surface should be small. Pixel sizes (at the target surface) ranging from 1.02 μm / px (micrometer per a pixel) to about 37.3 μm / px have been used in these references.

In two-dimensional (2D) DIC, the side faces of a fretting specimen and pad(s) are typically measured. This can differ from a single point displacement measurement (e.g. LVDT), in which displacements at the centre region (in a width direction) of the specimen / pad are measured. At the centre region, the plane strain condition stands, as the strain in the lateral direction may be approximated to zero. Basically, the plane stress condition applies on the faces. Some edge effects may exist at the edges of the side faces. This has been studied numerically in almost complete contacts (a flat pad with rounding at the contact edge) and it was shown that the edge effects were minor, i.e., the calculated axial stress, contact pressure and relative displacements were similar at the free edge and at the center of the contact (23). Good correlation has been achieved in measured displacements between 2D DIC and an LVDT (14,19). This suggests that the plane strain condition, which can be more relevant in terms of

fretting, can be used in modelling when employing 2D DIC data. In the test device used here, fatigue cracks have been nucleated in the central region (plane strain region) of the contact edge in the lateral direction (24). In reality, contact between solids is discontinuous and the real area of contact is only a fraction of the nominal area of contact. Contact models covering such micromechanical aspects are complex and time consuming and are still in their development phase. Coulomb's friction model and plane strain assumptions are typically utilized in numerical fretting analyses (14,15,25,26). Bulk material has typically constant elastic properties. However, in (14) a thin compliant layer was introduced at the contacting surfaces in the FE-model to incorporate surface effects, such as surface roughness. This layer enabled matching tangential contact stiffness to the corresponding experimental results.

In this study, experimentally measured displacements in partial slip conditions were compared to numerically predicted values within a complete contact. The numerical part represents a model that is commonly used in fretting contact modelling. In the experiments, test device compliances were minimized by measuring displacements close to the contact interface. Measurements were made of relative slip and its characteristics, including maximum slip amplitude, slip variation (distribution) across the contact length and also the size of slip zones. The calculated and measured cyclic slips were then compared. Finally, the friction coefficient was calibrated using FEM and DIC and the friction coefficient was determined as a function of the loading cycles of fatigue tests.

2. EXPERIMENTS

A complete contact fretting test device was used in this study, a detailed description of which is given in (24). The material used was quenched and tempered steel. The experimental test results originally obtained in (21) were used here.

2.1. Test device and test parts

A schematic overview of the test device is shown in Figure 1.

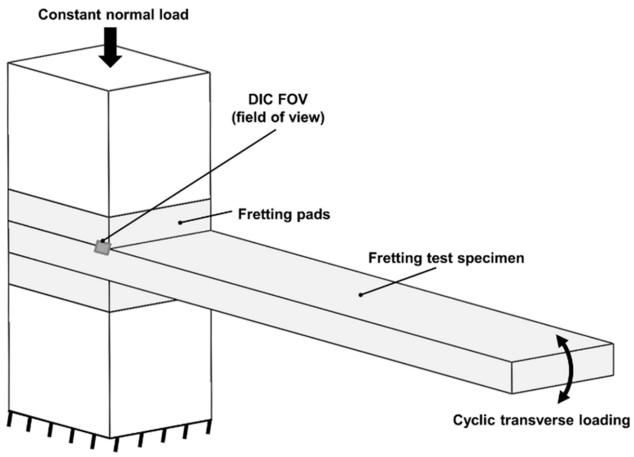

Figure 1. Schematic overview of the test device.

Two test contacts are established by clamping a flat fretting test specimen between two flat fretting pads by a normal load. A theoretical singularity occurs at the edge of the contact due to the complete contact created. The fretting movement in the contact and the fatigue loading of the test specimen is created by deflecting the specimen's free tip by an eccentric mechanism. At the contact edge, relative slip between the specimen and pads is induced due to the strain in the specimen, which is created by the transverse bulk loading. Relative slip is the result of the loadings, compliances of the design and tribological behavior (e.g., COF) and cannot be determined solely by the bulk loading mechanism. Due to the design of the test device and the specimen, tests are carried out in partial slip conditions, i.e., relative slip at the contact edge covers only a part of the nominal contact area. The major part of the contact is stuck where no slip occurs when using typical operating parameters (normal and bulk loading).

The size of the specimen and pad are as follows: the transverse width of the specimen and the pads is 40 mm; the length of the specimen is 250 mm and the length of the pad is 50 mm, which is also the nominal contact length. The thickness of the parts is

10 mm. The material of the specimen and the pads was EN 10083-1-34CrNiMo6+QT. Grinding direction was longitudinal and the grinding produced *Sa* value (arithmetic mean surface roughness) of 0.25 µm, measured with a Wyko NT1100 optical profilometer. The analyzed surface area was 4.9 × 3.8 mm^2, with a 6.72 µm sampling interval. For the DIC measurements, it is important that the specimen and pads are in the same depth of focus as close as possible. A jig was used to align the fretting specimen, pads and the blocks of steel. The tests were carried out in dry contact conditions. Acetone was used to clean the parts before testing. The tests were conducted under normal laboratory conditions. The relative humidity in the testing room was under 25 % during the experiments.

2.2. Digital image correlation

Displacements at the contact edge area were measured with a digital image correlation system. Detailed presentation of the measurement system used is given in (21). Basically, a five megapixel digital camera, equipped with a long distance microscope, was employed to capture images from the lateral (side) face of the specimen and pad at the contact edge area. The size of the field of view (FOV) was approximately 4.5 mm × 3.8 mm, giving pixel size of about 1.8 µm at the target surface. A calibration plate was used to define the scale. No special preparation was done to the target surface, i.e., pure ground steel surface was used. Displacements were calculated using the Least Squares Matching (LSM) approach (27). The spatial resolution of displacements was 32 µm – 37.2 µm, depending on minor differences in camera set-ups between tests (i.e., in the field of views). About 30 points were measured during one loading cycle of the specimen and short-term measurements were taken at specific points during the fatigue tests. Due to the huge amount of measurement data created, the entire fretting fatigue test cannot be practically measured with DIC. The loading frequency during DIC measurements was decreased from 41 Hz to 0.5 Hz or 1 Hz.

3. MODELING

The fretting contact was modeled using ABAQUS 6.13-3 finite element programme (28). A quasi-static analysis was considered adequate, given the small loading frequency in the experiments during DIC imaging. The implicit FE-model used here consists of the fretting test specimen, pads and blocks of steel as shown in Figure 2.

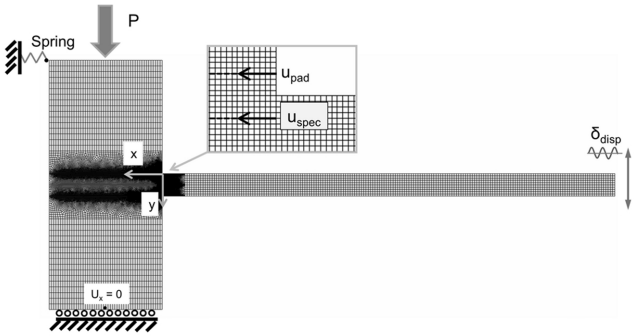

Figure 2. Finite element model of the fretting test device.

Plane strain, four node CPE4I elements with full integration were employed in the contact along with the ABAQUS's master-slave contact algorithm. An incompatible mode element was used to improve the bending behavior of the elements. The element size close to the contact edge is similar to the spatial resolution of DIC data (35 µm), though the elements are oversized for stresses to converge at the contact corner point. However, the displacements here are analyzed some distance away from the contact edge where the displacements converge, i.e., a smaller element size does not markedly change the displacement values there. Surface-to-surface contact discretization was used, which enforces contact over the regions nearby nodes, rather than at individual nodes. This provides more accurate results than node-to-surface discretization (28). The tangential behavior was described using the Penalty method with an elastic slip value of 5 nm. Elastic slip is a small amount of slip that is allowed to occur when the surfaces should be sticking. Normal direction was described using the Augmented Lagrange method with default stiffness. The

Coulomb friction model was adopted and constant COF was assumed along the contact surface. COF was increased monotonically to a desired value with small increments, starting from 0.1. This is assumed to describe real contact behavior better than using only the desired COF value. Three load cycles were performed with each COF to achieve steady-state contact conditions. The contact between the pads and the blocks of steel was not modelled because it was observed numerically that the contacts are stuck under the loading parameters used here. An elastic, isotropic material model was used having a Young's Modulus of 206 GPa and a Poisson's ratio of 0.28. Geometric nonlinearity was taken into account using the 'NLGEOM' (nonlinear geometry) option in ABAQUS.

A multi-point constraint (MPC) was applied at the top of the upper block to introduce the normal load. The lower end was fixed in the *y*-direction and the midpoint was fixed in the *x*-direction. Transverse bulk loading was created by displacing the specimen tip. A spring was fitted to the upper block to take into account compliances and rotation of the test device. The stiffness of the spring was adjusted using displacements measured with DIC. The displacement amplitude of the tip of the fretting specimen is measured by a laser sensor in the test device and this data was used in the FE model. Each loading cycle was divided into 58 increments. It has been reported that load incrementation in FE fretting analysis can have a marked effect on the accuracy of the slip distribution (29). First, the normal load was applied (and kept constant throughout analysis) and then, the cyclic transverse loading was applied. This is how the loading was applied in the measurements. Post-processing of raw DIC displacement data and FEM data was made in Matlab (30) with specially developed scripts. The FE results were processed in such a way that they can be directly compared to the corresponding measured DIC values, e.g., nodal displacements were adjusted to zero at the beginning of a loading step.

Figure 3 shows some features of the device and the contact arrangement. The figure shows normalized contact pressure p/p_{nom} during one loading cycle, when the nominal contact pressure p_{nom} is 100 MPa, the maximum nominal bending stress is 190 MPa and COF is 0.2.

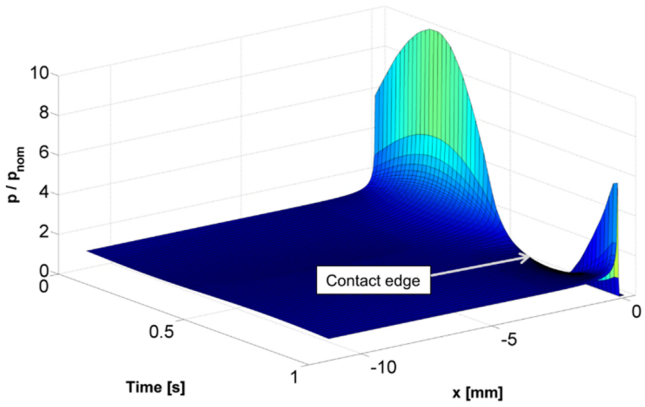

Figure 3. Contact pressure distribution during one loading cycle (FE calculation).

Initially, when the specimen and pads are clamped together by the normal load (time = 0 s), a local and steep contact pressure concentration exists at the contact edge. When bending the specimen against the pad, the magnitude of pressure increases (time 0.25 s). When the specimen is bent away from the pad, the contact pressure reaches to zero very close to the contact edge, meaning that the contact opens (time 0.75 s). With the normal load and bulk loading values used here, the contact opening occurs in every test. Contact opening always leads to at least some degree of slip (31) and therefore, fretting.

4. RESULTS AND DISCUSSION

The results are presented for two normal loads, corresponding to nominal contact pressures of 30 MPa and 100 MPa. The displacement amplitude of the specimen tip was between 2.5 mm and 2.7 mm, corresponding to the maximum nominal bulk (bending) stress in the specimen of about 190 MPa and 210 MPa, respectively. The maximum nominal bulk stress is the stress at the contact edge due the pure transverse loading, excluding any contact

effects. The tests were carried out with fully reversed loading (R = -1).

4.1. Displacement field

Measured and calculated displacements at the contact edge are compared between DIC (top) and FEM (bottom) in Figure 4. The figures show x-displacements (displacement field) at the upper position of the specimen, i.e., bending the specimen 'against' the fretting pad, during the first cycle of a fatigue test. The upper part is the pad and the lower part the specimen; the contact interface can be clearly seen between the parts. The COF used in the FE model was 0.2.

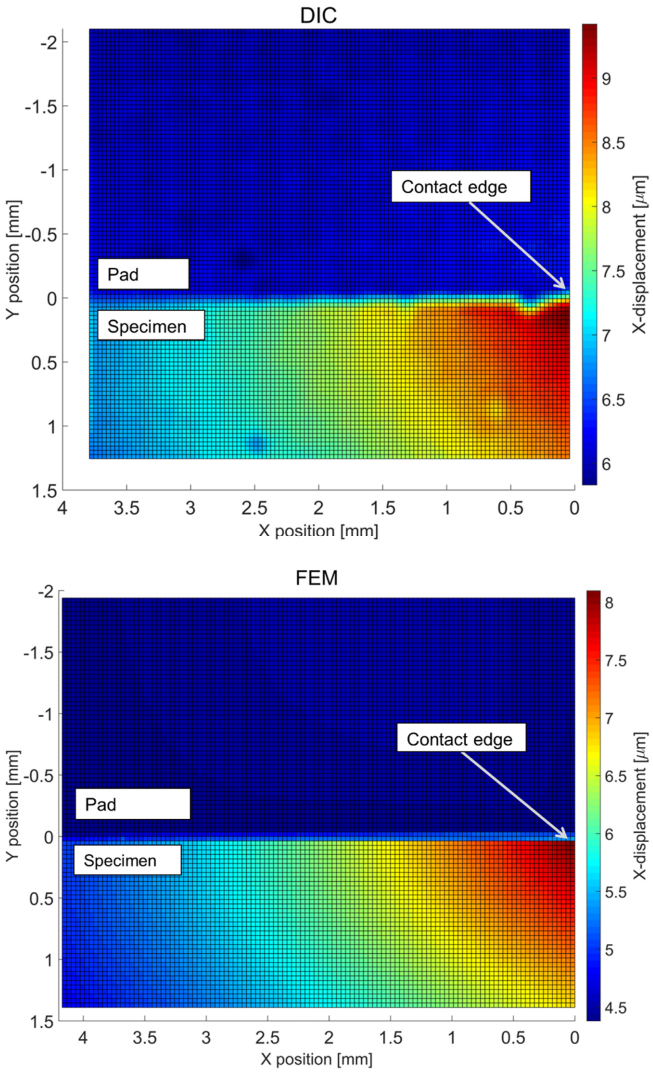

Figure 4. Comparison of x-displacements, specimen at upper position (upper: DIC, lower: FEM).

The displacement fields between DIC and FEM show similar behavior. Due to the unequal x-displacements between the specimen and pad at the contact interface, relative slip exists across the contact length shown. Maximum displacement of the specimen exists at the contact edge. This is the point of maximum stress and typically the point of cracking (24). Figure 5 presents the results more visually, where the displacement is shown as a height (z-axis in graphs). Upper and lower positions of the specimen are shown. The scales are similar in both graphs.

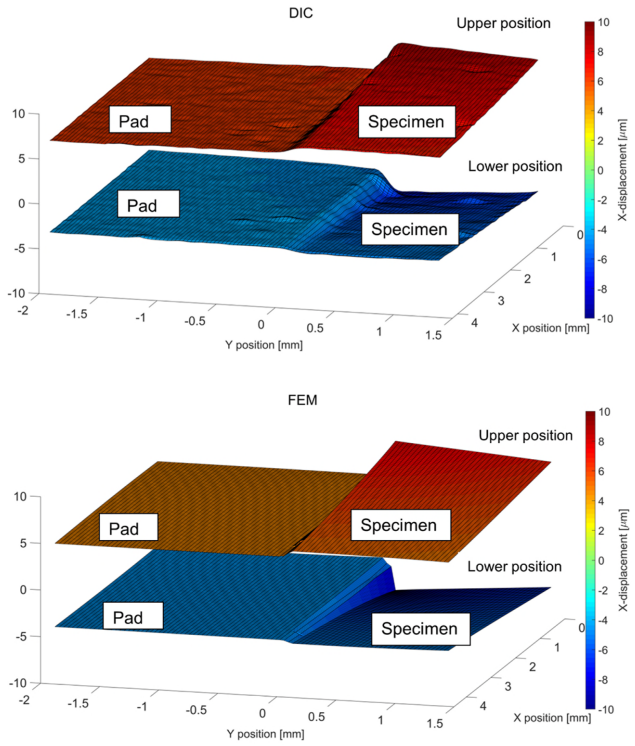

Figure 5. X displacements at upper and lower positions of the specimen (upper: DIC, lower: FEM).

The maximum displacement of the specimen is about ten micrometers, corresponding to approximately six pixels in captured images, thus making the movement clearly visible. Generally, somewhat similar values and behavior are observed for both DIC and FEM. Somewhat higher slip amplitude occurs when bending the specimen against the fretting pad. The bending moment caused by the transverse bulk loading of the specimen will cause rotation of the pads. The elastic compliances and the rigid body movement are

considerable, approximately equal to the amount of relative slip between the parts. These effects should be minimized. The DIC data is relatively smooth but some spots exist where displacements diverge from the surrounding values. In both positions, the relative movement exists throughout the length shown, i.e., the field of view is too small to capture the whole slip region.

4.2. Relative tangential movement (slip)

In practice, displacements at some distance away from the contact interface can be determined with DIC, depending on the disturbances in the measurements caused by the contact interface and parameters used in the displacement calculation. Therefore, the actual slip in the contact interface is difficult to determine. The slip δ between the specimen and pad at time moment t is defined here as the relative tangential displacement of the points in the specimen (u_{spec}) and pad (u_{pad}), i.e., the relative displacement between points that have the same x position and an equal but opposite y position (see Figure 2). This minimizes the rigid body movement and compliance effects.

$$\delta_i(t) = u_{spec}(t) - u_{pad}(t) \quad (1)$$

Figure 6 shows relative displacements as a function of the distance from the contact interface in the y-direction. The minimum examination distance is 150 µm, which is at least a factor of ten less than the distance of an extensometer from the contact interface.

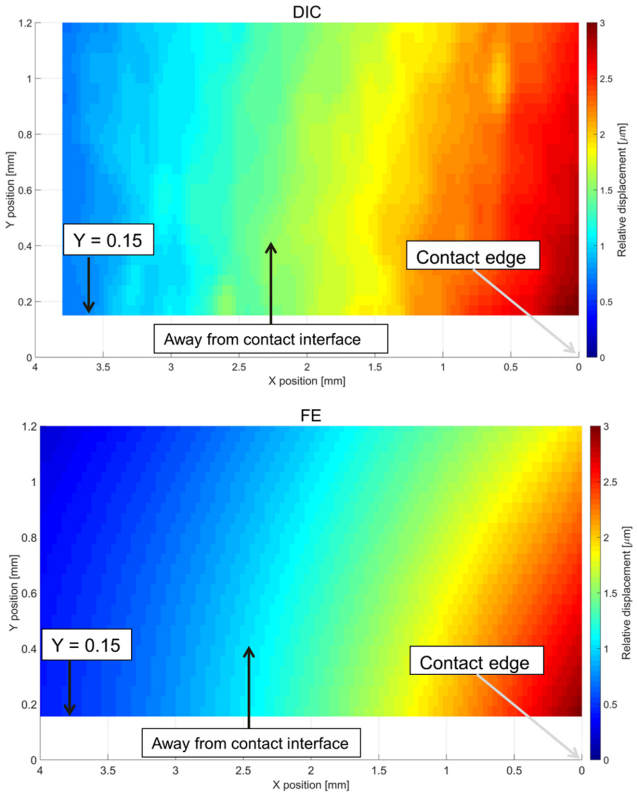

Figure 6. Relative displacement as a function of the distance from contact interface in y direction (upper: DIC, lower: FEM).

The FEM calculations are matched with the DIC results to within a 1 % difference in maximum slip amplitude (at the contact edge). The COF used in the model was varied. Thus, the COF was 0.245. Relative movement decreases when moving away from the contact interface. The maximum decrease (between values along a path in the y-direction) exists at the contact edge. With DIC, the slip 1.2 mm away from the contact edge is about 20 % lower than 150 µm away from the contact edge. With FEM, the corresponding value is about 30 %. It should be noted that the distance (1.2 mm) is nonetheless small and may not be comparable to displacements that an extensometer would measure from farther away. In subsequent DIC and FEM results, displacements are investigated at a distance approximately 150 µm from the contact edge.

Slip amplitudes and slip region lengths were computed using different COFs and the results are presented in Figure 7. The slip amplitude is the average of the two values of maximum slip in both

directions (i.e., at the extreme positions) during a loading cycle. The slip region length is the maximum length observed during a cycle. In the experiments (21), the threshold value for slip was 0.3 µm and values below this were neglected. This value was chosen on the basis of the disturbances shown in the DIC measurements and on the evaluation of the accuracy of the measurements. The same threshold was used in Figure 7.

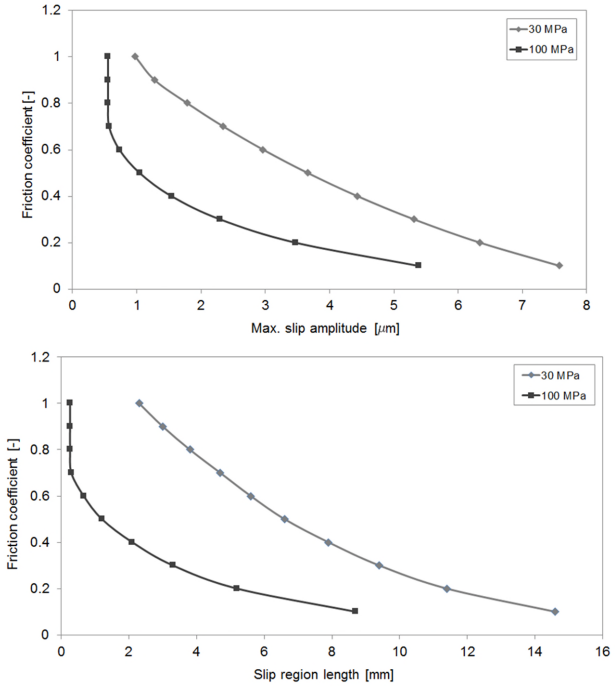

Figure 7. Calculated slip amplitude and slip region length using different friction coefficients.

The effect of COF on slip is clearly shown in the graphs. Both slip region length and slip amplitude decrease markedly as the COF increases. For example, in the 30 MPa case, the increase in COF from 0.2 to 0.8 decreases the slip amplitude by 70 %. In the case of 100 MPa, at COFs above, say, 0.7, the visible small amplitude is mostly due to elastic compliances, nor to slip between the surfaces. Basically, FEM shows that the contact sticks when bending the specimen against the pad. In addition, when bending the specimen downwards, the slip is very small. In contrast, in the 30 MPa case the slip varies markedly up to a COF of one. These graphs are, of course, valid only for the loading parameters used.

The FEM model was used to repeat the cyclic slip measured with DIC. The FEM results were matched with the measured data within the slip amplitude when bending the specimen upwards. Cyclic slip results with a nominal contact pressure of 100 MPa are shown in Figure 8.

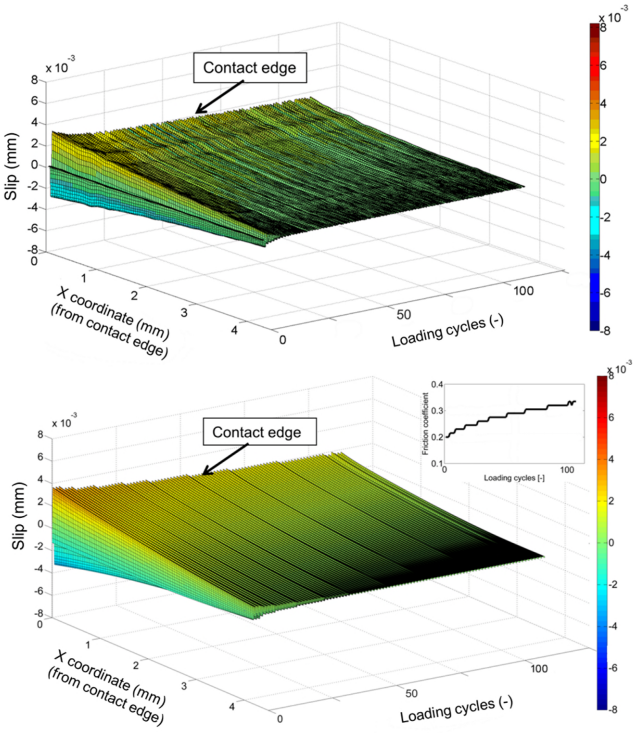

Figure 8. Cyclic slip as a function of the first 107 loading cycles of a fretting fatigue test, nominal contact pressure 100 MPa (upper: DIC, lower FEM).

The top half of the figure shows the DIC results of the first 107 cycles of a fatigue test and below are the corresponding FEM results. During the cycles shown, the COF is increased from about 0.2 to 0.33, as shown in the inset. Slip amplitude and slip region length decrease immediately at the beginning of the test. During the cycles shown, the maximum slip amplitude at the contact edge decreases almost 50 %. Figure 9 shows the corresponding results of the lower nominal contact pressure (30 MPa), during the first 31 cycles of a fatigue test.

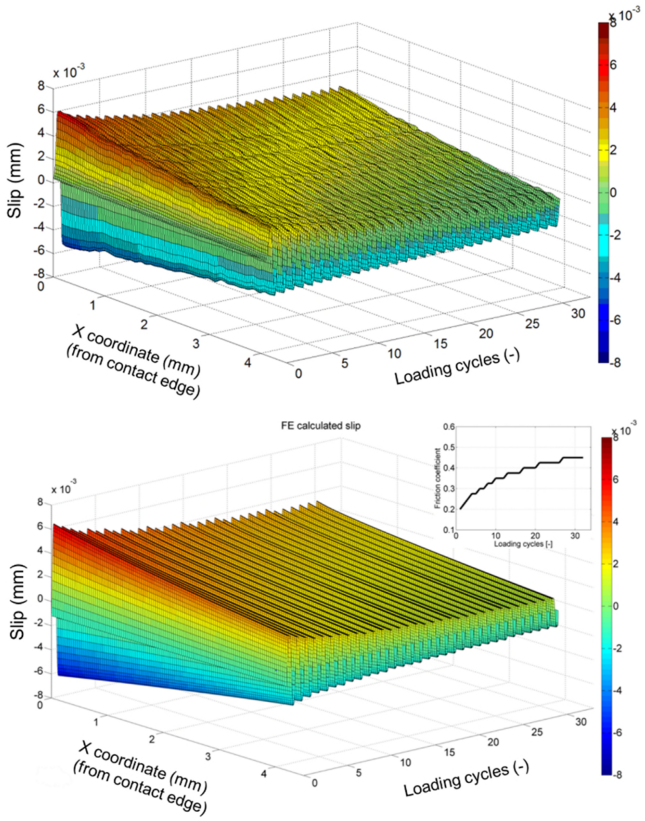

Figure 9. Cyclic slip as a function of the first 31 loading cycles of a fretting fatigue test, nominal contact pressure 30 MPa (upper: DIC, lower FEM).

As expected, slip is clearly higher in this case as the normal loading is decreased while the bulk loading stays the same. Both the slip amplitude and slip region length are appreciably higher than in the 100 MPa case. Again, there is a marked drop in these values during the initial cycles.

4.3. Friction coefficient

The COF was calibrated in three ways. Figure 10 shows COFs calculated from the experimentally measured slip region length using the previously shown relationship between COF and slip region length (Figure 7). As noted earlier, the length is rather difficult to determine experimentally because slip decreases somewhat exponentially and measurement noise is increased in this area because of the very small slip amplitudes. In addition, the slip region length is in most cases extrapolated outside the field of view (see (21)).

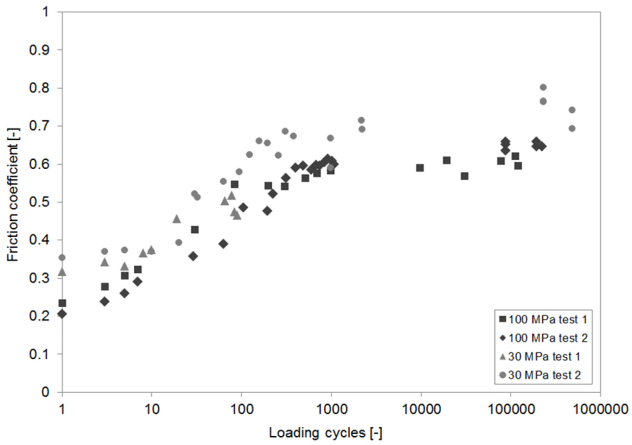

Figure 10. Calculated friction coefficients (from slip region length) as a function of loading cycles.

In both normal load cases, COFs start from a relatively low value, but increase rapidly and stabilize after about 1000 cycles, which is in line with the general observations. The steady-state values are between 0.55 and 0.8. Due to scattering in the results, no definitive conclusions can be drawn on the difference between the contact pressures. However, it seems that COF increases as contact pressure decreases. Figure 11 shows COFs calculated from the experimentally measured maximum slip amplitude value.

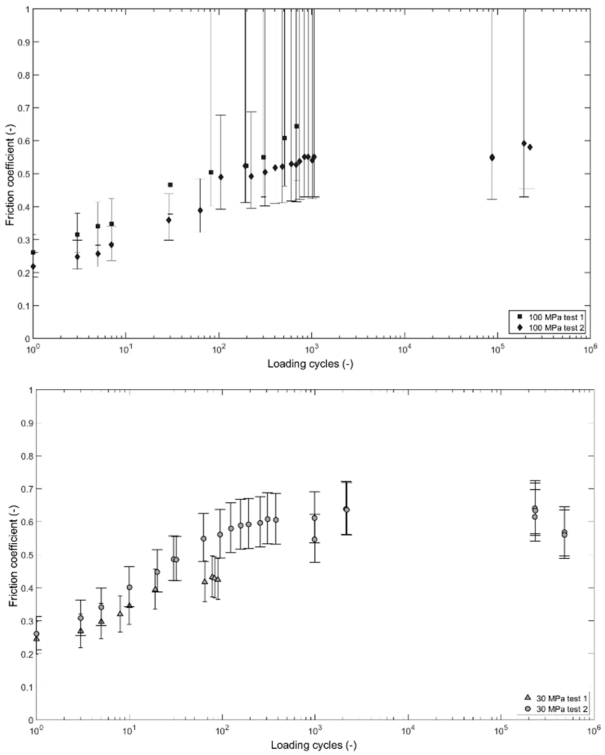

Figure 11. Calculated friction coefficients (from slip amplitude) as a function of loading cycles.

The error bars shown are calculated assuming variations of ± 0.5 µm in the measured displacements. This level of accuracy should be reached in careful measurements (21). The steady-state values are between 0.5 and 0.65. In the 100 MPa case, COFs over ~0.5 have a very large range of variation and, clearly, COFs above ~0.6 cannot be determined due to the almost sticking contact. In the 30 MPa case, however, the variation is reasonably smooth and the results are somewhat similar to the results calculated from the slip length.

Accumulated slip (29) over contact length was employed to calibrate the COF (22). It has been estimated as giving a better 'measure of contact' than slip amplitude alone (22). The cumulative slip in Figure 12 and Figure 13 is the sum of slips (in absolute values) over one loading cycle, i.e., a single up and down movement of the specimen. The same time incrementation was used by interpolating FEM data to correspond to the DIC results.

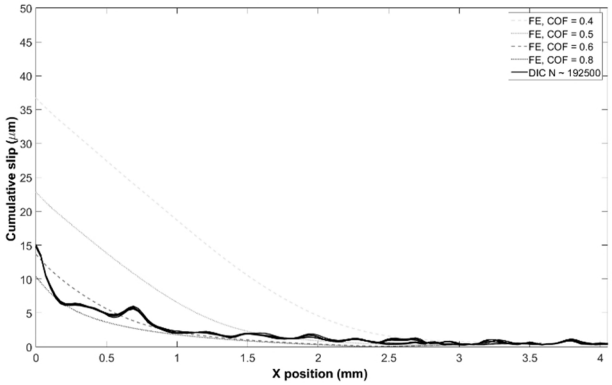

Figure 12. Calculated and measured cumulative slip, nominal contact pressure 100 MPa.

Figure 12 shows the results for the 100 MPa case after about 192 500 loading cycles, so these represent steady-state, i.e., stabilized, COF values in the fretting fatigue test. The figure shows cumulative slip for COFs of 0.4, 0.5, 0.6 and 0.8. Of these, COFs of between 0.6 and 0.8 give the closest correspondence to the experimental results, which are shown as a solid black line.

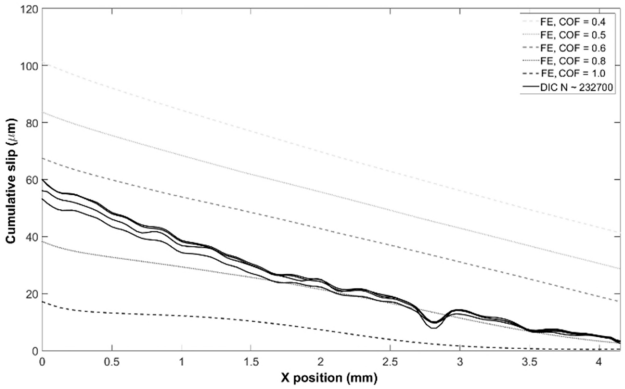

Figure 13. Calculated and measured cumulative slip, nominal contact pressure 30 MPa.

Figure 13 presents the corresponding results in the case of 30 MPa, after about 232 700 cycles. COFs of between 0.6 and 0.8 provide the best correspondence to the experimental results at the contact edge though the higher COF correlates better away from the contact edge. The accumulated slip distributions show differences between FEM and DIC, as can be seen also in (22). A major reason here can be the accumulation of measurement uncertainties. In terms of modeling, the assumptions, e.g., plane strain conditions and constant friction coefficient, may have had an effect on the results. On the other hand, however, the accumulated slip is sensitive to COF. Calibration of the friction coefficient using accumulated slips seems, therefore, to be an efficient and practical method.

The results presented show that DIC is a suitable method to apply in fretting conditions. Besides the relative slip amplitude, used typically to characterize fretting contact, it can provide the slip distribution over the contact and, therefore, the size of the slip and stick regions. However, at very small relative slips, measurement errors can be considerable and care is needed. Local disturbances at the contact boundary (e.g. local adhering at the contact edge side) may cause errors. It is, therefore, recommended that several tests be performed with similar parameters to minimize these uncertainties. In addition, full-field displacement data from DIC

measurements provide a useful and comprehensive means for comparison with full-field FE data to verify numerical models and to calibrate the friction coefficient, for example.

5. CONCLUSIONS

Full field displacement data measured from a complete contact using the Digital Image Correlation method and corresponding finite element model data were used to analyze the fretting contact.

- Test device compliances and rigid body movement were minimized by measuring displacements close to the contact interface.
- The displacement field and its derivates, relative slip amplitude, slip distribution across the contact, length of the slip region and accumulated slip distribution, were compared between both methods using the friction coefficient as a variable in the numerical model.
- The friction coefficient was calibrated in three ways using the finite element method and displacements measured with the digital image correlation method and, in addition, the friction coefficient was determined as a function of loading cycles in fretting fatigue tests.
- Friction coefficient has a considerable effect, i.e., slip decreases markedly as the friction coefficient increases and also decreases markedly as the nominal contact pressure is increased.
- The friction coefficient was found to increase at the beginning of the tests and stabilize after about 1000 cycles, which is in agreement with general observations.

ACKNOWLEDGEMENTS

This study was conducted as part of SCarFace Research Project (Tekes decision no. 40205/12). We are grateful for the financial support provided by Tekes - the Finnish Funding Agency for Innovation, Wartsila Finland Oy, Nome Oy, and Global Boiler Works Oy.

DECLARATION OF CONFLICTING INTERESTS

The authors declared no potential conflicts of interest with respect to the research, authorship, and/or publication of this article.

FUNDING

This work was supported by the Finnish Funding Agency for Innovation [grant number 40205/12], Wartsila Finland Oy, Nome Oy, and Global Boiler Works Oy.

REFERENCES

1. Dobrominski JM. Variables of Fretting Process: Are There 50 of Them? In: Attia, MH and Waterhouse RB (ed.) *Stand Frett Fatigue Test Methods Equip.* 1992;ASTM STP 1:60–66.
2. Hills D, Nowell D. *Mechanics of Fretting Fatigue.* Dordrecht: Kluwer Academic Publishers; 1994.
3. Fouvry S, Kapsa P, Vincent L. A global methodology to quantify fretting damages. *ASTM Spec Tech Publ 1425*. 2002;(1425):17–32.
4. McColl I, Ding J, Leen SB. Finite element simulation and experimental validation of fretting wear. *Wear*. 2004;256(11-12):1114–1127.
5. Hintikka J, Lehtovaara A, Mantyla A. Fretting-induced friction and wear in large flat-on-flat contact with quenched and tempered steel. *Tribol Int.* 2015;92:191–202.
6. Ruiz C, Boddington PHB., Chen KC. An investigation of fatigue and fretting in a dovetail joint. *Exp Mech*. 1984;24(3):208–217.
7. Spink GM. Fretting fatigue of a 2.5%NiCrMoV low pressure turbine shaft steel: The effect of different contact pad materials and of variable slip amplitude. *Wear*. 1990;(136):281–297.
8. Vingsbo O, Soderberg S. On fretting maps. *Wear*. 1988;126(2):131–147.

9. Nishida T, Kondoh K, Xu JQ, Mutoh Y. Observations and analysis of relative slip in fretting fatigue. In: Mutoh Y, Hoeppner DW and Kinyon SE (ed.) *Fretting fatigue: Advances of Basic Understanding and Applications.* West Conshohocken, PA, USA: ASTM; 2003. p. 33–43.
10. Sabelkin V, Mall S. Investigation into relative slip during fretting fatigue under partial slip contact condition. *Fatigue Fract Eng Mater Struct*. 2005;28(9):809–824.
11. Wittkowsky BU, Birch PR, Dominguez J, Suresh S. An apparatus for quantitative fretting fatigue testing. *Fatigue Fract Eng Mater Struct.* 1999;22(4):307–320.
12. Noraphaiphipaksa N, Kanchanomai C and Mutoh Y. Numerical and experimental investigations on fretting fatigue: Relative slip, crack path, and fatigue life. *Eng Fract Mech* 2013; 112-113: 58–71.
13. Sutton MA, Orteu J-J, Schreier HW. *Image Correlation for Shape, Motion and Deformation Measurements.* New York, Springer; 2009.
14. Kartal ME, Mulvihill DM, Nowell D, Hills DA. Determination of the Frictional Properties of Titanium and Nickel Alloys Using the Digital Image Correlation Method. *Exp Mech*. 2011;51(3):359–371.
15. Kartal ME, Mulvihill DM, Nowell D, Hills DA. Measurements of pressure and area dependent tangential contact stiffness between rough surfaces using digital image correlation. *Tribol Int*. 2011;44(10):1188–1198.
16. Mulvihill DM, Brunskill H, Kartal ME, Dwyer-Joyce RS, Nowell D. A Comparison of Contact Stiffness Measurements Obtained by the Digital Image Correlation and Ultrasound Techniques. *Exp Mech*. 2013;53(7):1245–1263.
17. Crevoisier J, Swiergiel N, Champaney L, Hild F. Identification of In Situ Frictional Properties of Bolted Assemblies with Digital Image Correlation. *Exp Mech*. 2012;52(6):561–572.
18. Hojjati R. *Numerical Modelling Techniques for Fretting Fatigue Crack Initiation and Propagation.* PhD Thesis, University of Ghent, Belgium, 2014.
19. De Pauw J, De Waele W, Hojjati-Talemi R, De Baets P. On the use of digital image correlation for slip measurement during coupon scale fretting fatigue experiments. *Int J Solids Struct*. 2014;51(18):3058–3066.
20. Winkler J, Geǫrgakis CT, Fischer G. Fretting fatigue behavior of high-strength steel monostrands under bending load. *Iïnt J Fatigue*. 2015;70:13–23.
21. Juoksukangas J, Lehtovaara A, Mantyla A. Applying the digital image correlation method to fretting contact for slip measúrement. *Proc Inst Mech Eng Parť J J Eng Ťribol*. 2015.
22. Nesladek M, Spaniel M, Jurenka J, Růzička J, Kuzelka J. Fretting fatigue – Experimental and numerical approaches. *Int J Fatigue*. 2012;44:61–73.
23. Kim HS, Mall S. Investigation into three-dimensional effects of finite contact width on fretting fatigue. *Finite Elem Aïnal Ďes*. 2005;41(11-12):1140–1159.
24. Juoksukangas J, Lehtovaara A, Mantyla A. Development of a complete contact fretting test device. *Proc Inst Mech Eng Part J J Eng Tribol.* 2013;227(6):570–578.
25. Sabelkin V, Mall S. Relative Slip on Contact Surface under Partial Slip Fretting Fatigue Condition. *Strain*. 2006;42(1):11–20.
26. Ding J, Leen SB, McColl IR. The effect of slip regime on fretting wear-induced stress evolution. *Int J Fatigue*. 2004;26(5):521–531.
27. Lavi̇sion. Davis 8.2 Commercial DIC-software. 2013.
28. Systemes D. Abaqus Theory Manual 6.12-EF. 2014;
29. Leen SB, Richardson IJ, McColl IR, Williams EJ, Hyde TR. Macroscopic fretting variables in a splined coupling under combined torque and axial load. *J Strain Anal Eng*. 2001;36(5):481–497.
30. MATLAB and Statistics Toolbox Release 2010b, The MathWorks, Inc., Natick, Massachusetts, United States.
31. Hills DA, Paynter RJH and Dini D. An overview of the quantification of fretting fatigue lives of complete contacts. *Eng Fract Mech* 2012; 80: 3-12.

Notation

DIC	Digital image correlation (method)
LSM	Least Squares Matching method in Davis (DIC) program to calculate displacements
t	Time
u_{pad}	Displacement of fretting pad
u_{spec}	Displacement of fretting specimen
δ	Relative tangential movement between fretting pad and specimen
δ_{disp}	Transverse bulk loading
N	Loading cycles
p	Contact pressure
p_{nom}	Nominal contact pressure
P	Normal load
R	Stress ratio
U_x	x-displacement

Publication VI

Experimental and numerical investigation of fretting fatigue behavior in bolted joints

by

J. Juoksukangas, A. Lehtovaara and A. Mäntylä

Tribology International, 103, 2016, 440–448, doi:10.1016/j.triboint.2016.07.021

Tribology International 103 (2016) 440–448

Contents lists available at ScienceDirect

Tribology International

journal homepage: www.elsevier.com/locate/triboint

Experimental and numerical investigation of fretting fatigue behavior in bolted joints

Janne Juoksukangas [a,*], Arto Lehtovaara [a], Antti Mäntylä [b]

[a] Group of Tribology and Machine Elements, Department of Materials Science, Tampere University of Technology, P.O. Box 589, 33101 Tampere, Finland
[b] Research & Development, Wärtsilä Finland Oy, P.O. Box 244, 65101 Vaasa, Finland

ARTICLE INFO

Article history:
Received 11 April 2016
Received in revised form
25 July 2016
Accepted 26 July 2016
Available online 27 July 2016

Keywords:
Fretting
Contact
Fatigue
Finite-element method

ABSTRACT

Bolted joints may suffer from fretting damage which can significantly decrease fatigue life. A testing arrangement was developed to study the effect of different operating and design parameters of a single bolted joint on fretting fatigue life. Fretting fatigue stress-life (S-N) tests were conducted to investigate in particular the effect of bolt preload and cyclic bulk loading on fatigue life. Fretting fatigue life decreased when increasing the preload and also when increasing the bulk stress. The Digital Image Correlation method was applied to measure tangential displacements close to the contact. A corresponding finite element model of the test setup was used to analyze contact variables in greater detail. The numerical results corresponded well to the experimental results.

1. Introduction

In mechanical engineering, bolted joints are often used in assemblies to clamp parts together and to transfer loads. However, bolted joints may suffer from fretting damage, which is one of their major failure mechanisms [1]. Fretting refers to small oscillatory relative movement between connected parts under normal loading. Fretting can lead to high local stresses, surface damage and wear that can further lead to fatigue crack nucleation.

The main operating parameters in bolted joints are bolt preload (creating normal load in the contact) and external cyclic bulk loading of bolted parts. The purposes of the bolt preload are to clamp parts together and to create frictional forces between the bolted parts to carry shear loading. Preload affects the sizes of the stick (adhesion) and slip zones of contacts during fretting loading [2]. Typically, at low or negligible preload, the point of fatigue cracking is at the bolt hole where the hole induced stress concentration exists [2,3]. A preloading with compressive stress can decrease the stress concentration effect at the bolt hole and thus increase fatigue life [1,3–6], which has also been shown in riveted joints [7]. An increase in preload can move the point of cracking away from the area of the hole and produce a further increase in fatigue life [1]. However, even when the cracking point is moved outside the stress concentration area, fatigue life can be decreased due to fretting [2,3]. In addition, the value of coefficient of friction (COF) has an effect on the point of cracking. In an experimental study [3], the COF was reduced by lubricating the contact and the point of cracking moved to the hole edge area, resulting in reduced fatigue life. The predominant wear mechanism has been observed to change from adhesive wear to abrasive wear when increasing preload [2]. A hybrid joint (e.g. an adhesive layer between bolted plates) can notably decrease stress concentration at the bolt's hole [8,9] and it can have longer fatigue life compared to pure bolted joints [8]. An interference-fitted bolt may also increase the fatigue life of a joint [10].

Typically, experimental testing relating to bolted joints is carried out using commercial material fatigue testing machines with axial loading of the specimens [1–3,8,11–16]. Considering practical bolted connections, bending loading may commonly exist. However, bending loading has been used less frequently, e.g. [17]. Ultrasound technique has been used to study contact pressure distribution [18] and cracking [5,11]. Numerical studies, based mainly on the finite element method (FEM), have been carried out to study the contact behavior of bolted joints [2,6,9,19–24], to predict fretting fatigue life [6,14,19,25–27] and to apply fracture mechanics [6,8]. Analytical solutions have been developed to study contact quantities [28], and to control the preload [29]. The bolt loosening has practical importance and has been studied, for example, in Ref. [29,30].

Relative tangential movement, slip, between contacting parts is an important variable in fretting. Tangential displacements in the contact are typically measured using a linear variable differential

* Corresponding author.
E-mail addresses: janne.juoksukangas@tut.fi (J. Juoksukangas), arto.lehtovaara@tut.fi (A. Lehtovaara), antti.mantyla@wartsila.com (A. Mäntylä).

http://dx.doi.org/10.1016/j.triboint.2016.07.021
0301-679X/

transformer (LVDT) or an extensometer, but such measurements also include compliances of the test device. Moreover, displacement of only one point can be measured. Alternatively, a Digital Image Correlation ('DIC') can be used to measure the displacement field of a fretting contact and, in turn, the relative tangential displacements (slip). DIC is an optical method that uses captured digital images of loaded structures to resolve displacements [31]. DIC has previously been applied to fretting contacts, e.g., [32,33]. In bolted joints, numerical results have been compared to DIC measurements with good accuracy and the coefficient of friction has been identified as a function of loading cycles using the FEM and DIC [15]. The materials in contact were aluminum alloy and carbon/epoxy. DIC has been used to analyze a bolted joint under vibration loading [34].

Although there are several studies relating to fretting fatigue in bolted joints, there is still a need for further research to gain a more complete understanding of fretting behavior in bolted connections. Though quenched and tempered steels are commonly used materials in heavy load conditions, relatively little attention has been given to their fretting fatigue behavior. For example, in medium speed combustion engines, parts are under heavy loading conditions where the contact surfaces need to transfer high contact tractions. In bolted lap joint studies, the focus is on aluminium and titanium alloys in the literature. Therefore, there is a need for fretting research in bolted joints made of quenched and tempered steels**.** Here, a single bolted joint was studied both experimentally and numerically. A test setup was developed to study, mainly, the effect of joint preload and bulk loading on fretting fatigue life using bending loading. Several fretting fatigue tests were carried out with different operating and design parameters. The Digital Image Correlation method was applied to measure tangential displacements close to the contact which were used further together with a corresponding finite element model to evaluate the coefficient of friction of the contact. The model was used to study contact variables in greater detail.

2. Experiments

2.1. Test device

A previously developed complete contact fretting test device was used here [35]. Only minor modifications were needed to study bolted joints. Two flat test specimens, shown schematically in Fig. 1, are clamped together at one end (main clamping). The test contact (single bolt joint) is 30 mm away from the main clamping. The cyclic bulk loading in the specimens is established by the transverse loading (displacement) applied at the specimens' free tips by an eccentric mechanism. This loading also induces the shear load to the joint under examination. Relative slip between the specimens is created as a result of the different strains in the specimens (i.e., the contact surface of one specimen is in tension at the same time as the contact surface of the other specimen is in compression). The specimens are clamped together from the free end to apply the bulk loading. Though clamping obviously induces fretting at this point, it is supposed that it would have no significant effect on the actual test contact.

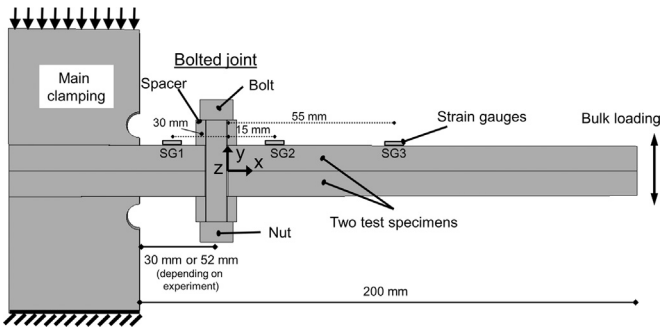

Fig. 1. Schematics of the bolted joint testing arrangement.

The specimen had a length of 250 mm, width of 40 mm and thickness of 10 mm. The material was EN 10083-1-34CrNiMo6+QT. Grinding direction was longitudinal and the grinding produced a *Sa* value of 0.25 μm, measured with a Wyko NT1100 optical profilometer. The normal load created by the bolt was transferred to the fretted contact via spacers. The spacers were made of steel with a height of 10 mm and the outer and inner diameters were 16 mm and 8.5 mm, respectively. The diameter of the bolt hole in the specimen was 9 mm. M8 12.9 hex socket bolt was used with a corresponding nut. FEM analysis showed that the bolt shank and the specimens do not touch under cyclic loading and this was further confirmed in the experiments.

Strain gauges were attached to the bolt to continuously measure the preload during testing. A device was built to calibrate the preload measuring arrangement against an external force sensor. Three strain gauges were attached to the upper test specimen having *x*-positions of −30 mm, 15 mm and 55 mm (Fig. 1). The bulk loading frequency was 20 Hz but during DIC measurements the loading frequency was decreased to 0.6 Hz. The tests were conducted under normal laboratory conditions with relative humidity under 45 RH and temperature between 24 and 29 °C. The tests were carried out in dry (unlubricated) conditions. Before testing, the specimens were wiped with acetone.

The experimental test matrix is shown in Table 1. Parameters were the bolt preload, bulk (bending) stress, spacer outer diameter and bolted joint position in the specimen. Three bolt preloads were used (20 kN, 25 kN and 30 kN). The preload was either close to the design value or markedly below practical loading conditions (56%, 70% and 85% of the bolt's proof strength). In series 1 and 2, the three bulk stress amplitudes at the location of the center point of the hole were approximately 130 MPa, 170 MPa and 205 MPa and were linearly scaled from the strain gauge measurements (SG2 and SG3, Fig. 1). The contact contributes to the measured stress values which can be seen in the measurements. The reported values are selected after about 80,000 loading cycles, after which the bulk stress values have somewhat stabilized. These stresses correspond to specimen tip displacement amplitudes of about 1.4, 1.8 and 2.3 mm, respectively. In series 3 and 4, the bulk stress amplitudes were 180–200 MPa. In all tests, the bulk loading was fully reversed, i.e., the desired value for stress ratio *R* was −1. Fatigue tests were run until one or both of the specimens cracked completely or the cut-off limit of three million cycles was reached.

In series 1, three preloads and three bulk stresses were used. Series 2 was a repeat series, where two tests with 25 kN preload were conducted with all three bulk loadings. In series 3, the active contact area was increased by using a larger spacer, having an outer diameter of 24 mm. The slip was increased in series 4 by moving the bolt position towards the free end. In series 5, four interrupted tests were performed to study fretting damage development. The number of cycles was approximately 40,000, 200,000, 400,000 and 600,000. The preload was 25 kN and the highest bulk loading amplitude (205 MPa) was used. A new specimen was introduced in every test. A total of 24 experimental tests were carried out.

2.2. Digital image correlation measurements

A five megapixel digital camera with 200 mm lens and an extension tube was positioned behind the test device, and with the aid of a mirror, the lateral surface of the specimens was

Table 1
Experimental test matrix.

Series	Description	Bolt preload [kN]	Bulk stress [MPa]	Spacer outer diameter [mm]	Bolted joint position (from main clamping) [mm]	Number of tests
1	Reference	20, 25, 30	130, 170, 205	16	30	9
2	Repeat	25	130, 170, 205	16	30	6
3	Increased contact area	25	180	24	30	2
4	Increased slip	25	180–200	16	52	3
5	Interrupted (with DIC)	25	205	16	30	4
Total number of tests						24

photographed. A complete contact has been previously measured in a similar way [36], where a more detailed presentation of the DIC-system is given. The DaVis program by Lavision [37] was used to obtain the images and to calculate displacements. The target surface was sprayed with black paint using an airbrush. The size of the field of view was approximately 12.2 × 10.2 mm^2, resulting in a pixel size of 5 μm at the target surface. A calibration plate provided by the manufacturer of the DIC equipment [37] was used to define the scale. Displacements were computed in the DaVis program using the Least Squares Matching (LSM) approach [37]. The size of a subset was 33 pixels and the step size was 16 pixels. The resulting spatial displacement resolution was, therefore, 80 μm. About 24 points were measured during a single loading cycle and short term measurements were taken at specific points during the fatigue tests.

3. Modelling

An FE-model of the test setup, with some simplifications, was built to analyze the contact in more detail using the commercial ABAQUS programme [38]. The parts shown in Fig. 1 were modelled. Only one half of the geometry was modelled due to the assembly's symmetry (Fig. 2). Elastic material model with Poisson's ratio of 0.28 and Young's Modulus of 206 GPa was used.

Some simplifications were made to the model. The bolt and nut were attached, i.e., tied, to the spacers. The lower end of the block (main clamping) was fixed. A stiff spring was added to the top end to take into account the rotation of the test device due to the transverse loading. The bolt preload was modelled as “bolt load” in Abaqus. Loads corresponding to the experiments were applied in four steps. First, the bolt preload was applied. Then, the specimens were clamped (main clamping) resulting in nominal contact pressure of 100 MPa, and after that, the clamping of the free end was applied. The clamping was modelled using 1.5 kN point loads. Finally, cyclic loading was introduced by displacing the specimens' free tips. Experimentally measured displacement amplitude data of the tip of the fretting specimen was used in the model.

After a mesh convergence study, the element size of about 1 mm was adopted in the contact area. At the hole, however, smaller elements may be needed to capture the stress concentration. In this case, the inspection point is at the fretting area where the element size used is sufficiently small. The element type used was C3D8I. The master-slave contact algorithm was used with finite sliding contact condition and the surface-to-surface contact discretization. Penalty friction with elastic slip value of 0.05 μm was used to describe the contact tangential behavior together with the Coulomb friction model. COF of the contact between the spacer and specimen, as well as between the blocks of steel and specimen (main clamping) was 0.6. The normal direction was described using the Augmented Lagrange method. Each loading cycle was divided into 50 increments. Three cycles were performed to represent steady-state loading conditions.

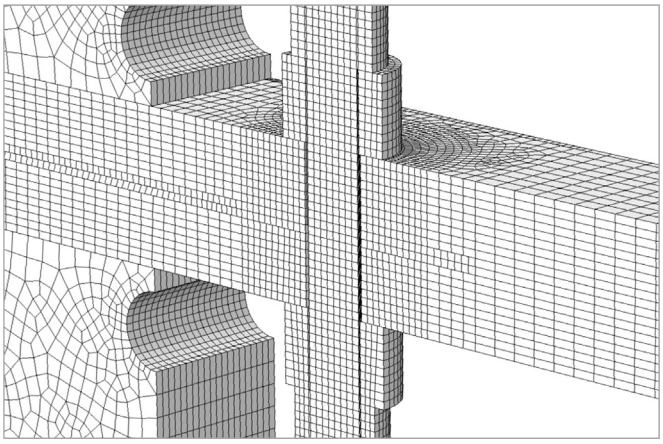

Fig. 2. FE-mesh.

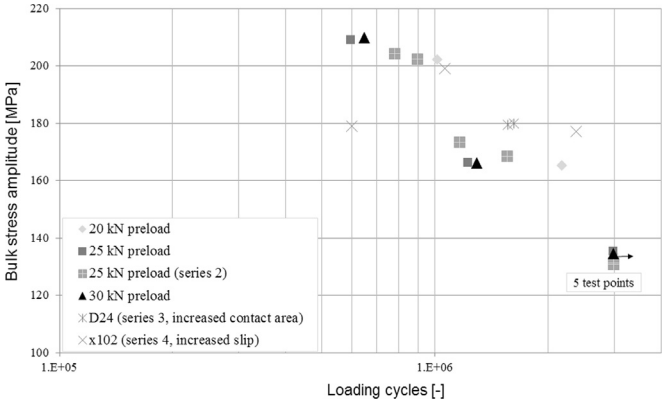

Fig. 3. Fretting fatigue S-N test results of series 1, 2, 3 and 4.

4. Experimental results

4.1. Fretting fatigue results

The results of series 1, 2, 3 and 4 are presented in the S-N graph in Fig. 3, where the bulk stress amplitude is shown as a function of loading cycles. At the lowest bulk stress, no complete fracture occurred. However, small cracks (similar to those shown in Fig. 6, the last subfigure) were observed in three specimens. Some of them were very small and barely visible. Therefore, fretting readily led to nucleation of cracks but the bulk stress was not high enough to allow cracks to grow further. The cracks were mainly inspected visually though a micro-level inspection might have detected more small (microscopic) cracks. At higher bulk stresses, all specimens fractured completely. Increasing the bulk loading decreases fatigue life, regardless of the preload. Two tests were made with a larger spacer diameter (24 mm, series 3) and with a preload of 25 kN. Here, naturally, the active contact area increases and the maximum contact pressure decreases compared to the previous

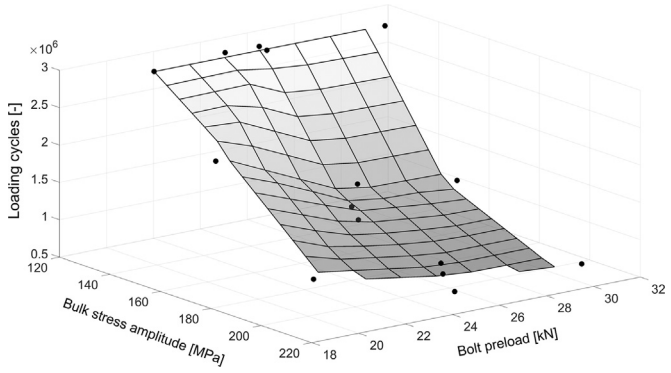

Fig. 4. Experimental fretting fatigue tests results of series 1 and 2.

case. These tests indicated increased fatigue lives. Slip amplitude was increased by re-positioning the hole (series 4). A high scatter was observed in the series 4 tests and so no conclusion can be drawn. Although major cracks were nucleated at the test contact surface in these tests, in both of the series (2 and 3) cracking was also observed under the spacer in one of the tests, which may have had an effect on fatigue lives. In one test (series 4, 'x102', 2.4e6 loading cycles), major cracking was observed under the spacer and therefore, this test point was rejected because the focus is on the contacting surfaces between the two test specimens.

The effect of the preload on fatigue life can be more clearly seen in Fig. 4. The results of series 1 and 2 are shown. The experimental results indicate that fretting fatigue life decreases as the preload is increased. For example, in the 170 MPa case, the use of 20 kN preload roughly doubles the fatigue life compared to 30 kN preload. It is worth noting that in all the tests, the bolt preload was relatively constant during testing and the difference between the lowest and highest value during a test was typically under a few percent.

4.2. Surface damage

Fretting scars were analyzed visually. The images of the specimens of series 1 are shown in Fig. 5. The right side of each figure relates to the free end of the specimen. The contact surfaces of both the upper and lower specimen are shown. The surfaces of the specimens in the outermost column (right-hand side) were not wiped with acetone after testing, thus showing their surfaces 'as is'. The fact that fretting particles (brown area) exist on the right side of the crack with a strict boundary indicates that the contact opens at that point. It is also worth noting that some specimens had seized together somewhat and some force was needed to separate them.

The following observations can be made from Fig. 5:

- Fretting damage occurs in all tests.
- More wear is observed at the bulk loading (free end) side creating 'arch' type scar.
- The point of severe damage and cracking is situated at some distance away from the hole.
- A stick zone or a zone with small slip can be created around the hole when increasing preload.

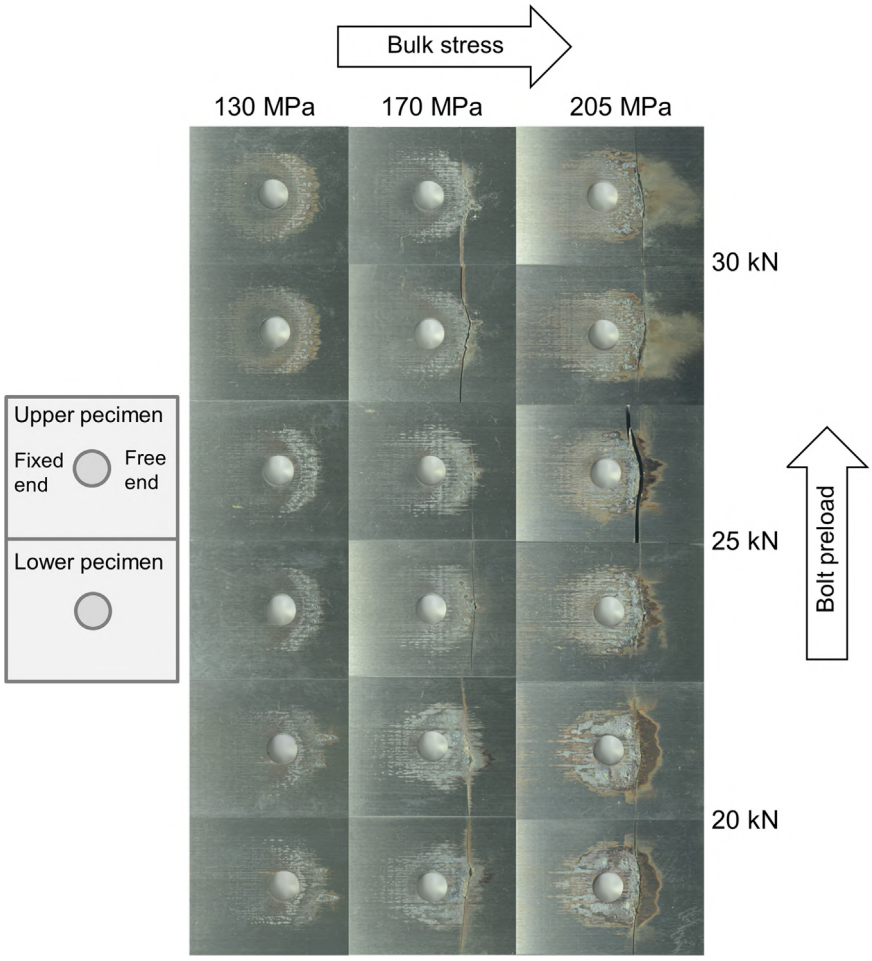

Fig. 5. Fretting scars of the specimens of series 1. (For interpretation of the references to color in this figure, the reader is referred to the web version of this article.)

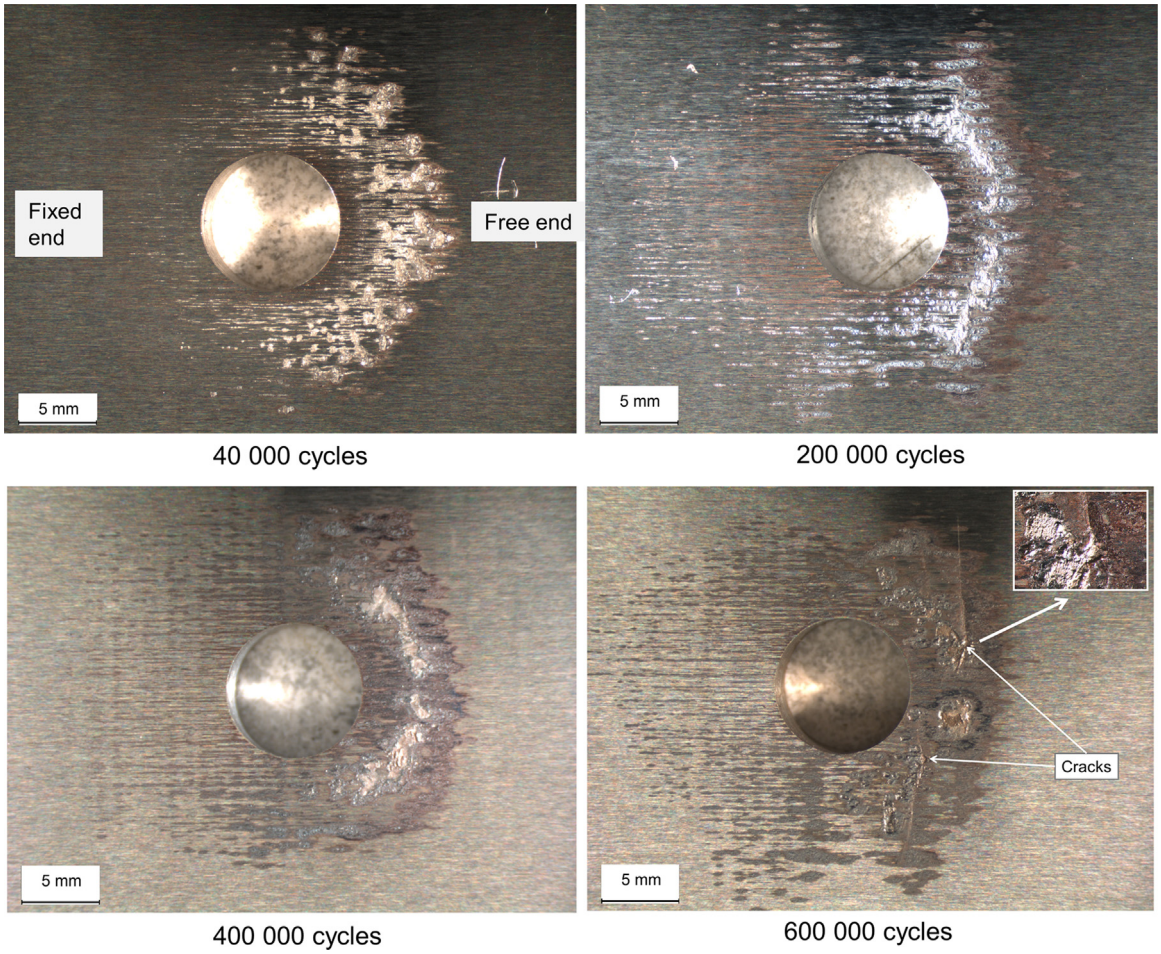

Fig. 6. Evolution of fretting scars (interrupted test series 5). (For interpretation of the references to color in this figure, the reader is referred to the web version of this article.)

- Contact size is fairly insensitive to the preload and bulk loading.
- Counterparts show rather similar fretting scars and cracks.

The actual contact has a circular shaped form around the hole. This is an example of 'common edge' contact [39]. Here, this means that two bodies of the same nominal contact dimensions are pressed together and after preloading, the contact opens around the hole some distance away. Thus, a receding contact is created, where contact pressure falls to zero at the outer edges of the contact.

Several conclusions can be drawn relating to cracking (series 1–4):

- Cracks leading to complete fracture were always formed at the free end side of the hole and were caused by fretting and not by the stress concentration of the hole.
- Cracks formed close to the contact outer edge, in front of the region of most severe fretting damage.
- The main cracks leading to complete fracture have typically been nucleated in the central area (in a lateral direction), whereas minor cracks may have been nucleated at the areas of severe damage around the hole.
- By increasing the active contact area, the cracking point moves farther from the hole.
- In rare cases, small crack was found at the hole edge, even though the point of final cracking was inside the fretting area.

Four interrupted tests were made to study the evolution of fretting damage (series 5). The fretting scars are shown in Fig. 6. Generally, the scars look similar to each other. Fretting damage was evident in all tests. Adhesion and material transfer was observed between the specimens; however, it is generally known that similar metal contacts promote welding of asperities. Severe surface degradation can "concentrate" in tests to a smaller area to form 'spot-like' damage zones that are also associated with cracking, i.e., cracks were often found at these locations. In the fourth test, small cracks have been nucleated but these did not progress to complete fracture.

4.3. DIC results

The Digital Image Correlation method was applied in series 5 in order to determine relative tangential displacement between the specimens. An example of a measured displacement field is shown in Fig. 7. The specimens are loaded downwards. The magnitude of x and y displacements is shown: these are notable and multiple times the pixel size. Here relative tangential displacements (in x-direction) between the specimens are determined at a distance of 0.5 mm from the contact interface to minimize bulk material compliances. It is impractical to measure displacements precisely at the contact interface due to disturbances caused by the interface.

Fig. 8 shows relative tangential displacements at two points, at the hole edge, x_1 (x=0 mm) and at a distance of approximately 9 mm from the hole edge, x_2 (x=9mm). The relative tangential displacements ($u_{spec1}-u_{spec2}$) shown are the average of the maximum relative tangential displacements (specimen at upper and

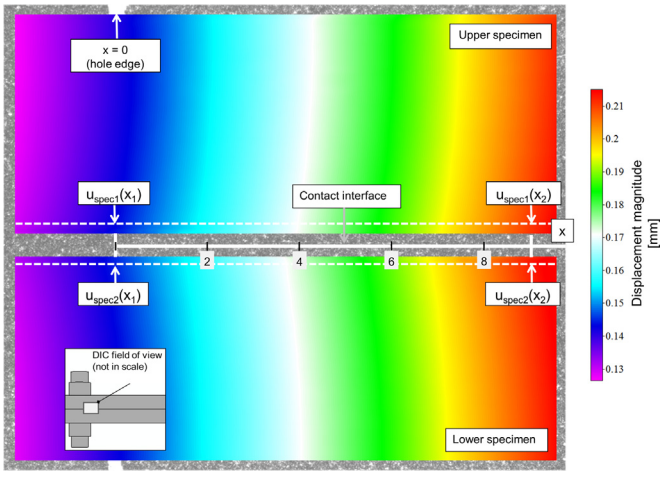

Fig. 7. An example of displacement field measured with DIC. (For interpretation of the references to color in this figure, the reader is referred to the web version of this article.)

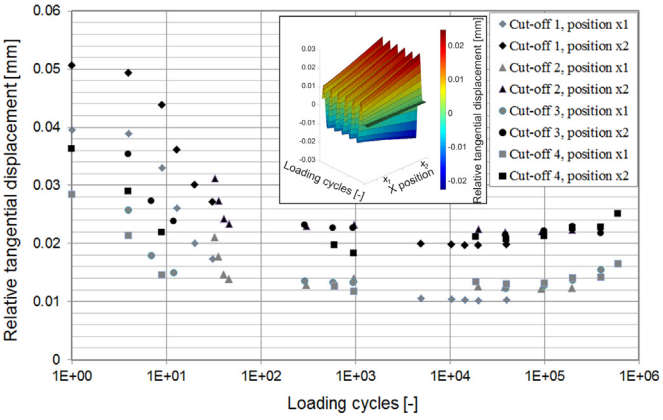

Fig. 8. Measured relative tangential displacements at points x_1 ($x=0$ mm) and x_2 ($x=9$ mm). (For interpretation of the references to color in this figure, the reader is referred to the web version of this article.)

lower position). Clearly, the amplitude decreases during the initial cycles of a fatigue test when the coefficient of friction is expected to increase. Initially, there is some scatter. The bulk loading needs to be fine-tuned after the start-up of a test in order to achieve the desired bulk loading. In order to measure displacements immediately, such fine tuning was not made and this led to somewhat fluctuating bulk loading amplitude. The bulk loading was adjusted after about 1000 cycles, except in cut-off test 1. The results of the four tests are similar in the steady-state phase and repeatability of the tests seems to be reasonable. In the figure, an example of distribution of cyclic relative tangential displacements is shown (cut-off test 4, about 600,000 loading cycles). As expected, the relative displacement increases towards the free end.

5. Numerical results

5.1. Evaluation of the coefficient of friction

The steady state COF was evaluated using the relative tangential displacements measured with DIC. The COF was varied in the FE-model and accumulated slip was computed and compared to the corresponding accumulated slip in the experiments [33], as has been done previously in [40]. In this way, steady-state COFs around 0.8 – 1.0 were evaluated. An indication of high COF can be

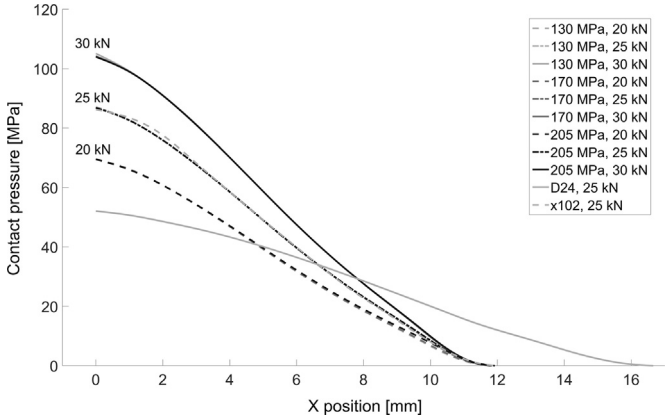

Fig. 9. Contact pressure distribution of different tests.

achieved and in the following modeling results, a COF of 1.0 is used.

5.2. Stresses and contact variables

Stresses and contact variables were studied to evaluate the experimental results in more detail. A continuum level numerical model was used without taking wear into account. For the sake of brevity, parameters were examined mainly at the centerline of the specimen. Fig. 9 shows the contact pressure distributions of different tests when the specimens are at the extreme position. The maximum of the non-uniform contact pressure distribution occurs at the hole edge and the contact pressure decreases smoothly towards zero when going farther from the hole. The preload has only a negligible effect on contact size, as was also seen in the experiments. Clearly, maximum contact pressure increases as the preload increases. Bulk loading, on the other hand, has a small or negligible effect on the contact pressure distribution.

Fig. 10 shows the effect of COF on the axial stress in the contact surface. The maximum stress at COF 1.0 occurs close to the active contact outer edge and the cracking point. The figure also shows stress with COF of 0.1, which may represent an initial contact condition or lubricated contact. The point of maximum stress is at the hole edge, at the point of minimum cross section and the hole-induced stress concentration. COF greater than 0.6 is needed to clearly move the point of maximum stress away from the hole area. This level of COF is typical in fretting conditions. Since cracks leading to complete fracture were always nucleated away from the hole, it seems to confirm that COF is indeed relatively high.

Axial stress distributions with different loading conditions and with a coefficient of friction of 1.0 are shown in Fig. 11. The stress increases by increasing the preload (keeping the bulk loading constant), which is in line with the measured fatigue results, i.e., increasing preload decreases fatigue life. The effect is more pronounced with higher bulk loads. With a larger spacer, the point of maximum stress moves farther from the hole, which corresponds to the experiment results. Fig. 12 shows the axial stress amplitudes as a function of loading cycles of the experimental tests and also a stress component history (at the point of maximum axial stress) during a loading cycle. To some extent, the stress state can be approximated as uniaxial loading. The plain fatigue limit of 517 MPa has been measured for similar material [35], so fretting markedly decreases fatigue life. The results of series 3 and 4 match the other results somewhat accurately.

Fig. 13 show computed slip amplitude with different load cases. The figure shows that the preload and bulk loading has a major effect on slip and slip increases when increasing the bulk loading and also when decreasing the preload. In many cases, the contact sticks near

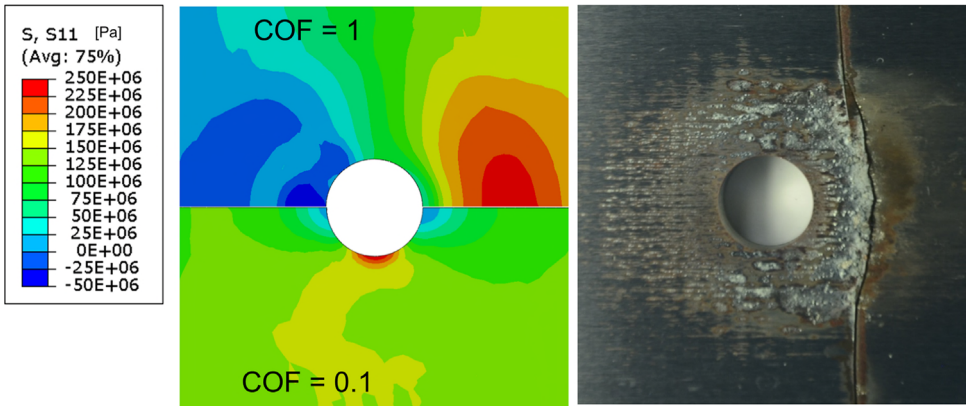

Fig. 10. Axial stress of the specimen in tension (at extreme position) (205 MPa, 25 kN). (For interpretation of the references to color in this figure, the reader is referred to the web version of this article.)

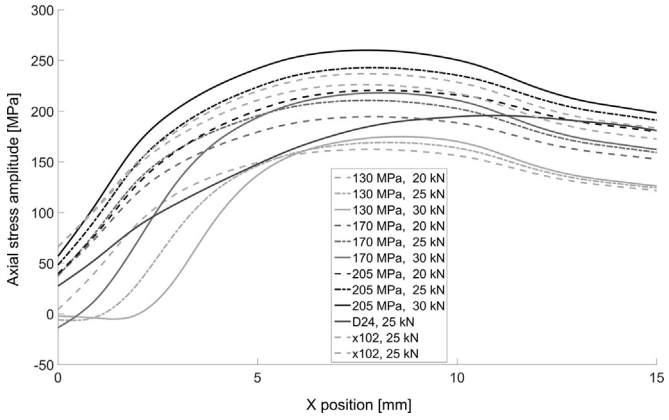

Fig. 11. Axial stress amplitudes with different load cases.

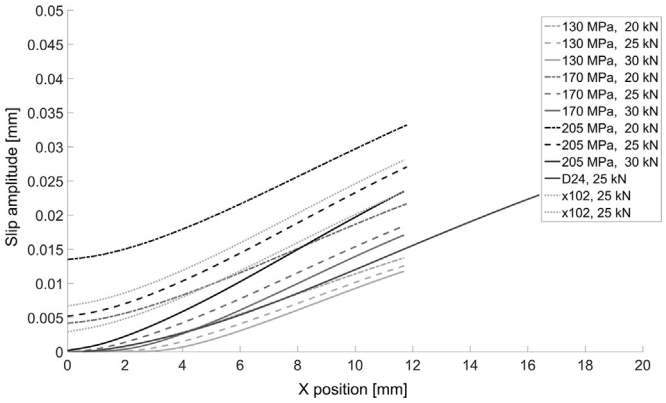

Fig. 13. Slip amplitude with different load cases.

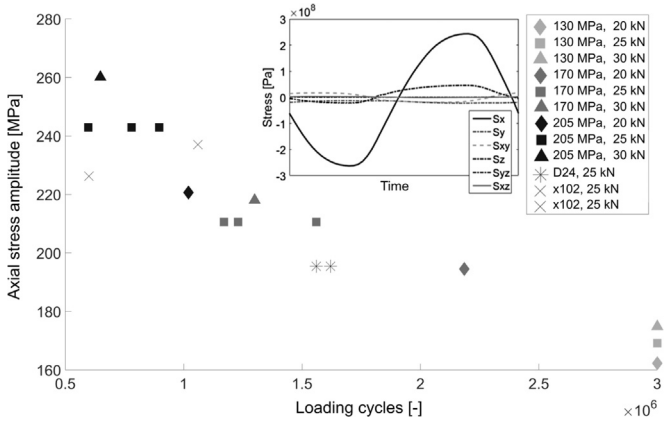

Fig. 12. Axial stress amplitude in experimental tests.

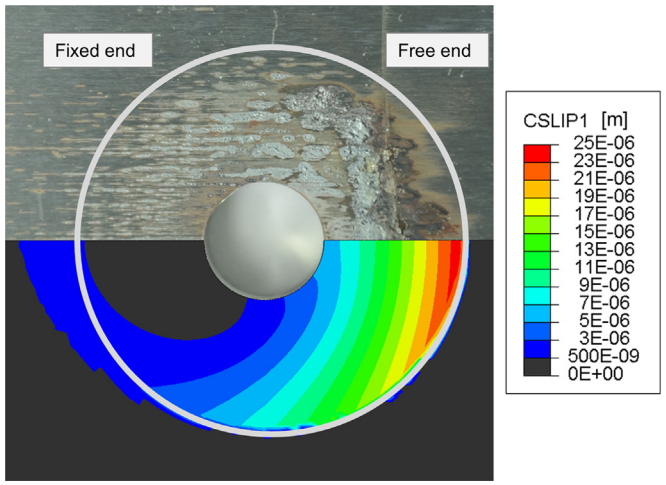

Fig. 14. Slip field compared to fretting scars (205 MPa, 25 kN). (For interpretation of the references to color in this figure, the reader is referred to the web version of this article.)

the hole, i.e., no slip occurs. To some extent, this is visible in the experimental scars shown in Fig. 5. Slip is clearly an important factor affecting fretting fatigue life. However, bulk loading is not constant at the points and cracking cannot be predicted solely on the basis of slip amplitude. Computed slip (CSLIP1 in Abaqus) is compared to fretting scars in Fig. 14. Higher slip occurs at the free end side but on the left side the slip is small. Contact area and slip distribution correspond relatively well with the experimental scars.

Fretting wear has been linked to the dissipated energy of contacts and this methodology is used here locally [41]. The fretting loop energy is computed at individual nodes. The energy Ed corresponds to the area inside the (instantaneous) shear traction (τ) - slip (δ) curve:

$$Ed(x) = \oint \tau(x) d\delta(x) \tag{1}$$

The normalized distribution of the dissipated energy along the contact in an x-direction is shown in Fig. 15. The bulk loading is 205 MPa and preload 25 kN. The maximum point of the dissipated

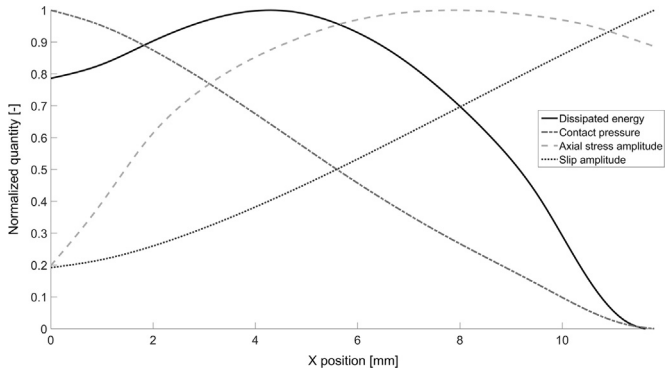

Fig. 15. Distributions of normalized dissipative energy, contact pressure, slip amplitude and axial stress amplitude.

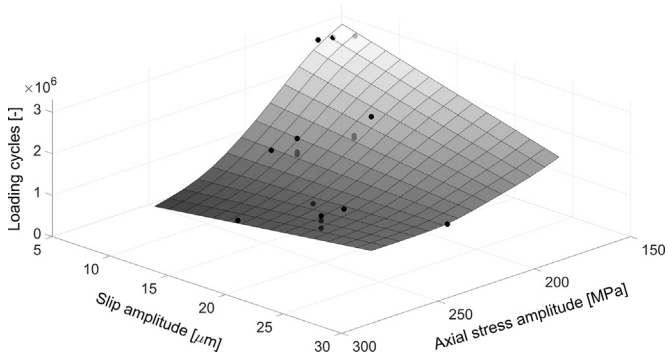

Fig. 16. Slip amplitude, axial stress amplitude in the contact and loading cycles of experimental test points.

energy is on the left side from the point of maximum stress. The distribution of dissipated energy corresponds well with the area of most severe damage and cracking observed in the experiments. The macroscopic cracks observed were found to nucleate at the outer edge side (free end side) of the most severe fretting scar where axial stress is higher. Small cracks may also be found at other locations. The scatter seen in the cracking points in the experiments is rather predictable due to the widespread distribution of frictional energy and stress.

Fig. 16 presents slip amplitude, axial stress amplitude and loading cycles of the experimental results together on the same graph. The figure shows the local variables at the point of maximum axial stress. Such data ('design map') may be useful for a designer to determine a suitable loading condition for a fretting problem.

6. Conclusions

A testing arrangement was developed to study different operating and design parameters of a single bolted joint on the fretting fatigue life. A corresponding finite element model of the test setup was built to analyze contact variables in greater detail using continuum level numerical analysis, i.e., what are the initial contact conditions and what kind of conditions may lead to fretting damage. A detailed contact and fatigue analysis was outside the scope of this study and therefore approximations were made. The material of the specimens was quenched and tempered steel. Applying the Digital Image Correlation method gave important information about the contact in terms of displacements. This data was further used together with the FE-model, to evaluate the coefficient of friction in the contact. The computed contact variables (contact area, contact slip, axial stress and dissipated energy) corresponded well to the experimental results in terms of fretting scars and cracking. Fretting damage was observed in all tests and also at a relatively early stage in the loading history. Fatigue cracks were nucleated close to the actual contact edge boundary. Fretting fatigue life decreased when increasing the bulk stress and also when increasing the preload. Cracking was observed with relatively low stresses in the specimens. The results show that fretting significantly decreases fatigue life in bolted joints. A promising kind of design map based on local contact variables (slip and stress) was also developed, which may be useful for a designer to determine a suitable loading condition for a fretting problem.

Acknowledgements

This study was conducted as part of SCarFace Research Project (Tekes decision no. 40205/12). We are grateful for the financial support provided by Tekes - the Finnish Funding Agency for Innovation, Wärtsilä Finland Oy, Nome Oy, and Global Boiler Works Oy. Atte Hokkanen, MSc, conducted all the experimental tests and carried out the photographic inspection.

References

[1] Benhamena A, Amrouche A, Talha A, Benseddiq N. Effect of contact forces on fretting fatigue behavior of bolted plates: numerical and experimental analysis. Tribol Int 2012;48:237–45. http://dx.doi.org/10.1016/j.triboint.2011.12.008.

[2] Benhamena A, Talha A, Benseddiq N, Amrouche A, Mesmacque G, Benguediab M. Effect of clamping force on fretting fatigue behaviour of bolted assemblies: case of couple steel–aluminium. Mater Sci Eng A 2010;527:6413–21. http://dx.doi.org/10.1016/j.msea.2010.06.080.

[3] Chakherlou TN, Razavi MJ, Aghdam AB, Abazadeh B. An experimental investigation of the bolt clamping force and friction effect on the fatigue behavior of aluminum alloy 2024-T3 double shear lap joint. Mater Des 2011;32:4641–9. http://dx.doi.org/10.1016/j.matdes.2011.04.022.

[4] Chakherlou TN, Oskouei RH, Vogwell J. Experimental and numerical investigation of the effect of clamping force on the fatigue behaviour of bolted plates. Eng Fail Anal 2008;15:563–74. http://dx.doi.org/10.1016/j.engfailanal.2007.04.009.

[5] Wagle S, Kato H. Ultrasonic detection of fretting fatigue damage at bolt joints of aluminum alloy plates. Int J Fatigue 2009;31:1378–85. http://dx.doi.org/10.1016/j.ijfatigue.2009.03.017.

[6] Taghizadeh H, Chakherlou TN, Ghorbani H, Mohammadpour A. Prediction of fatigue life in cold expanded fastener holes subjected to bolt tightening in Al alloy 7075-T6 plate. Int J Mech Sci 2015;90:6–15. http://dx.doi.org/10.1016/j.ijmecsci.2014.10.026.

[7] Skorupa M, Machniewicz T, Skorupa A, Korbel A. Effect of load transfer by friction on the fatigue behaviour of riveted lap joints. Int J Fatigue 2016;90:1–11. http://dx.doi.org/10.1016/j.ijfatigue.2016.04.005.

[8] Samaei M, Zehsaz M, Chakherlou TN. Experimental and numerical study of fatigue crack growth of aluminum alloy 2024-T3 single lap simple bolted and hybrid (adhesive/bolted) joints. Eng Fail Anal 2016;59:253–68. http://dx.doi.org/10.1016/j.engfailanal.2015.10.013.

[9] Esmaeili F, Chakherlou TN. Investigation on the effect of tigthening torque on the stress distribution in double lap simple bolted and hybrid (bolted-bonded) joints. J Solid Mech 2015;7:268–80.

[10] Li J, Zhang K, Li Y, Liu P, Xia J. Influence of interference-fit size on bearing fatigue response of single-lap carbon fiber reinforced polymer/Ti alloy bolted joints. Tribol Int 2016;93:151–62. http://dx.doi.org/10.1016/j.triboint.2015.08.044.

[11] Wagle S, Kato H. Depth evaluation of fretting fatigue crack appearing at bolt joints of aluminum alloy plates by synchronized surface acoustic wave measurement. Mater Trans 2012;53:256–63. http://dx.doi.org/10.2320/matertrans.I-M2011838.

[12] Esmaeili F, Chakherlou TN, Zehsaz M, Hasanifard S. Investigating the effect of clamping force on the fatigue life of bolted plates using volumetric approach. J Mech Sci Technol 2013;27:3657–64. http://dx.doi.org/10.1007/s12206-013-0911-3.

[13] Ferrero JF, Yettou E, Barrau JJ, Rivallant S. Analysis of a dry friction problem under small displacements: application to a bolted joint. Wear 2004;256:1135–43. http://dx.doi.org/10.1016/j.wear.2003.07.003.

[14] Ferjaoui A, Yue T, Abdel Wahab M, Hojjati-Talemi R. Prediction of fretting fatigue crack initiation in double lap bolted joint using continuum damage mechanics. Int J Fatigue 2015;73:66–76. http://dx.doi.org/10.1016/j.ijfatigue.2014.11.012.

[15] Crevoisier J, Swiergiel N, Champaney L, Hild F. Identification of in situ frictional properties of bolted assemblies with digital image correlation. Exp Mech 2012;52:561–72. http://dx.doi.org/10.1007/s11340-011-9518-8.

[16] Schön J. Coefficient of friction for aluminum in contact with a carbon fiber epoxy composite. Tribol Int 2004;37:395–404. http://dx.doi.org/10.1016/j.triboint.2003.11.008.
[17] Jayaprakash M, Mutoh Y, Yoshii K. Fretting fatigue behavior and life prediction of automotive steel bolted joint. Mater Des 2011;32:3911–9. http://dx.doi.org/10.1016/j.matdes.2011.02.061.
[18] Marshall MB, Lewis R, Dwyer-Joyce RS. Characterisation of contact pressure distribution in bolted joints. Strain 2006;42:31–43. http://dx.doi.org/10.1111/j.1475-1305.2006.00247.x.
[19] Benhaddou T, Chirol C, Daidie A, Guillot J, Stephan P, Tuery J-B. Pre-tensioning effect on fatigue life of bolted shear joints. Aerosp Sci Technol 2014;36:36–43. http://dx.doi.org/10.1016/j.ast.2014.03.003.
[20] Oskouei RH, Keikhosravy M, Soutis C. A finite element stress analysis of aircraft bolted joints loaded in tension. Aeronaut J 2010;114:315–20. http://dx.doi.org/10.1017/S0001924000003766.
[21] Cho Y, Kim T. Estimation of ultimate strength in single shear bolted connections with aluminum alloys (6061-T6). Thin-Walled Struct 2016;101:43–57. http://dx.doi.org/10.1016/j.tws.2015.11.017.
[22] Murugesan J, Mutoh Y. Fretting fatigue strength prediction of dovetail joint and bolted joint by using the generalized tangential stress range-compressive stress range diagram. Tribol Int 2014;76:116–21. http://dx.doi.org/10.1016/j.triboint.2013.11.006.
[23] Abad J, Medel FJ, Franco JM. Determination of Valanis model parameters in a bolted lap joint: experimental and numerical analyses of frictional dissipation. Int J Mech Sci 2014;89:289–98. http://dx.doi.org/10.1016/j.ijmecsci.2014.09.014.
[24] Abazadeh B, Chakherlou TN, Alderliesten RC. Effect of interference fitting and/or bolt clamping on the fatigue behavior of Al alloy 2024-T3 double shear lap joints in different cyclic load ranges. Int J Mech Sci 2013;72:2–12. http://dx.doi.org/10.1016/j.ijmecsci.2013.03.001.
[25] Abazadeh B, Chakherlou TN, Farrahi GH, Alderliesten RC. Fatigue life estimation of bolt clamped and interference fitted-bolt clamped double shear lap joints using multiaxial fatigue criteria. Mater Des 2013;43:327–36. http://dx.doi.org/10.1016/j.matdes.2012.06.050.
[26] Chakherlou TN, Mirzajanzadeh M, Vogwell J, Abazadeh B. Investigation of the fatigue life and crack growth in torque tightened bolted joints. Aerosp Sci Technol 2011;15:304–13. http://dx.doi.org/10.1016/j.ast.2010.08.003.
[27] Esmaeili F, Chakherlou TN, Zehsaz M. Prediction of fatigue life in aircraft double lap bolted joints using several multiaxial fatigue criteria. Mater Des 2014;59:430–8. http://dx.doi.org/10.1016/j.matdes.2014.03.019.
[28] Zografos A, Dini D, Olver AV. Fretting fatigue and wear in bolted connections: A multi-level formulation for the computation of local contact stresses. Tribol Int 2009;42:1663–75. http://dx.doi.org/10.1016/j.triboint.2009.03.007.
[29] Zhu L, Hong J, Jiang X. On controlling preload and estimating anti-loosening performance in threaded fasteners based on accurate contact modeling. Tribol Int 2016;95:181–91. http://dx.doi.org/10.1016/j.triboint.2015.11.006.
[30] Kounoudji KA, Renouf M, Mollon G, Berthier Y. Role of third body on bolted joints' self-loosening. Tribol Lett 2016. http://dx.doi.org/10.1007/s11249-016-0640-8.
[31] Sutton MA, Orteu J-J, Schreier HW. Image correlation for shape, motion and deformation measurements.New York: Springer; 2009.
[32] Kartal ME, Mulvihill DM, Nowell D, Hills DA. Determination of the frictional properties of titanium and nickel alloys using the digital image correlation method. Exp Mech 2011;51:359–71. http://dx.doi.org/10.1007/s11340-010-9366-y.
[33] Nesladek M, Spaniel M, Jurenka J, Ruzicka J, Kuzelka J. Fretting fatigue – experimental and numerical approaches. Int J Fatigue 2012;44:61–73. http://dx.doi.org/10.1016/j.ijfatigue.2012.05.015.
[34] Kounoudji KA, Mollon G, Renouf M, Berthier Y. Tribological analysis of bolted joints submitted to vibrations. Tribol Online 2016;**11**:255–63. http://dx.doi.org/10.2474/trol.11.255.
[35] Juoksukangas J, Lehtovaara A, Mäntylä A. Development of a complete contact fretting test device. Proc Inst Mech Eng J: J Eng Tribol 2012;227:570–8. http://dx.doi.org/10.1177/1350650112466162.
[36] Juoksukangas J, Lehtovaara A, Mäntylä A. Applying the digital image correlation method to fretting contact for slip measurement. Proc Inst Mech Eng J: J Eng Tribol 2015. http://dx.doi.org/10.1177/1350650115601695 Published online ahead of print August 20, 2015.
[37] Lavision. Davis 8.2 Commercial DIC equipment and software; 2014.
[38] Dassault Systèmes Simulia Corp. Abaqus Theory Manual 6.13; 2015.
[39] Ramesh R, Hills D. Recent progress in understanding the properties of elastic contacts. Proc Inst Mech Eng C: J Mech Eng Sci 2015;229:2117–26. http://dx.doi.org/10.1177/0954406214556667.
[40] Juoksukangas J, Lehtovaara A, Mäntylä A. A comparison of relative displacement fields between numerical predictions and experimental results in fretting contact. Proc Inst Mech Eng J: J Eng Tribol 2015. http://dx.doi.org/10.1177/1350650116633573 Published online before print March 7, 2016.
[41] Fouvry S, Kapsa P, Vincent L. Quantification of fretting damage. Wear 1996;200:186–205. http://dx.doi.org/10.1016/S0043-1648(96)07306-1.

Publication VII

Influence of a surface treatment on fretting fatigue life in complete contacts

by

J. Juoksukangas, A. Lehtovaara, T. Koivula and A. Mäntylä

Unpublished manuscript

Influence of a surface treatment on fretting fatigue life in complete contacts

J. Juoksukangas[1*], A. Lehtovaara[1], T. Koivula[1] and A. Mantyla[2]

[1]Group of Tribology and Machine Elements, Department of Materials Science, Tampere University of Technology, P.O. Box 589, 33101 Tampere, Finland
[2]Research & Development, Wartsila Finland Oy, P.O.Box 244, 65101 Vaasa, Finland
*Corresponding author, e-mail: janne.juoksukangas@tut.fi

ABSTRACT

Fretting can be the reason for serious and unexpected damage in press-fitted components, where small amplitude relative tangential movement takes place between the contacting bodies. Fretting fatigue life can be increased by introducing compressive residual stresses on surfaces. Shot peening and nitriding are techniques often used for such purposes. This study experimentally investigated the effect of these treatments on the fretting and plain fatigue life of quenched and tempered 34CrNiMo6 steel in a complete contact. Shot peening and nitriding increased not only fretting fatigue life, but also plain fatigue life. Fretting relaxed residual stresses and made the initially uniform residual stress field anisotropic.

Keywords: fretting fatigue, surface treatment, complete contact, shot peening, nitriding.

1. INTRODUCTION

Fretting fatigue or wear may exist if small amplitude tangential movement takes place between contacting bodies [1]. Fretting fatigue can significantly decrease fatigue life of components consisting of frictional joints, like press-fits. Fretting induces high stresses on the surface that promotes fatigue crack nucleation that can grow further due to cyclic stresses in the body. Cracking can lead to serious and unexpected failure because the cracks can grow invisibly inside a contact.

Fretting fatigue and plain fatigue life can be increased by introducing compressive stresses on the surfaces, for example, using shot peening and nitriding. Both methods develop compressive residual stresses that inhibit fatigue crack propagation. In addition, the hardness of the surface and surface roughness may be altered. [2,3]

Shot peening is a cold working process, where small (typically ball-formed) particles are shot on the surface. The kinetic energy of the balls is converted into work that causes elastic and plastic deformation in the target surface and produces compressive residual stresses. The residual stress distribution depends on the material and parameters used in the process. Typically, on metals, the residual stress can be slightly over a half of the material's ultimate stress limit at maximum. Shot peening may significantly increase the surface roughness and may also give rise to small initial cracks [2]. [4]

Nitriding is a heat treating process, in which a case hardened surface with compressive residual stresses

is created by diffusing nitrogen into the target surface. A thin compound layer of iron nitride is created on the surface as a by-product. With 34CrNiMo6 specimens, the brittle compound layer was attributed to affect fatigue behaviour at high stress amplitude [5] but, on the other hand, the compound layer had no major effect on fatigue life in [6]. The hard layer is wear-resistant and generally, the diffusion layer provides the enhanced fatigue properties. [7]

A major increase in fretting fatigue life is reported due to shot peening [8,9]. The fretting fatigue limit has been increased up to the level of plain fatigue limit [10]. The intensity of shot peening process may affect the plain fatigue behaviour [2,9]. Nitriding also has a beneficial effect by increasing plain and fretting fatigue life. Depending on the steel grade used, the plain fatigue limit increased 10 - 25 % and the fretting fatigue limit 50 - 150 % [11]. The fretting fatigue limit may be increased to the same level as the plain fatigue limit [12]. Nitriding increased the fretting and plain fatigue life of specimens made of 34CrNiMo6 steel up to same level and the cracks in fretting specimens nucleated from subsurface [5], instead of surface. In bending fatigue with notched steel specimens [3], nitriding increased fatigue limit 8 % and the combination of nitriding and shot peening 35 %. Ion nitriding increased fatigue strength by up to 91 % of quenched and tempered steel [13] and plain fatigue strength by up to 45 % with a low-alloy steel [6]. In plain carbon steel fatigue tests, gas nitriding and plasma nitriding produced the same level of increase in fatigue limit [14]. By combining the shot peening nitrided methods, fretting fatigue limit was increased from a value of 110 to 300 MPa in specimens made of 709M40 steel [15].

Fatigue cracks typically nucleate at the surface, but the compressive layer can cause cracks to nucleate below the layer. Subsurface crack initiation with a “fish-eye” type crack is typical of nitrided fretting [5] and plain fatigue specimens [6,13]. This is associated with non-metallic inclusions below the surface. [5,13]. Fretting can relax the residual compressive stresses of shot peened specimens [16]. Residual stresses can be relaxed also in notched fatigue specimens [3].

Shot peened steel specimen had the same coefficient of friction as the untreated specimen, but nitriding resulted in lower value of coefficient of friction [17]. In a complete contact, i.e. ‘sharp-ended’ contact, in which the nominal contact area is independent of the normal load, nitrided fretting test specimens, made of titanium alloy, had lower friction force compared to the untreated ones [18]. It is well known that the value of coefficient of friction greatly affects contact stresses and therefore, coefficient of friction can have a major effect on the risk of fretting fatigue crack nucleation, as has been reported also within the complete contact setup used here [19].

The effect of nitriding and shot peening on fretting fatigue life has been studied with several steel grades, mainly in individual studies, and only a little of this research relates to quenched and tempered 34CrNiMo6 steel. However, this steel grade is commonly used in heavily loaded conditions in machine components. Thus, there is a need for studying the effect of both shot peening and nitriding on fretting fatigue behaviour using the quenched and tempered steel within the same test conditions.

This study experimentally investigated the effect of shot peening and nitriding on fretting fatigue (using a complete contact) and plain fatigue life with quenched and tempered 34CrNiMo6 steel. Complete contacts can be often found in practical frictional connections. Both fretting and plain fatigue tests were carried out that allow comparison of the results. The achieved test results were compared to previously conducted tests with untreated specimens (the results originally presented in [20]). In addition, the effect of fretting on residual stresses was investigated.

2. EXPERIMENTS

A complete contact fretting test device, schematically shown in Figure 1, was used in the experimental tests. A detailed description can be found in [20]. Here, only a brief overview of the experimental device and testing procedure is presented.

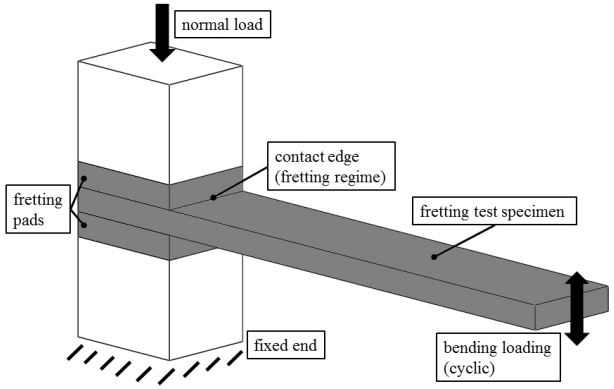

Figure 1. Schematics of an in-house complete contact fretting test device.

The fretting specimen and pads creating the test contacts are clamped together by a normal load. Thus, an asymptotic contact pressure distribution is created at the contact edge, which is, therefore, the point of stress concentration. Slip amplitude has its maximum value also at the edge [21]. The specimen is loaded transversally at the free end (displacement controlled), which creates bulk (bending) stresses in the specimen. The bulk loading forms relative movement (slip) between the specimen and the pads.

The nominal fretting contact area created by the specimen and pad is 2000 mm^2. The width of the plain fatigue specimen is reduced outside the contact to move the point of maximum bending stress away from the contact [20]. The specimens and pads are self-mated using EN 10083-1-34CrNiMo6+QT steel. Before surface treatments, the specimens and pads were ground longitudinally producing 3D roughness *Sa* of 0.3 µm, measured with a Wyco NT1100. The analyzed surface area was 4.9 × 3.8 mm^2, with a 6.72 µm sampling period. The front face of the pads was also ground.

The Almen value, indicating the intensity of the shot peening, was 0.24 mm (type A). Steel balls were used with 100 % coverage. *Sa* value of the shot peened specimens was about 3 µm. The gas nitriding process with ammonia lasting for 33 hours produced a diffusion layer having a thickness of about 0.4 mm. *Sa* value of the nitrided specimens was 0.4 µm. Therefore, nitriding had only a minor effect on the surface roughness, as shot peening increased it by a factor of about ten. A microscope image of the cross-section of a nitrided specimen is shown in Figure 2.

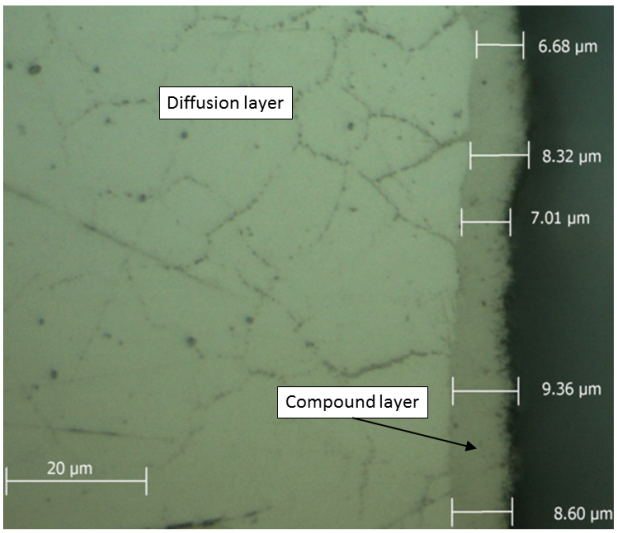

Figure 2. Compound layer of a nitrided specimen.

The compound layer has an average thickness of about 8 µm. In some nitrided test specimens the layer was left intact, while in the rest of the specimens it was removed by grinding.

In the shot peening case, 13 fretting fatigue and 5 plain fatigue tests were performed with the treated specimens. Similarly, 13 fretting fatigue and 17 plain fatigue tests were performed with the nitrided specimens. A new specimen was introduced at each individual test. Tests were run in dry conditions without any lubrication and acetone was used to clean the specimens and pads before testing. The nominal contact pressure was 100 MPa and the testing frequency was 41 Hz with a fully reversed loading (R = -1). Tests were stopped after three million cycles, if no failure occurred and the specimen was treated

as having infinite fatigue life. The tests were run at a normal laboratory room temperature and humidity.

The outcome of the experimental tests was *S-N*-curves, where the maximum bulk (nominal bending) stress amplitude in the specimen, excluding the contact stresses, is plotted as a function the cycles of complete fracture. This allows straightforward comparison of the results between treated and untreated specimens as well as treated fretting and plain fatigue specimens. Several bulk stress levels were used to determine the finite regime. The fatigue limit was determined by reproducing a staircase test [22].

3. RESULTS AND DISCUSSION

The experimental results achieved are compared to the untreated fretting and plain fatigue tests made previously using the same material [20]. Prior to the surface treatment, the specimens were similar and therefore comparable.

3.1. Fatigue life

The fretting fatigue test results for the shot peened specimens are shown in Figure 3.

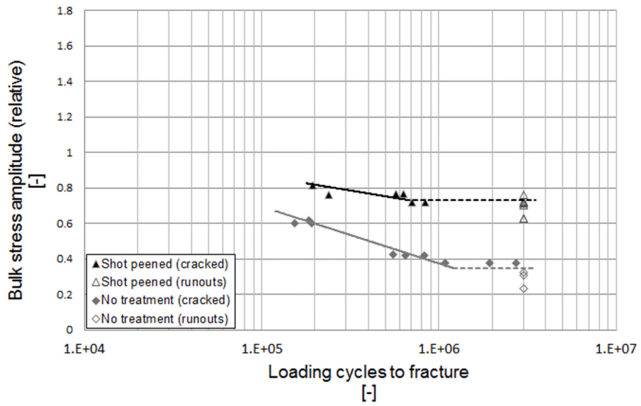

Figure 3. Shot peening test results: fretting fatigue.

The black markers represent the shot peened specimens and the grey markers the reference specimens having no surface treatment [20]. The solid markers represent specimens with finite lifetime and the open markers those with infinite lifetime (run-out). The values are scaled to the nominal plain fatigue limit of untreated specimens.

The results clearly demonstrate the beneficial effect of shot peening on fretting fatigue life. The fretting fatigue limit increased 110 %. Further, the fretting fatigue limit is about 73 % of the reference plain fatigue limit, being only about 35 % with untreated specimens. Figure 4 presents the shot peening plain fatigue results.

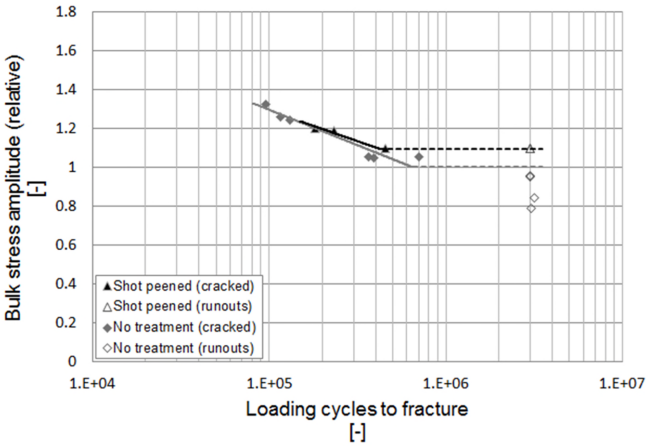

Figure 4. Shot peening test results: plain fatigue.

A slight increase in fatigue limit is achieved, about 10 %. However, more tests would be needed to show that the small difference is statistically reliable.
Similar graphs are presented for the nitrided specimens. Figure 5 presents the fretting fatigue results. Nitrided specimens are marked by a black square and specimens from which the compound layer has been removed are marked by a grey circle.

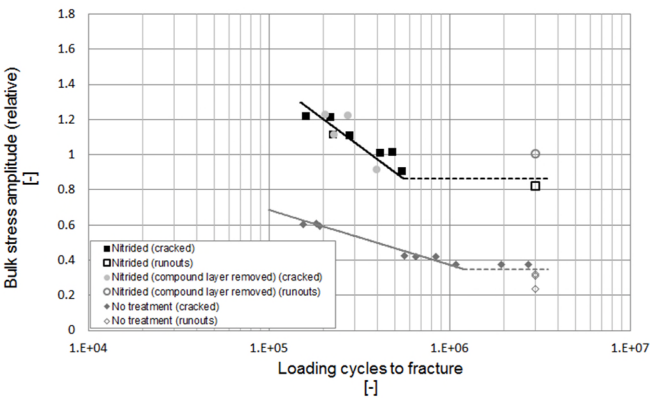

Figure 5. Nitriding test results: fretting fatigue.

As in the shot peening case, a notable increase in fretting fatigue life is achieved. The fretting fatigue limit has now increased by about 150 % which is 86 % of the reference plain fatigue limit. Nitriding notably increases fatigue life at high bulk stress amplitudes. Nitriding has a greater improving effect on fretting fatigue behaviour compared to shot peening. In a few specimens fracture occurred completely outside the contact; these test points are rejected from the analysis and the figure. The plain fatigue results are presented in Figure 6.

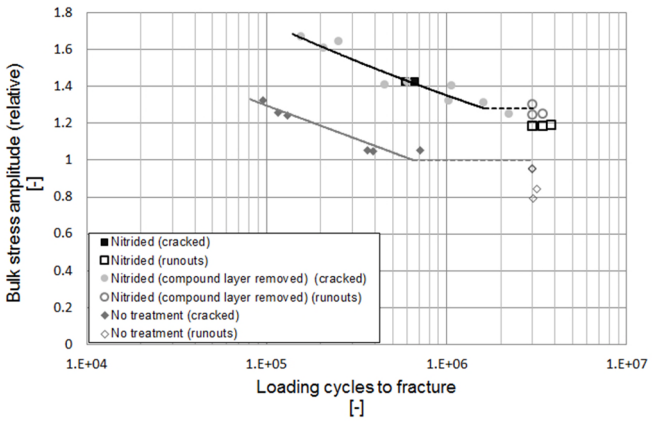

Figure 6. Nitriding test results: plain fatigue.

The plain fatigue limit has increased by about 25 %. Nitriding also has a more beneficial effect on plain fatigue behaviour compared to shot peening. The compound layer had no major effect on fatigue life in either the fretting or plain fatigue cases. In all cases, fatigue life decreased as the bulk loading increased. The results in both shot peening and nitriding cases are at a similar level to the results in the literature discussed in the introduction.

3.2. Fretting scars and cracking

Fretting scars and crack surfaces were inspected with an optical microscope. In the shot peening case, the fretting specimens cracked at the contact edge, the point of stress concentration and maximum slip, and the plain fatigue specimens at the point of maximum bending stress. A fretting scar of a shot peened specimen is shown in Figure 7.

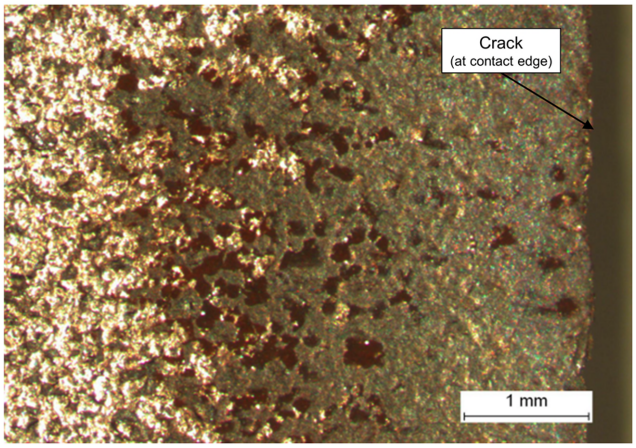

Figure 7. Fretting scar of a shot peened specimen.

In the figure, the cracking point (contact edge) is on the right. On the left, an unaltered surface is seen, showing the initial surface after shot peening. Fretting movement has clearly modified the surface over a zone of a few millimetres to the left of the contact edge. The cracks leading to complete fracture were invariably nucleated at the centre of the specimen.

Figure 8 shows a fretting scar of a nitrided specimen. Bulk stresses were higher in the nitrided test series than in the shot peened case and therefore the fretting scars cannot be directly compared.

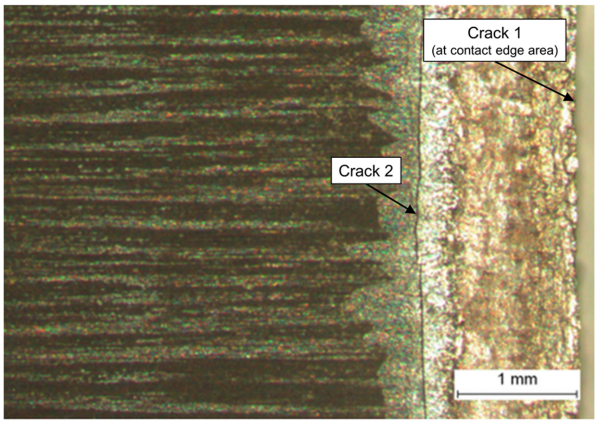

Figure 8. Fretting scar of a nitrided specimen.

The crack surface (Crack 1) is on the right. Here a region of more severe surface degradation can be seen slightly over one millimetre from the contact edge. To the left is a region of mild fretting (slip) marks. There was another crack nucleated inside the contact at the boundary seen in the figure (Crack 2 in Figure 8) that typically led to final fracture. Most of

the nitrided specimens contained both of these differently located cracks shown in the figure.

Nitrided plain fatigue specimens cracked invariably at the central region of the specimen and at the point of maximum bulk (bending) stress in the specimen longitudinal direction. An example of a crack nucleation point is shown in Figure 9.

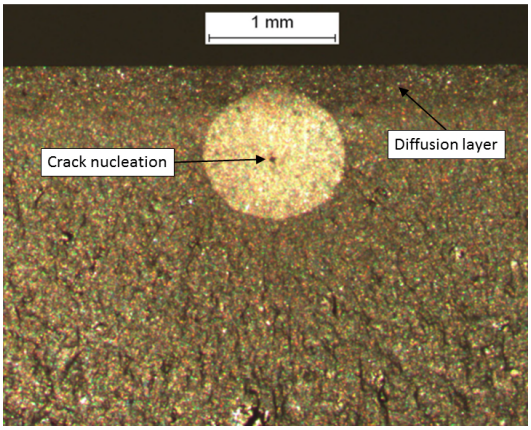

Figure 9. "Fish eye" crack nucleation of a nitrided plain fatigue specimen.

The crack has been nucleated from a defect below the diffusion layer, forming a "fish eye" crack. Due to bending loading, the stress is already notably decreased at that depth, which emphasizes the positive effect of nitriding on fatigue behaviour. The diffusion layer can be seen as a darker area at the surface.

3.3. Residual stress relaxation

The residual stresses in some of the shot peened specimens were measured after grinding (specimen manufacturing), after surface treatment process and also after fretting testing. The residual stresses for one specimen were measured as a function of the depth. The measurements were made by a sub-contractor using X-ray diffraction and the material removal was made by electropolishing. The measuring point was in the middle of the specimen, in a longitudinal direction 1 mm inside the contact in the fretting regime. Table 1 shows the values in both a longitudinal and transversal direction.

Table 1. Residual stress measurement results.

Specimen	Cracked/ runout	No treatment		Shot peened		Fretting tested		Effect of fretting fatigue
		Measured residual stress [MPa]	± [MPa]	Measured residual stress [MPa]	± [MPa]	Measured residual stress [MPa]	± [MPa]	Residual stress relaxation (%)
Longitudinal (0°)								
QT_1	runout	-18	10	-592	3	-245	17	58.6
QT_2	runout	-183	9	-599	8	-242	16	59.5
QT_3	cracked	-206	7	-571	8	-109	14	80.9
Transversal (90°)								
QT_1	runout	-223	5	-568	7	-362	6	36.4
QT_2	runout	-304	7	-561	5	-393	6	30.1
QT_3	cracked	-327	3	-548	3	-351	6	35.9

Shot peening produced a spatially uniform compressive residual stress field, even though there was some scatter in the values after grinding. Fretting relaxed the stresses noticeably and made the residual stress field anisotropic. In the longitudinal direction (the direction of fretting movement) the stresses relaxed about 60 %. The results of the completely cracked specimen (QT_3) may not be comparable due to possible relaxation of stresses at the proximity of the crack surface. In the longitudinal direction notably lower residual value is measured in that specimen. In a transversal direction, the stresses relaxed slightly over 30 %. Figure 10 shows the residual stresses for a single specimen (QT_1) after fretting testing as a function of depth in both directions.

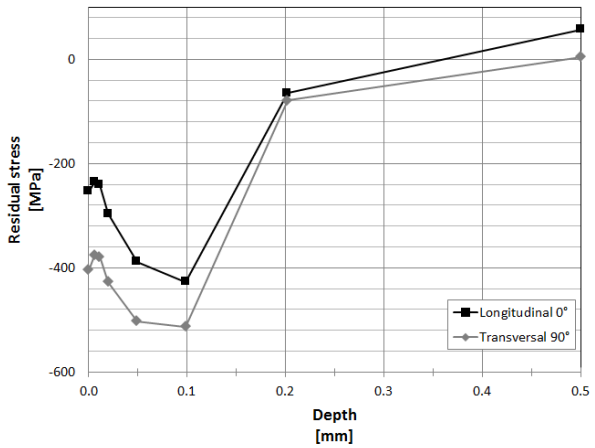

Figure 10. Residual stresses as a function of depth (after fretting testing).

A major decrease in residual stresses occurs close to the surface especially in the longitudinal direction. It can be seen that the maximum residual stresses occur down to about 0.1 mm below the surface. At that

depth fretting induced stresses have at least mostly vanished [19].

4. CONCLUSIONS

Fretting fatigue can notably decrease the fatigue life of components such as press fits. The effect of shot peening and nitriding on the fretting fatigue behaviour of specimens made of 34CrNiMo6 quenched and tempered steel was studied in dry conditions. The results were compared with untreated fretting and plain fatigue results achieved with the same test device. The nominal contact pressure was 100 MPa of the complete contact used having a nominal contact area of 2000 mm^2. The transversally applied cyclic bulk (bending) loading amplitude of the specimen ranged between about 300 - 600 MPa.

Both the nitriding and shot peening processes notably increased fretting fatigue life. Nitriding had a greater improving effect on both fretting and plain fatigue behaviour. Shot peening increased the fretting fatigue limit by 110 % and the plain fatigue limit by about 10 %. Similarly, nitriding increased the fretting fatigue limit by 150 % and the plain fatigue limit by around 25 %. The compound layer produced by the nitriding process had no effect on fatigue life in either the fretting or plain fatigue cases. Fretting caused residual stress relaxation at the contact surfaces and made the initially uniform residual stress field anisotropic.

ACKNOWLEDGEMENTS

The work was carried out within FIMECC Ltd and its DEMAPP program. We gratefully acknowledge the financial support of Wartsila Finland Oy, Metso Paper Oy and Tekes (Finnish Funding Agency for Technology and Innovation). Tomi Koivula, MSc, carried out the experimental tests, analysed the data and made the microscopic inspections. Some of the material analysis was made at the Department of Materials Science.

REFERENCES

[1] Hills DA, Nowell D. Mechanics of Fretting Fatigue. Dordrecht: Kluwer Academic Publishers; 1994.

[2] Waterhouse RB, Trowsdale AJ. Residual stress and surface roughness in fretting fatigue. J Phys D Appl Phys 1992;25:236–239.

[3] Terres MA, Laalai N, Sidhom H. Effect of nitriding and shot-peening on the fatigue behavior of 42CrMo4 steel: Experimental analysis and predictive approach. Mater Des 2012;35:741–748.

[4] Kritzler J, Wubbenhorst W. Inducing Compressive Stresses through Controlled Shot Peening. In: Totten G, Howes M, Inoue T, editors. Handb. Residual Stress Deform. Steel, Ohio: ASM International; 2002, p. 345–358.

[5] Costa JD, Ferreira JM, Ramalho AL. Fatigue and fretting fatigue of ion-nitrided 34CrNiMo6 steel. Theor Appl Fract Mech 2001;35:69–79.

[6] Alsaran A, Karakan M, Celik A. The investigation of mechanical properties of ion-nitrided ´AISI 5140 low-alloy steel. Mater Charact 2002;48:323–327.

[7] Kolozsvary Z. Residual Stresses in Nitriding. In: Totten G, Howes M, Inoue T, editors. Handb. Residual Stress Deform. Steel, Ohio: ASM International; 2002, p. 209–219.

[8] Cadario A, Alfredsson B. Influence of residual stresses from shot peening on fretting fatigue crack growth. Fatigue Fract Eng Mater Struct 2007;30:947–963.

[9] Torres MAS, Voorwald HJC. An evaluation of shot peening, residual stress and stress relaxation on the fatigue life of AISI 4340 steel. Int J Fatigue 2002;24:877–886.

[10] Waterhouse RB. Fretting fatigue. London: Applied Science Publishers; 1981.

[11] Allen C, Li CX, Bell T, Sun Y. The effect of fretting on the fatigue behaviour of plasma nitrided stainless steels. Wear 2003;254:1106–1112.

[12] Linhart V, Cipera M, Cerny I, Ciperova L. The Effect of Ion Nitriding and Carbonitriding on Fretting Fatigue of Steels. World Acad Sci Eng Technol 2011;76:373–378.

[13] Sirin SY, Sirin K, Kaluc E. Effect of the ion

nitriding surface hardening process on fatigue behavior of AISI 4340 steel. Mater Charact 2008;59:351–358.

[14] Ashrafizadeh F. Influence of plasma and gas nitriding on fatigue resistance of plain carbon (Ck45) steel. Surf Coatings Technol 2003;174–175:1196–1200.

[15] Li CX, Sun Y, Bell T. Shot peening of plasma nitrided steel for fretting fatigue strength enhancement. Mater Sci Technol 2000;16:1067–1072.

[16] Lee H, Sathish S, Mall S. Evolution of residual stress under fretting fatigue. J Mater Sci 2004;39:7089–7092.

[17] Kubiak K, Fouvry S, Wendler BG. Comparison of Shot Peening and Nitriding Surface Treatments Under Complex Fretting Loadings. Mater Sci Forum 2006;513:105–118.

[18] Rajasekaran B, Ganesh Sundara Raman S. Plain fatigue and fretting fatigue behaviour of plasma nitrided Ti-6Al-4V. Mäter ¨Lett 2008;62:2473–2475.

[19] Juoksukangas J, Lehtovaara A, Mantyla A. The effect of contact edge geometry on fretting fatigue behavior in complete¨contäcts. Wear 2013;308:206–212.

[20] Juoksukangas J, Lehtovaara A, Mantyla A. Development of a complete contact fretting test device. Proc Inst Mech Eng P¨art J¨J Eng Tribol 2013;227:570–578.

[21] Juoksukangas J, Lehtovaara A, Mantyla A. A comparison of relative displacement fields between numerical predictions and experimental results in fretting contact. Proc Inst Mech Engg ¨Part J J Eng Tribol 2016;230:1273–1287.

[22] Rabb R. Todennakoisyysteoriaan pohjautuva vasymisanalyysi. Helsinki: BoD - Books On Demand; 2013.

Tampereen teknillinen yliopisto
PL 527
33101 Tampere

Tampere University of Technology
P.O.B. 527
FI-33101 Tampere, Finland

ISBN 978-952-15-3944-2
ISSN 1459-2045